Host-Pathogen Interactions at the Intestinal Epithelial Barrier

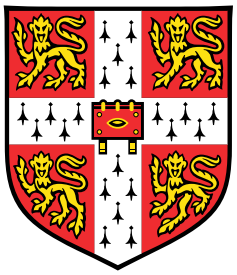

Joana Patricia Fernandes de Moura Guedes

Babraham Institute

University of Cambridge

This dissertation is submitted for the degree of

Doctor of Philosophy

Darwin College

September 2017

Declaration

I hereby declare that except where specific reference is made to the work of others, the contents of this dissertation are original and have not been submitted in whole or in part for consideration for any other degree or qualification in this, or any other university. This dissertation is my own work and contains nothing which is the outcome of work done in collaboration with others, except as specified in the text and Acknowledgements. It does not exceed the prescribed word limit for the relevant Degree Committee. The research in this thesis was carried out at the Babraham Institute, Cambridge, between October 2013 and September 2017.

Joana Patricia Fernandes de Moura Guedes

September 2017

Acknowledgements

The completion of this work would not have been possible without the contribution of many people who supported me during the past 4 years.

First, I want to express my gratitude to my scientific mentors. Jörg Stange, thank you for your unbelievable support and friendship. We both know that we are very different. but you were always there every time I didn't know where to begin, to provide me with the much needed guidance (and sometimes pressure). Thank you for being my role model and for helping me grow so much, both as a scientist and as a person.

To Dr. Geoff Butcher for showing me that even though life might be unfair, it is very important not to get discouraged and to keep trusting people around me. A very special thank you for helping me putting this thesis together - I am not sure I would have had the strength to do it without you. Also thank you for your kind English teaching and discussions about Spanish words or Portuguese food - they were always good fun!

Silvia Innocentin thank you for your incredible support through my PhD dark times. I was very fortunate to have you around and I am very thankful for your kind words when I most needed them. Sometimes giving strength to someone else can be as easy as telling them to just keep going. You were one of my rocks!

Marisa Stebegg thank you for all your help in the lab, but mostly thank you for being such a good friend, someone that I know I can always count on (even for port wine tastings in Porto)! I'll miss having you around!

Even though we did not collaborate during my Phd, I need give a very special thank you to Dr. Margarida Saraiva, for making me believe in science and providing me with strong scientific values. This would not be possible without your training and early stage support.

To Dr. Fátima Santos and Dr. Simon Walker, I apologise for having bombarded you both with so many questions and thank you for always providing me answers and pointing me towards the right direction.

Second, this journey would not be possible without the support of my very talented friends. I will thank you all, without any order of preference, because you are all my favourite!

Isak Herman, a big fat thank you for being a great writing companion! We've made it!

Magda Reis, you know you are my person and friend for life! I'm sorry for that. Thank you for the many phone calls and unrequested advice, I really appreciated it, but mostly I needed it! Ana Cardoso, I'm sorry I kept pushing your buttons, mostly by being constantly distracted. As Magda you are stuck with me for life! Thank you both for being there for me, I know I can always count on you to seek for comfort or tough love.

To Ana Lima, for pointing out that some references are not acceptable in a PhD thesis! Thank you for your friendship (mostly, roof and breakfast), my soon to be flatmate! But mostly thank you for listening to my long crying hours and for taking me, a "countryside" girl, to the "city".

To Mário Pereira and Joel Alves, thank you for making sure that during my thesis writing, I was fed and presentable! Thank you for the many advice that I didn't listen to, except maybe my favourite one by Joel: "that's a problem for future Joana"! Mário Pereira thanks for putting up with me on my antisocial and moody days, you were a great flatmate! (only except when you gave me poisoned food!).

José Reis, thanks for connecting people and make sure I've made it to president of CUPortSS! Can't wait to be your flatmate! Remaining members of 'colhão esquerdo' thank you for all the amazing moments we shared together.

Elsa Sousa and Tomás Gomes, thank you for your feedback and writing company! Mostly, thank you for being the best secretary and treasurer I could ask for! It felt really good bossing you around...

Master Marco Mickalski and Jo Mitchelmore thank you for all the hours we spent together at kelsey kerridge, I've learned so much with you both but mostly I had loads of fun! I'll miss our road trips!

To Jack, Azad and Steph, it was a pleasure to work with you both at Biotech YES and SymBLS. I'm sure Jack didn't had much fun, but I think that the rest of us had a blast!

Fiore Cugliandolo and Christina Courreges, you showed up from nowhere when I couldn't be bothered to make new friends! Thanks for your persistence and thank you so much for believing in me the way you do! Christina thank you for the long hours reading my thesis, as I said before I believe that you are tailor-made for science!

To Pedro Albuquerque, for always being young at heart and showing me that there's much more to life than work. Luis Pureza and Luis Figueiredo thank you for everything but mostly for the Saturday Portuguese breakfasts!

I also want to say a very special thank you to all the members of different groups who always welcomed me as one of their one. And the Institute for being my home for the past 4 years, where I've always felt protected and met the most wonderful people.

Thank you to all of my friends from Darwin college, my other Cambridge home, where I've spend many hours complaining, drinking, discussing very weird topics or playing table football. A very special thank you to my former flatmates, Gerry and Giles (also known as Gerry 2.0), I miss our long conversations!

Finally, the biggest thank you of all to the most important people in my life. Mum, dad and Pedro. Thank you for your unconditional love, for believing in me and for always supporting my choices. I wouldn't be here without your help. I personally don't fell very competitive, even so, I do have high expectations for myself because you believe in me

(sometimes a bit too much, it is a tiny bit delusional) and I work really hard to meet those expectations just to please you. I hope you're proud, this one was a tough cookie! There were times that I was so sure I didn't have the strength to keep going but somehow your incredibly support always kept me on the right path! Love you!

There are not enough words to thank you all, I'm incredibly lucky and privileged to have been able to meet amazing people while at Cambridge. I was astonishingly happy here and I'll miss you all.

Acknowledgement of assistance

1) Initial training in techniques and laboratory practice and subsequent mentoring:

Dr. Jörg Stange - Training in parasitology and animal work; mentoring and assessment

Dr. Geoff Butcher - Mentoring

Dr. Simon Walker - Training in microscopy and image analysis

Dr. Marc Veldhoen, Dr. Patrick Varga-Weisz - Mentoring and assessment

2) Data obtained from a technical service provider:

Dr. Silvia Innocentin - Mouse genotyping

3) Data produced jointly:

Dr. Jörg Stange - *E. falciformis* confocal microscopy image acquisition

4) Data/materials provided by someone else:

Dr. Simon Andrews - Bioinformatics analysis of data published by Middendrop *et al.*

Abstract

This thesis reports investigations of the interactions between the intestinal epithelial barrier and the intracellular apicomplexan *Eimeria spp*., both *in vivo* and *in vitro*.

Initially, conventional *in vivo* studies using genetically modified animals were used to investigate the contribution of innate lymphoid cells (ILCs) to immune protection of the intestinal barrier. Additionally, to understand complex epithelial host-pathogen interactions a novel *in vitro* model of small intestine organoids was developed. Data suggest that immunoprotection against *Eimeria vermiformis* infections is mediated by T cells. Furthermore, there is an indication that ILCs have a detrimental effect in *Eimeria vermiformis*-infected immunocompromised animals. However, the role for ILCs in the regulation of the immune response remains unclear.

The life cycles of *Eimeria vermiformis* and *Eimeria falciformis* are highly complex, comprising multiple schizogonies followed by a gametogony. *In vitro* life cycle completion has not been achieved to date due to the limitations of monolayer cell line models. It is likely that for a successful parasite development the interaction of the different epithelial cell types present in intestinal organoids is required.

The development of intestinal organoids by Sato and colleagues gave rise to a breakthrough in cellular studies, providing the tools to study complex interactions between host tissues and invading pathogens *in vitro*. I showed that small intestine-derived organoids grow exponentially after passage and that each organoid contains distinct specialised epithelial cell types, such as Paneth, Goblet or enteroendocrine cells, suggesting that the organoid

model closely resembles the native intestinal epithelium and that *Eimeria spp.* benefit from the three-dimensional structure and physiological characteristics of the organoid model. Intestinal organoids were infected with *E. vermiformis* or *E. falciformis* sporozoites. These completed several rounds of asexual replication, but did not proceed to the final gametogony.

Despite the need for the development of sensitive techniques applicable to three-dimensional cell culture models, these results indicate that intestine-derived organoids are a promising model to study host-parasite interactions at the intestinal epithelial barrier at the cellular and molecular levels.

Table of contents

List of figures

List of tables

List of abbreviations

AMP	Antimicrobial peptide
ATG16L1	Autophagy related 16 like 1 gene
Ag	Antigen
BCEC	Bovine colonical epithelial cells
BFGC	Bovine foetal gastrointestinal cells
BI	Babraham Institute
BMP	Bone morphogenetic protein
BSA	Bovine serum albumin
BSLEC	Bovine spleen lymphatic endothelial cells
BUVEC	Bovine umbilical vein cells
CBC	Columnar base cell
DC	Dendritic cell
DMEM	Dulbecco's Modified Eagle's medium
EDTA	Ethylenediaminetetraacetic acid

EGF	Epidermal growth factor
EtBr	Ethidium bromide
FDA	Fluorescein diacetate
Foxp3	Forkhead box P3
GALT	Gut-associated lymphoid tissue
GATA3	GATA binding protein 3
HIV	Human immunodeficiency virus
IEC	Intestinal epithelial cell
IEL	Intraepithelial Lymphocyte
IESC	Intestinal epithelial stem cell
IFN	Interferon
IL	Interleukin
ILC	Innate lymphoid cell
ILF	Isolated lymphoid follicles
IRGM1	Immunity-related GTPase family M member 1
Il15r	Interleukin-15 receptor
Il2rγ	Interleukin-2 receptor gamma
Il7r	Interleukin-7 receptor
$K_2Cr_2O_7$	Potassium dichromate

LPL	Lamina propria lymphocytes
Lgr5	Leucine-rich repeat-containing G-protein coupled receptor 5
M cell	Microfold cell
MAIT	Mucosal associated invariant T cell
MDBK	Madin-Darby bovine kidney cells
MHCII	Major histocompatibility complex class II
MLN	Mesenteric lymph nodes
NK cell	Natural killer cell
NOD2	Nucleotide binding oligomerization domain containing 2
NaOCL	Sodium hypochlorite
NaOCl	Sodium hypochlorite
P/S	Penicillin/Streptomycin
PBS	Phosphate buffered saline
PBS	Phosphate-buffered saline
PCK	Primary chicken kidney cells
PCR	Polymerase chain reaction
PRR	Pattern recognition receptor
RATEC	Rat epithelial-like cells
REGIIIγ	Regenerating islet-derived protein IIIγ

RELMβ	Resistin-like molecule-β
RIMS	Refractive index matching solution
RORγ	RAR-related orphan receptor gamma
RT-PCR	Real-time PCR
SILT	Solitary isolated lymphoid tissues
STAT	Signal transducer and activator of transcription
TA cell	Transient-amplifying cell
TCF4	Transcription factor 4
TCR	T cell receptor
TFF3	Trefoil factor 3
TNF	Tumor necrosis factor
Th	T helper cell
Treg	Regulatory T cell
iNKT	Invariant natural killer T cell

Chapter 1

Introduction

1.1 Anatomy and physiology of the intestine

The intestine is host to a larger number of immune cells than any other organ in the body. Given its regional organisation and continuous exposure to a large spectrum of antigens and potential immune stimuli, the intestine mounts diverse immune responses, which differ amongst other factors, according to the anatomical site of infection.

Typically divided into small and large intestines, the intestine is lined by a barrier of intestinal epithelial cells (IECs) and it extends from the outlet of the stomach to the beginning of the anus. The small intestine is divided into 3 segments: duodenum, jejunum and ileum. The large intestine comprises the caecum, ascending (proximal) colon, transverse colon, descending (distal) colon and rectum. The small intestine is organised into villi, finger-like projections that extend into the lumen to increase epithelium surface area; and crypts of Lieberkühn, invaginations that comprise the intestinal stem cell niche, responsible for the continuous intestinal self-renewal.

The intestinal immune system must adapt to the constantly changing environment driven by the nature of lumen contents. To a great extent, immune responses take place in the mucosa that is organised into epithelium, underlying lamina propria and muscularis mucosa.

Under the mucosa lies an area of connective tissue, known as the submucosa, important due to its plexus of parasympathetic nerves. Under the submucosa extends a layer of muscle tissue, and finally the serosa, which grants a thick fibrous layer that separates the intestine from the peritoneal cavity.

The different anatomical regions of the intestine provide the organ with the tools to fulfil different physiological functions. Absorptive epithelial cells of the small intestine have their apical side covered in microvilli, cell membrane protrusions that increase their surface area and are involved in the digestion of dietary components and the transport of nutrients. The large intestine lacks villi and microvilli; however, it also has little nutrient absorptive function compared to the small intestine, being its main role the absorption of water and the removal of undigested food. Furthermore, it is the main reservoir of microbiota, essential for the homeostatic regulation of the intestine.

1.2 The intestinal epithelial barrier

The intestinal epithelial barrier consists of a single-cell layer of intestinal epithelial cells (IECs) that protects the host against the external environment. By being selectively permeable, the barrier allows nutrient and water absorption while maintaining an efficient defence against enteric microorganisms [1]. The intestinal epithelium is highly dynamic and the IECs are renewed every 4 to 7 days [2, 3]. The continual turnover creates the opportunity for breaches in the epithelial barrier. However, this process is accompanied by a redistribution of the apical junction complex, which is responsible for the formation of an intercellular barrier between the lateral cell membranes, thus helping to strengthen the barrier function [4].

The maintenance of homeostasis at the intestinal barrier is reliant on the physical and biochemical properties of the mucus layer, which separate the microbiota from the epithelial layer [5]. Without the mucus layer, the microbiota would get in direct contact with IECs, leading to spontaneous development of colitis and an increased susceptibility to intestinal carcinomas [6, 7].

IECs also exert an important immunoregulatory role which takes advantage of their ability to sense and respond to microbial stimuli [1]. Compromised intestinal barrier function and consequent bacterial translocation leads to an increased risk of developing inflammatory bowel disease [8]. Furthermore, loss of the intestinal barrier function is also associated with the systemic immune activation, which can contribute to the progression of chronic infections, such as HIV and hepatitis virus, as well as metabolic disease [9–11]. Additionally, innate immunity and intestinal microbiota interactions can also contribute to autoimmune and inflammatory diseases, including type 1 diabetes, rheumatoid arthritis and multiple sclerosis [12–14].

A thorough understating of the immunoregulatory roles of IECs stemming from their location and function at the intestinal barrier could be crucial for the development of new targeted strategies to treat inflammation, infection or metabolic diseases.

1.2.1 IEC regulation of barrier function

The intestinal epithelium is composed of various cell types, such as: $Lgr5^+$ (leucine-rich-repeat-containing G-protein-coupled receptor 5, previously called Gpr49) stem cells, absorptive enterocytes, mucus-secreting goblet cells, antimicrobial peptide-secreting Paneth cells and hormone-secreting enteroendocrine cells [15, 16]. It is continually renewed by multipotent $Lgr5^+$ intestinal epithelial stem cells (IESCs), which reside at the base of the crypts, as part of the stem cell niche. The intestinal stem cell niche promotes the proliferation of epithelial cell progenitors, giving rise to the various specialised IEC lineages [3].

Enteroendocrine cells

Enteroendocrine cells are secretory IECs which specialise in the epithelium barrier function by bridging the central and enteric nervous systems through hormone regulators, such as chromogranin A [17].

Goblet cells

The first line of defence against microbial invasion is provided by the physical and biochemical protection of the epithelium barrier, which is established through the secretion of mucins and AMPs by goblet cells and Paneth cells, respectively [1]. Mucin secretion by goblet cells lubricates the luminal surface and it has been shown to be essential in the organisation of the intestinal mucus layer. The absolute number of goblet cells increases along the intestinal tract, being found in highest numbers in the distal colon. Therefore, a thick mucus coating can be found in the colon - the glycocalyx - that is formed by two different layers: a dense inner layer attached to the epithelial surface and a loose outer layer, that resembles the one in the small intestine and in which bacteria can be found (Figure 1.1) [5]. The main function of the mucus layer is to trap bacterial flora before they attach to the epithelial cells. Mucus production is regulated by immune mediators like leukotrienes, interferon (IFN)-γ,

interleukin (IL)-9 and IL-13 [18, 19]. Defects in mucus synthesis has been shown to increase the predisposition for the development of both spontaneous colitis and inflammation-induced colorectal cancers [5–7].

Furthermore, production of trefoil factor 3 (TFF3) and resistin-like molecule-β (RELMβ) by goblet cells also contributes to the regulation of the barrier function and its integrity [20, 21].

Paneth cells

Regulation of both commensal and pathogenic bacteria is further strengthened by enterocytes secreting AMPs into the mucus barrier, such as the C-type lectin regenerating islet-derived protein IIIγ (REGIIIγ) [22]. Paneth cells can only be found in the small intestine and are particularly abundant in the ileum. In response to IL-22 or pattern-recognition receptor (PRR) triggering, Paneth cells secret AMPs including defensins, cathelicidins and lysozyme [1, 23]. Interactions between AMPs and mucins are often observed. Their combined function is responsible for a reinforced control of the antimicrobial activity, preventing IEC from bacterial attachment and invasion (Figure 1.1) [24].

In contrast to the other epithelial cells, Paneth cells are long-lived and, after differentiation, they migrate downward towards the bottom of the crypt, residing next to the stem cells. Apart from their antibacterial role, Paneth cells are crucial for the maintenance of stem cell function, through production of pro-EGF, Wnt3 and Notch ligands [25–27]. Furthermore, it has been shown that susceptibility to chronic intestinal inflammation can be increased in response to deregulation of Paneth cell function. Crohn's disease-associated genes, including ATG16-like 1 (ATG16L1), transcription factor 4 (TCF4), NOD2 and immunity-related GTPase family M protein 1 (IRGM1) are expressed by Paneth cells [28]. Ablation of expression of these genes has been shown to be associated with functional defects in Paneth cells, which

consequently increase the susceptibility of mice to microbiota-dependent, spontaneous or experimentally-induced intestinal inflammation [29–33].

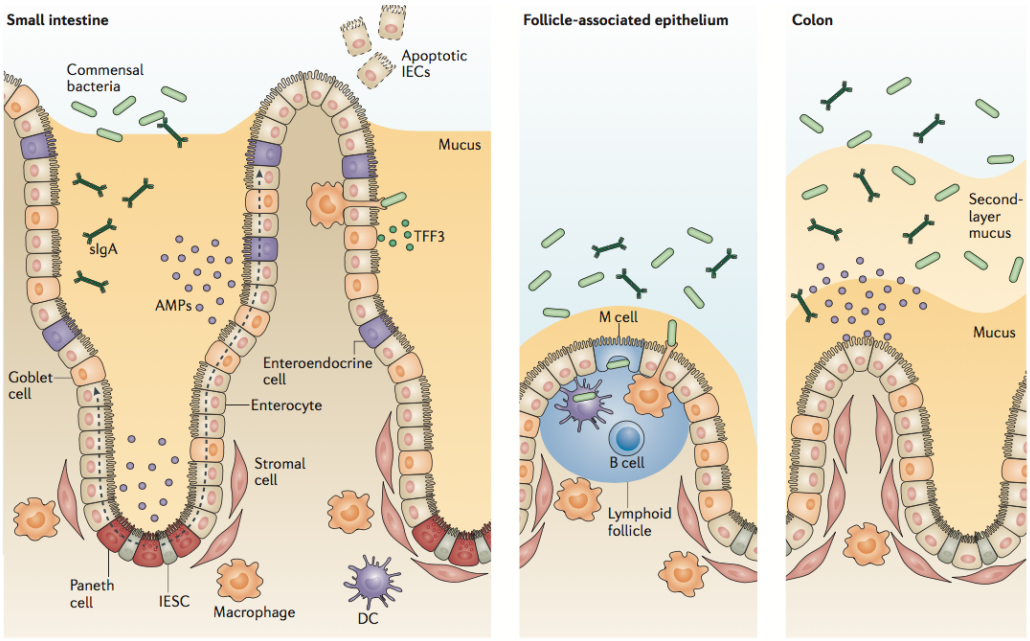

Fig. 1.1 The intestinal epithelial barrier

IECs secure the intestinal biochemical and physical barrier which limits the immune reactivity to luminal contents. The stem cell niche, located at the bottom of the intestinal crypt, is responsible for the continual renewal of IECs. With exception of Paneth cells that migrate to the bottom of the crypt, differentiated IEcs migrate along the crypt-villus axis (dashed arrows). Paneth cells and goblet cells secrete mucus and AMPs into the intestinal lumen, which, in addition to secretion of secretory IgA (sIgA), restrict the contact between the lumen microbiota and the intestinal epithelium. Production of trefoil factor 3 (TTF3) by goblet cells further regulates the function and integrity of the epithelial barrier. M cells, found in lymphoid follicles, mediate the transport of luminal antigens and bacteria across the intestinal epithelial barrier to dendritic cells (DCs) and intestinal macrophages. *From Peterson and Artis, 2014 [1]*

Collectively, the accumulated evidence shows that IECs are crucial for host protection from its continuous exposure to potentially inflammatory bacteria present in the microbiota. Nevertheless, analysis is required to further understand how interactions with the intestinal lumen contents shape IEC response regulation.

1.2.2 Stem cell niche

Intestinal self-renewal is driven by multipotent stem cells that reside at the base of the intestinal crypts. Stem cells give rise to transient-amplifying (TA) daughter cells, which also reside at the intestinal crypt, and move upwards along the flank of the villi where they differentiate into absorptive enterocytes, secretory cells or M cells.

Intestinal stem cells, known as crypt base columnar (CBC) cells, were first described by Cheng and Leblond, in 1974 [34]. CBC cells were shown to reside at the crypt bottom, intercalated with post-mitotic Paneth cells [34]. Baker and colleagues, using genetic lineage tracing, further described a CBC cell marker, known as Lgr5 [35]. Hereafter, I will refer to these cells as Lgr5-CBC cells.

$Lgr5^+$ cells are cycling and long-lived whereas their progeny of epithelial differentiated cells are renewed every 3 to 5 days. Also, a second quiescent stem cell type has been identified that resides at position 4 of the crypt, directly above Paneth cells, known as "+4 cells" [3]. These cells can be identified by several markers, including Bmi-1, Hopx, mTert and Lrig1 [36–39]. An additional an quiescent secretory precursor has also been identified that co-expresses both Lgr5 and the +4 cell markers. These are located close to the crypt bottom and undergo terminal differentiation within weeks. Interestingly, after tissue damage, these cells are able to revert into a cycling $Lgr5^+$ stem cell and differentiate into clones comprising the main epithelial cell types [40].

Lgr5-CBC cells divide symmetrically, and each daughter cell stochastically develops into a stem cell or a TA cell, depending on the availability of niche space [41, 2]. Intestinal homeostasis and Lgr5-CBC cell division are controlled by four well-defined signalling pathways: Wnt, Notch, EGF and BMP.

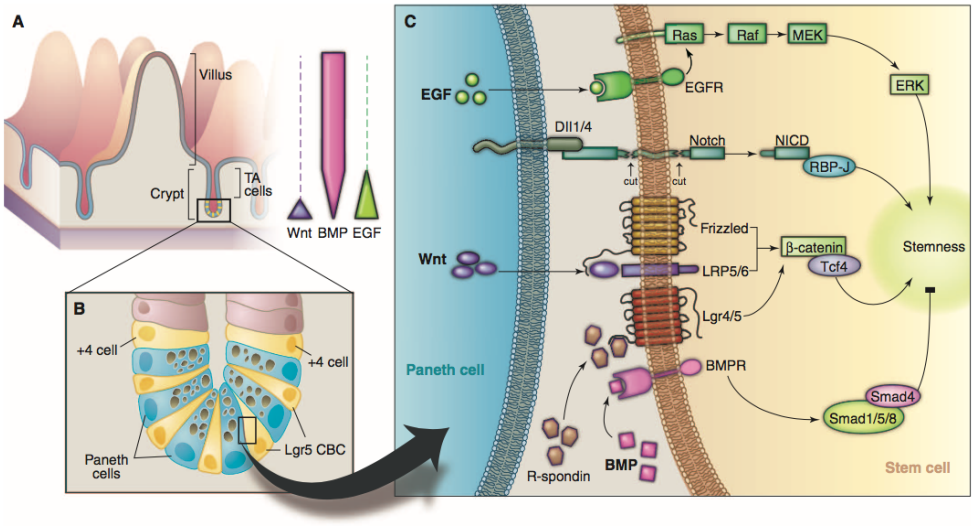

Fig. 1.2 Stem cell niche

(A) Schematic representation of the intestinal epithelial structure and location of stem cells. Gradients of Wnt, BMP, and EGF signals are formed along the crypt-villi axis. (B) Representation of the stem cell niche. Lgr5-CBC cells are in close proximity to Paneth cells, from which they receive signals for their stem cell function. (C) EGF, Notch, and Wnt signals are essential for maintenance of the Lgr5-CBC stem cell profile, whereas BMP negatively regulates stemness. R-spondin– Lgr4/5 signalling is required for Wnt activation. The source of R-spondin is unknown. *From Sato et al. 2013 [42]*

Wnt signalling

Wnt signalling is a key pathway in the regulation of small intestine stem cell fate which drives Lgr5-CBC and TA cell proliferation [43]. Wnt is also part of a signalling loop that drives terminal differentiation of Paneth cells [44]. As Paneth cells provide signals for Lgr5-CBC cell proliferation, this suggests that stem cell division is a self-sustained and tightly controlled mechanism [44].

Wnt factors trigger Frizzled-Lrp5/6 co-receptor signalling that drives β-catenin stabilisation, the latter in turn binding and activating the transcription factor Tcf4. Consequently, a "stemness" genetic programme gets activated (Figure 1.2) [45].

Notch signalling

Notch signalling is also indispensable for the maintenance of the Lgr5-CBC undifferentiated state. Blocking of Notch signalling leads to differentiation of the Lgr5-CBC and TA cells [46]. Notch signalling in Lgr5-CBC is activated by $Dll1^+$/$Dll4^+$ Paneth cells, thus maintaining intestinal progenitors and stem cells (Figure 1.2) [47]. Once daughter cells lose contact with $Dll1^+$/$Dll4^+$ Paneth cells, Notch signalling is downregulated whereas Dll1 signalling is upregulated, thus promoting their secretory differentiation [48]. Secretory precursors present Dll1 to neighbouring $Notch^+$ TA cells, promoting their development towards the enterocyte lineage. Thus, the blocking of Notch signalling controls the enterocyte-secretory switch.

EGF signalling

Mitogenic effects are mediated by epidermal growth factor (EGF), which is produced by Paneth cells. After engagement of EGF receptors, Lgr5-CBC and TA cells Ras/Raf/Mek/Erk signalling axis is triggered (Figure 1.2) [49].

BMP signalling

Bone morphogenic protein (BMP) signals are triggered in the villi. Noggin inhibition of BMP signalling leads to the formation of crypt-like structures along the villi, suggesting that BMP signalling represses *de novo* crypt formation [50]. Activation of BMP receptors leads to the formation of Smad1/5/8 and Smad4 complexes that repress stemness genes (Figure 1.2) [51].

Interactions between Lgr5-CBC cells and Paneth cells

Lgr5-CBC cells and Paneth cells are in close proximity at the bottom of the intestinal crypt (Figure 1.2). Besides the ability to secrete AMPs, Paneth cells also secret EGF and Wnt3. Furthermore, they also expresse the Dll1 and Dll4 ligands on their cell surfaces. Thus, Paneth

cell ablation leads to disruption of the intestinal stem cell niche, due to a concomitant loss of Lgr5-CBC cells [26, 27]. However, it has been observed that in *Math1* mice mutants, Paneth cells are depleted but Lgr5-CBC cells are retained, suggesting that Paneth cells are dispensable for the Lgr5-CBC cell function [52]. It has been shown that *Math1*-deficient crypts prevent Lgr5-CBC stem cell exhaustion in the absence of Paneth cell-derived Wnts, by preventing their dependence on Notch ligands [53]. Additionally, it has been noted that *Math1*-mutant crypts do not grow *in vitro*, providing an indication that Paneth cell signalling dependence is not restrict to Notch signals but might also include Wnt3. The authors of this study further showed that $Wnt3^{-/-}$ crypts were capable of growing *in vivo*, but failed to grow *in vitro* [25]. This suggested that Paneth cells provide Lgr5-CBC cells Notch ligands but are also a Wnt3 source, even though Wnt3 can also be produced by the surrounding mesenchyme *in vivo* [25].

1.3 Lymphoid structures in the intestine

Priming of adaptive immune responses in the intestine occurs mainly at the gut-associated lymphoid tissue (GALT) and draining lymph nodes. The GALT is formed by mucosal and submucosal lymphoid aggregates and is characterised by an overlying follicle-associated epithelium that contains microfold cells (M cells) (Figure 1.1). M cells are specialised in the immunosurveillance and transport of antigens from the lumen to immune cells, thus triggering immune responses or tolerance [54].

Peyer's patches are one of the best characterised tissues of the GALT, which can be found particularly concentrated in the distal ileum. They consist of isolated or aggregated B cell lymphoid follicles, flanked by smaller T cell areas. Peyer's patches major role consist in antigen (Ag) uptake and the development of mucosal secretory IgA (S-IgA) antibody responses [55].

Solitary isolated lymphoid tissues (SILTs) are smaller lymphoid aggregates that can also be found in the GALT, and can range in size from small cryptopatches to mature isolated lymphoid follicles (ILFs). SILTs display germinal centres that comprise B cells, suggesting ongoing humoral immune activation [56].

Mesenteric lymph nodes (MLN) comprise separate nodes that drain separate segments of the intestine. Given the different food and microbial differences along the intestinal lumen, MLN may display specialised immunological characteristics through the different sections of the intestine [57].

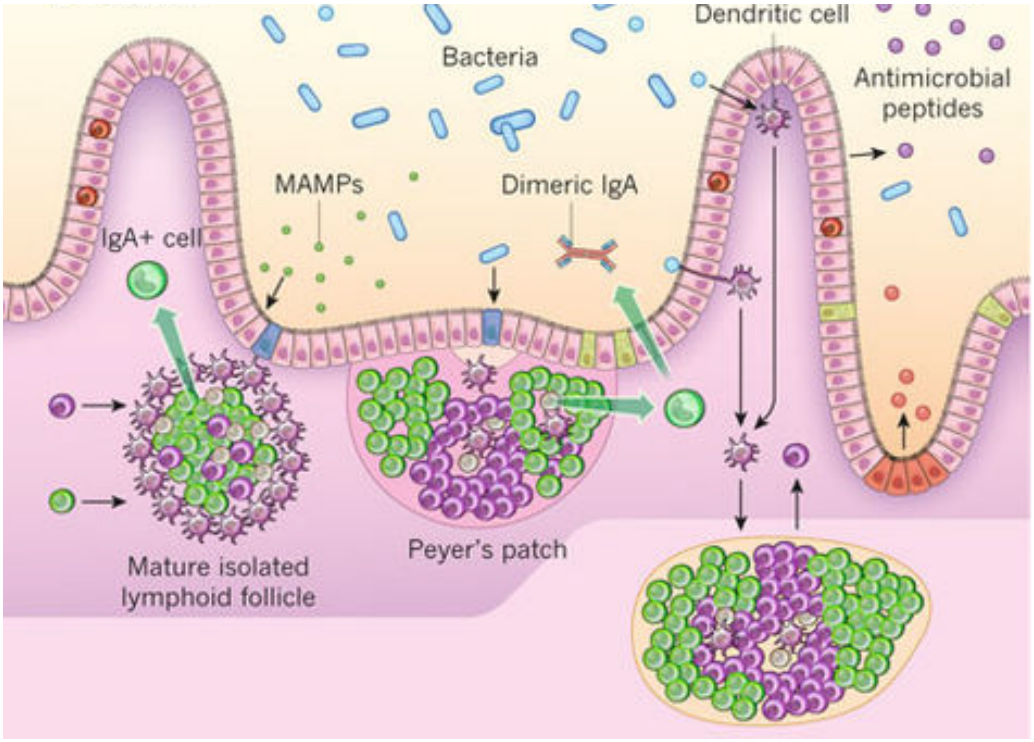

Fig. 1.3 Intestinal lymphoid structures

Intestinal epithelial cells (IECs), together with dendritic cells (DCs), express pattern-recognition receptors (PRRs), responsible for the local sensing of microbe-associated lymphoid patterns (MAMPs). After being triggered, these cells further stimulate the recruitment of T and B cells from adjacent cryptopatches, which in turn develop into mature isolated lymphoid follicles that release IgA-producing plasma cells into the lamina propria. Additionally, microbes can be transported by M cells through the epithelial barrier into Peyer's patches, where they are endocytosed by DCs in the subepithelial dome, leading to the induction of T-cell differentiation and T-cell-dependent B-cell maturation in the germinal centre. This leads to the development of IgA-producing plasma cells. MAMPs also stimulate IECs in the crypt, leading to an increase density of Paneth cells in the small intestine and the release of antimicrobial peptides. *From Maynard et al. 2012 [58]*

1.4 Lymphocyte distribution in the intestine

Given the constant stimulation from microbiota and food, the lamina propria and epithelium are major effector sites of the intestinal immune system. Lamina propria comprises B cells, T cells and various other immune cells, including dendritic cells (DCs), macrophages, eosinophils and mast cells. In this section, I shall address the distribution and function of the different lymphocytes subsets and their variation along the intestine. For more detail please refer to table 1.1.

Table 1.1 Lymphocyte distribution in the intestine

Intestinal site	Cell type	Function
Surface epithelium	Enterocytes (MHC II^+)	Antigen presentation and T cell stimulation
	IELs	Cytolitic activity
	M cells	Antigen transport
Peyer's patches	T cells (mainly $CD4^+T_H$)	Provide help to plasma cells and effector memory to $CD8^+$ memory T cells
	B cells	Generation of memory B cells and IgA-producing plasma cells
Lamina propria	Plasma cells	IgA secretion
	B cells	IgM secretion
	T cells	provide helper function for B cell Ig synthesis

1.4.1 Intraepithelial lymphocytes

Intraepithelial lymphocytes (IELs) are tissue-resident T cells that are in direct contact with IECs where they contribute to maintaining immune homeostasis at the intestinal immune barrier [59]. IELs represent the first line of defence against invading pathogens, as they are in direct contact with intestinal lumen antigens. IELs are almost exclusively T cells and develop from either a TCR$\gamma\delta$ or TCR$\alpha\beta$ lineage. Intestinal IELs comprise up to 60% TCR$\gamma\delta$ cells [60, 61]. Furthermore, intestinal IELs frequently express CD44 and CD69,

suggesting that they are antigen-experienced [62–64]. IELs have also been shown to have cytotoxic properties through the expression of effector cytokines including IFN-γ, IL-2, IL-4 and IL-17 [65–68].

Most TCR$\alpha\beta$ IELs express a homodimer of CD8$\alpha\alpha$, yet dimers can be formed, such as CD4$\alpha\beta$ or CD8$\alpha\beta$ [69]. Based both on the mechanism of activation and antigen recognition, IELs can be classified into two major subsets: 'natural' IELs and 'induced' IELs. Natural IELs develop an activated phenotype during thymus development through contact with self antigens. Conversely, induced IELs arise from conventional $CD4^+$ or CD8$\alpha\beta^+$ TCR$\alpha\beta^+$ T cells that are activated post-thymically, after encounter with peripheral antigens [70].

Due to their location within the intestinal epithelium, the immune protection provided by IELs is crucial for the control of invasion and spreading of pathogens. Thus, a stable equilibrium in IELs immune response to microbial and food components present in the lumen is required in order to keep a homeostatic intestinal environment. Deregulation of IEL function can lead to non-specific or exacerbated immune responses, which consequently can jeopardise the integrity of the intestinal barrier and induce immunopathology. Furthermore, it may also contribute to an increased susceptibility to intestinal inflammation or cancer [62].

1.4.2 Lamina propria T cells

Both $CD4^+$ T cells and $CD8^+$ T cells can be found in the intestinal lamina propria and are thought to originate from secondary lymphoid organs. In the secondary lymphoid tissue, they recirculate through the body before settling into the intestine. They display an effector memory phenotype and mount rapid responses to infection. Lamina propria $CD4^+$ T cells are greatly diverse, consisting of T_H1, T_H2 and T_H17 subsets. Additionally, regulatory T (T_{Reg}) cells, either forkhead box P3 $(FOXP3)^+$ or $FOXP3^-$ can be found in the lamina propria of the intestine, being particularly abundant in the colon [71].

1.4.3 Innate lymphoid cells

Innate lymphoid cells (ILCs) are important regulators of the intestinal epithelial barrier. They have been shown to have an important role in resistance to invading pathogens, regulation of autoimmunity, tissue remodelling, cancer and metabolic homeostasis [72]. ILCs are typically classified into three distinct groups based on their production of T_H cell-associated cytokines. Thus, group 1 comprises IFN-γ-producing ILCs, including NK cells and ILC1 cells. Group 2 comprises IL-5- and IL-13-producing ILCs, which are dependent on GATA-binding protein 3 (GATA3) and retinoic acid receptor-related orphan receptor-α (RORα) for their development. Group 3 comprises IL-17- and/or IL-22-producing ILCs that are dependent on the transcription factor RORγt for their development [73]. These include LTi cells, NCR^+ ILC3 and NCR^- ILC3 cells. ILC development is dependent on the common cytokine receptor γ-chain. While NK cell development requires IL-15 signalling, the remaining ILCs are dependent on IL-7 signalling [74, 75].

Numbers of ILC1s and ILC2s in the human intestine are very low, ILC3s being the largest ILC population in the intestine, notably NCR^+ILC3 and NCR^+ILC3 [76–78]. ILC3s have been shown to be important producers of IL-22 in the intestinal mucosa and may be involved in epithelium replenishing and repair, both in steady-state conditions and in response to infections [79–81]. As referred to above, ILCs are able to produce effector cytokines in response to infection. Additionally, it has been shown that in response to infection, ILC3s can express MHC II molecules, thus contributing to the intestinal immune regulation through suppression of T_H17 responses [82].

ILCs were shown to induce protective responses against intracellular pathogens, including parasites such as *Toxoplasma gondii* [83–85]. Conversely, ILCs were also shown to be associated with the pathophysiology of intestine inflammatory diseases [86–88]. Taken together, these studies show that ILCs can be crucial for protective immunity, but unbalanced ILC activation can have a pathogenic role in inflammatory diseases.

1.4.4 Intestinal B cells

The intestinal lamina propria consists of high numbers of predominantly secretory IgA- and IgG-producing plasma cells, thus contributing to the provision of a first-line of defence against invading pathogens [89]. These immunoglobulins have shown different roles in the intestinal immunoprotection. In particular IgA was shown to confer protection through a non-inflammatory response, whereas IgG triggers a pro-inflammatory response against invading pathogens [90, 91].

1.4.5 Invariant T cells

Mucosa-associated invariant T (MAIT) cells contains T cells with an invariant TCRα form that exert an innate and effector function [92]. In response to small organic molecules, presented by bacteria or fungi, MAIT cells are capable of producing pro-inflammatory cytokines, including IFN-γ and tumor necrosis factor (TNF), and exerting a cytolytic activity [93–95]. Furthermore, it has been shown that besides the ability to provide a first-line of defence against invading pathogens, MAIT cells also contribute to the enhancement of adaptive immune responses [93].

Intestinal invariant natural killer T (iNKT) cells also express an invariant TCRα-chain and have an important role in early stages of defence against invading pathogens [96]. In response to intestinal infections, iNKT cells produce IFN-γ, thus having an important contribution limiting bacterial spread [97–99].

1.5 Small Intestine Organoids

In 2009, Sato and colleagues established the first long-term culture for primary adult intestine tissue. The three-dimensional culture could be maintained and expanded for more than a year, without introducing genetic transformations [16]. The small intestine organoid culture was established from a single Lgr5-CBC cell or isolated intestinal crypts cultured in matrigel and supplemented with a cocktail of R-spondin 1, EGF and Noggin. Matrigel, a three-dimensional laminin- and collagen-rich matrix that resembles the basal lamina,was required for the support of the organoid structure [16]. R-spondin 1 is a ligand of Lgr5 and was shown to increase the Wnt signal strength triggered by the Wnt and Frizzled/Lrp interaction [100, 101].

The only source of Wnt in the small intestine organoid is the Paneth cells, which induce sharp Wnt gradients that surround the intestinal crypt [42]. The Wnt gradient also provides TA cells with the necessary signalling cues for terminal differentiation along the villus flanks, with Notch lateral inhibition triggering the enterocyte-secretory fate switch.

Furthermore, it has been shown that if Wnt is homogeneously distributed across the organoid, the crypt-villi architecture is lost and organoids become symmetric cysts comprising an homogeneous population of stem and progenitor cells [26]. Additionally, Wnt production by Paneth cells also controls Paneth cell differentiation, through a positive feedback loop and, consequently, the number of stem cells and crypt expansion [25, 102]. Stem cell proliferation is also regulated by the strength of EGF signalling [103]. Taken together, this shows that, like their *in vivo* counterparts, small intestine organoids are tightly regulated by the interaction between the different IECs present in the model.

Architecture of the small intestine organoid

Mouse or human crypts can be isolated in conditions involving EDTA-based Ca^{2+}/Mg^{2+} chelation. Once they are seeded under the conditions described above they start growing

into cysts with a central lumen and polarised epithelium. Multiple crypt-like structures, commonly denominated as buds, project outwards. The basal side of the epithelium is oriented towards the outside in contact with the matrigel, whereas enterocyte microvilli project into the lumen. Paneth and goblet cells secrete into the organoid lumen [16]. Small intestine organoid self-renewal kinetics and cell-type composition closely resemble their *in vivo* counterparts. Paneth cells, goblet cells and enteroendocrine cells were shown to be present in the small intestine organoid culture and terminally differentiated cells were shown to exfoliate into the organoid lumen [16].

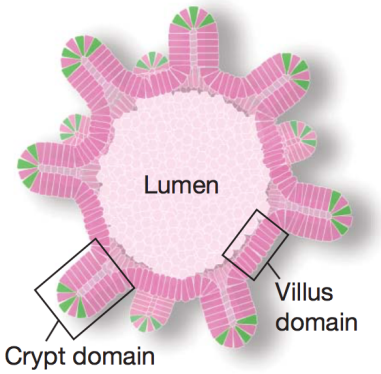

Fig. 1.4 Schematic representation of a small intestine organoid

Small intestine organoids comprise a central lumen lined by villus-like epithelium with multiple crypt-like domains projecting outwards. *From Sato et al., 2009 [16].*

Interestingly, it has been shown that engrafted epithelial organoids can regenerate epithelial lesions and are indiscernible from surrounding recipient epithelium [104]. These results demonstrated that organoids are transplantable and a promising tool for the development of new regenerative and gene-therapy strategies [104].

1.6 The intestinal Apicomplexan *Eimeria spp.* parasites

Eimeria spp. are intracellular protozoan parasites specifically adapted to infect and develop almost exclusively in the intestinal epithelium. *Eimeria spp.* are the most common causative agents of coccidiosis, highly prevalent among domesticated animal species, and accounting for more than US$3 billion annual costs worldwide in the poultry industry [105, 106]. As Apicomplexan parasites, *Eimeria spp.* belongs to the phylum that contains major human pathogens, as *Toxoplasma gondii*, *Plasmodium falciparum* and *Cryptosporidium parvum*, as well as other parasites of economic relevance to animal husbandry, such as species of *Sarcocystis*, *Leucocytozoon* and *Haemoproteus* [107, 108].

1.6.1 The life cycle of *Eimeria spp.*

The monoxenous life cycle of *Eimeria spp.* comprises exogenous and endogenous phases. During the exogenous phase, unsporulated multi-layered oocysts are shed into the environment (Figure 1.5H). At appropriate temperatures and humidities the oocysts undergo meiosis and mitosis forming 4 sporocysts that harbour 2 sporozoites each (Figure 1.5A) [109]. The endogenous phase occurs after host oral uptake of sporulated oocysts. The oocyst wall is most likely to get digested by the influence of pepsin during stomach passage and sporocysts get released into the intestinal lumen [110, 111]. Sporozoites actively excyst from the sporocyst, through mechanical abrasion followed by enzymatic digestion of the sporocyst wall (Figure 1.5B). Motile sporozoites migrate to the preferred site of development, the colon and caecum in the case of *E. falciformis* or the distal small intestine in the case of *E. vermiformis*, respectively. Once motile sporozoites invade IECs (Figure 1.5C), several rounds of schizogony take place, typically 3-4 rounds of asexual replication (Figures 1.5C and 1.5D), which are followed by sexual differentiation of gametes, known as gametogony (Figures 1.5E and 1.5F). The unsporulated oocyst results from fertilisation of macro- and microgametes, and this is then shed in the faeces (Figure 1.5G).

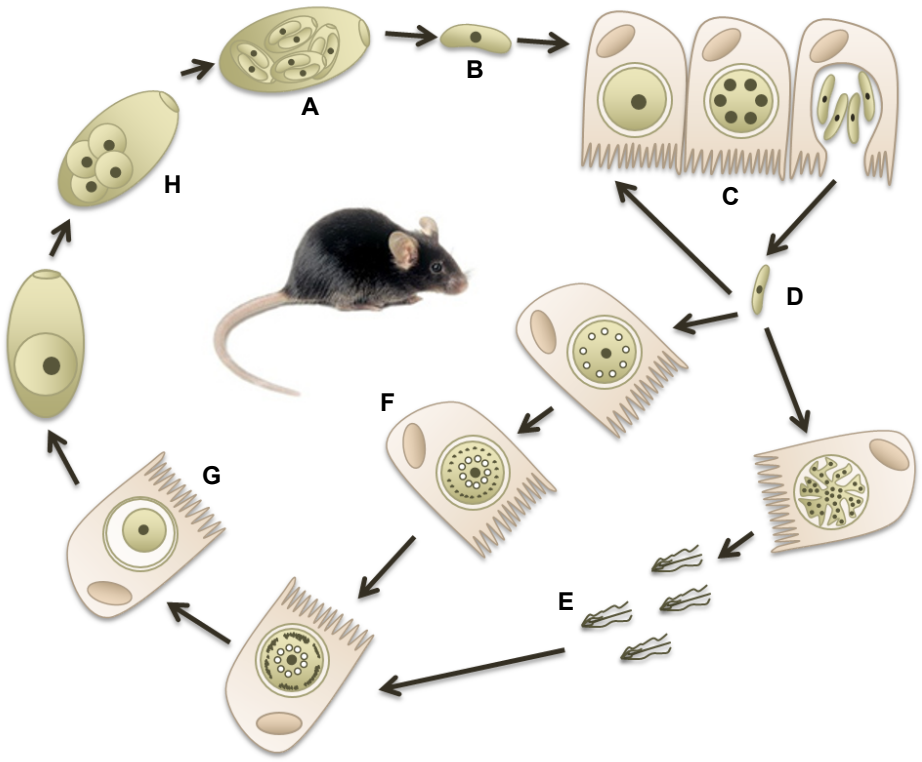

Fig. 1.5 *Eimeria spp.* life cycle

Sporulated oocysts (A) harbour sporocysts containing motile sporozoites (B) that undergo several rounds of schizogony (C) in intestinal epithelial cells. Merozoites (D) develop into micro- (E) and macrogametes (F) that fuse to form the zygote (G), which eventually develops into an unsporulated oocyst (H) that gets shed with the faeces and sporulates in the environment.

1.6.2 *Eimeria spp.* invasion of host epithelial cells

Invasion of host cells by apicomplexan parasites, such as *Eimeria spp.* is an active process that relies on actin-based motility.

Host cell attachment is mediated by a set of organelles that form the apical complex, such as rhoptries and micronemes, which sequentially secrete proteins - RON and AMA1/MIC, respectively - necessary for the formation of the moving junction (Figure 1.6) [112, 113]. The moving junction is both responsible for the invagination of the parasite as well as the simultaneous generation of the parasitophorous vacuole, which originates through the invagination of the host plasma membrane (Figure 1.6) [114]. In addition to the protection

that the parasitophorous vacuole membrane confers to the parasites, it also prevents the acidification of the intracellular environment environment [115].

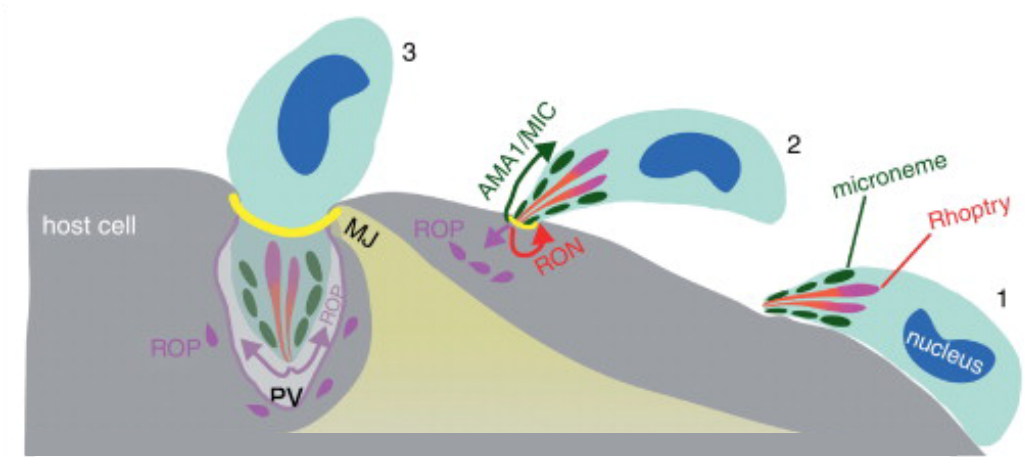

Fig. 1.6 *Eimeria spp.* invasion process of host cells

(1) Before invasion, the sporozoite loosely attaches to the target host cell. **(2)** Intimate association between the parasite and the host cell is mediated by protein secreted from the micronemes, such as AMA1 and MIC2. Proteins secreted from micronemes and the rhoptry neck, such as AMA1 and RON, respectively, lead to the formation of the moving junction and consequently the parasite invasion is initiated. **(3)** Simultaneously, vesicular clusters derived from contents of rhoptries (ROP) are secreted into the host cell. Te parasite moves into the parasitophorous vacuole through the moving junction. *From Shen and Sibley 2012 [116]*

In order to penetrate the host cell, the parasite constricts its body through the moving junction (Figure 1.6[3]). This process is mediated by either forces induced by the host cell or by forces induced by the parasite by activation of its actin/myosin motors that mediate invasion at the entry site [117].

The invasion process, exclusively mediated by the parasite, is a fundamental strategy for immune evasion. Some of the proteins involved in the *Eimeria spp.* invasion mechanism have been characterised [118, 114]. For example, a comparative proteomic analysis has shown the presence and dynamics of proteins involved in the *E. tenella* invasion process, including microneme and rhoptry [119, 120].

1.6.3 Pathology of *Eimeria spp.* infections

Eimeria infection can cause coccidiosis, a disease of the intestinal tract, usually self-limiting with spontaneous resolution typically occurring within a few weeks, unless reinfection occurs [121]. Depending on the dose of infection and the pathogenicity of the *Eimeria spp.* involved, animals can develop mild to severe pathologies. Infections with *E. falciformis* or *E. vermiformis* can cause epithelium necrotisation and bloody diarrhea, which typically results in dehydration and rapid weight loss [122] The symptoms and enteric lesions are most pronounced from day 8 to 10 post-infection, corresponding to the peak days of oocyst shedding [122].

Histopathological analysis of *E. falciformis*- or *E. vermiformis*-infected intestines has revealed destruction of the epithelium, submucosal edema and influx of neutrophils and mononuclear cells to the site of infection [123, 122]. Even though eimerian asexual replication and merozoite cell invasion may induce the destruction of the intestinal epithelium, it is likely that intestinal pathology is caused by the inflammatory immune response [122]. For example, TNF-α production was show to correlate with aggravated immunopathology in infection with *E. vermiformis* or *E. nieschulzi* [124, 125]. IFN-γ depletion was shown to result in exacerbated clinical effects, suggesting an immunoregulatory role for this cytokine [126]. Epithelium-resident immune cells can also impact pathology development during *Eimeria spp.* infections. It has been reported that during *E. vermiformis* infection, $\gamma\delta$ T cells sense exacerbated intestinal damage due to a failure in the regulation of $\alpha\beta$ T cell responses [127]. Furthermore, it has been shown that in *E. vermiformis*-infected animals, IELs help sustain the epithelial barrier function through the expression of junctional molecules [124].

IELs, producers of IFN-γ ad TGF-β, are increased during infection and have been shown to play an important role in the protection of the epithelium, through cytokine production or via direct contact with the epithelial barrier [124].

Information on the mechanisms that regulate protection and maintenance of the intestinal epithelial barrier against *E. vermiformis* infections is still very limited. What is known so far, has been reported based on *in vivo* descriptive animal models. Therefore, there is limited knowledge on the molecular mechanisms involving IEC activation in the context of *Eimeria spp.* infection.

1.6.4 Host immune response against *E. vermiformis*

Eimeria spp. infections are typically accompanied by a strong humoral and cellular immune response, essential for the control of primary infection and development of immunity against challenge infections. In this section I will focus on the immune response against *E. vermiformis*, which is known to infect specifically the distal small intestine.

E. vermiformis oocysts was first described by Ernst,Chobotar and Hammond in 1971 [128]. This description was followed by the reports from the same group and Todd and Lepp for the description of *E.vermiformis* life cycle [129–131]. One of the first descriptions of how distinct mouse strains were differently susceptible to *E. vermiformis* was published by Rose and colleagues in which was shown that athymic mice were highly susceptible to primary infections and remained susceptible to reinfection [132]. This is if relevance since a single *E. vermiformis* infection can lead to sterile immunity against secondary infections [126]. The primary *E. vermiformis* infection is typically characterised by a IFNγ-induced $CD4^+$ T_H1 cell immune response [133, 126, 134]. Thus, $\alpha\beta^+$ T cells have been shown to be crucial for immune protection against *E. vermiformis* primary and challenge infections [127, 135], whereas $CD8^+$ T cells were shown to play a role in resistance during challenge infections [133]. Moreover, it has also been shown that athymic (*nu/nu*) mice were completely susceptible to both primary and secondary infections [132]. On the contrary, $\gamma\delta^+$ T cells are not required to control infection; however, they do support the rapid activation of other

lymphoid cells during primary infections [136, 137]. Furthermore, $\gamma\delta^+$ cells have been shown to be crucial to limit immunopathology [138, 127].

Finally, effector mechanisms against intracellular stages of *E. vermiformis*, including production of reactive nitrogen intermediates, Fas ligand-mediated apoptosis of the host cell and lysis of the host cell by cytotoxicity, do not seem to play an essential role in the control of infection [139].

Considering recent advances in the understanding of the intestinal immune system, further research to provide evidence of the contributions of ILCs for the protection against *E. vermiformis* is required in order to clarify their immunoregulatory roles at the intestinal epithelial barrier.

1.6.5 *In vitro* culture of *Eimeria spp.*

Most cell lines are successfully invaded by *Eimeria spp.* but completion of the parasite's life cycle does not always occurs. With the exception of *E. tenella*, attempts to complete *Eimeria* endogenous development *in vitro* have not been successful.

E. tenella

The cultures conditions to grown *E. tenella* in primary chicken kidney (PCK) cells are very well established [140, 141]. These allowed for the development of *E. tenella* endogenous development *in vitro*, which successfully resulted in the *in vitro* production of oocysts [142, 143]. However, despite the continuous attempt to replace *in vivo* passage of *E. tenella*, the yield obtained from this cell culture system was very low, therefore, it has not proven suitable for the replacement of the conventional chicken passage of *E. tenella* stocks [144].

E. vermiformis

The first description of an *in vitro* cell culture of *E. vermiformis* was published in 1977 by Kelley and Youssef [145]. The authors cultured *E. vermiformis* sporozoites in bovine kidney cells, Madin-Darby bovine kidney (MDBK) cells and primary cultures of whole mouse embryos and described the *in vitro* development of first generation schizonts and merozoites [145].

Further attempts to culture *E. vermiformis* were made by Adams and colleges, using MDBK or PK-15 cells for the study of *E. vermiformis* sporozoite invasion. However, no details are given on the *in vitro* life cycle progression of the parasite [146]. *E. vermiformis in vitro* first generation schizonts were also described by Rose and co-workers. Sporozoite infection of murine fibroblast-like L-929 cells revealed the development of fully matured first generation schizonts at 45 hours post-infection. First generation schizont development was also achieved with sporozoite infection of rat epithelial-like cells (RATEC), yet parasite development was slower [147].

No other attempts to achieve the *in vitro* development of *E. vermiformis* have been reported.

E. falciformis

In vitro completion of *E. falciformis* first schizogony was described in a mouse intestine epithelial cell line (CMT-93). After sporozoite invasion, fist generation schizonts were observed at 39 hours post-infection. However, *E. falciformis* development did not progress [110]. To my knowledge there have been no other attempts to establish an *in vitro* culture system for the development of *E. falciformis*.

E. bovis

Various cell culture models have been established for the *in vitro* study of *E. bovis*, including human and porcine endothelial cell lines, bovine fetal gastrointestinal cells (BFGC), MDBK cells, African green monkey kidney epithelial (Vero) cells [148], bovine colonic epithelial cells (BCEC) [149], bovine umbilical vein cells (BUVEC) and bovine spleen lymphatic endothelial cells (BSLEC) [150, 151]. Successful development of the first asexual generation was often achieved but completion of *E. bovis* life cycle was only occasionally seen in BFGC. However, the *E bovis* life cycle is considerably different from that of avian or rodent species of *Eimeria*.

Hence, in order to achieve *in vitro* life cycle completion of mouse *Eimeria* species, the development of novel culture systems is required.

1.7 Aims and outlook

The principal aim of this thesis was to investigate whether *E. vermiformis* or *E. falciformis* life cycle could be replicated *in vitro*. If this could be attained, my goal was to further determine the molecular mechanisms triggered by intestinal epithelial cells in order to confer protection against *E. vermiformis* infection. Furthermore, I also proposed to dissect the immune cell contributions to the *in vivo* immune response to *E. vermiformis*, specifically the contribution of innate lymphoid cells. To tackle this question, Chapter 3 describes a series of *in vivo* studies in which various knock-out mice were infected with *E. vermiformis*. The contributions of different cell subsets was determined based on mice susceptibility to infection in the absence of the respective immune cells.

In Chapter 4, I proposed the establishment of an intestinal organoid primary culture for *Eimeria spp.* infections. Small intestine organoids were characterised and infected with *E. vermiformis* and *E. falciformis*, which completed several rounds of asexual replication.

Finally, in Chapter 5 I tested the contribution of different cytokines in the modulation of protection against *E. vermiformis* infection by the intestinal epithelial cells.

Chapter 2

Materials and Methods

2.1 Buffers and Media

2.1.1 Basal small intestine organoid medium

Advanced DMEM/F-12 (Life Technologies, Gibco #12634) containing 1% 1M HEPES buffer solution (Life Technologies, Gibco #15630), 1% GlutaMAX supplement (Life Technologies, Gibco #35050), 100 U/ml penicillin, and 100 μg/ml streptomycin (Life Technologies, Gibco #15140).

2.1.2 Complete small intestine organoid medium

Basal organoid medium containing 50 ng/ml recombinant murine EGF (Peprotech #315-09), 500 ng/ml recombinant murine Noggin (Peprotech #250-38) and 10% R-spondin 1 supernatant or, when specified, 500 ng/ml recombinant human R-spondin 1 (Peprotech #120-38).

2.1.3 193T-HA-RspoI-Fc growing medium

DMEM (Life Technologies, Gibco #31966) containing 10% FBS (Life Technologies, Gibco #12657011), 100 U/ml penicillin and 100 mg/ml streptomycin (Life Technologies, Gibco #15140).

2.1.4 193T-HA-RspoI-Fc selection medium

193t-HA-RspoI-Fc growing medium containing 300 μg/ml Zeocin (Invitrogen #R25001)

2.1.5 R-Spondin 1 supernatant

An aliquot of the 293T-HA-RspoI-Fc cell line (Calvin Kuo) was cultured in selection medium with Zeocin, in a 175cm^2 flask and incubated at 37º C, 7% CO_2. Cells were split when reached 100% confluency, in 6 x 175 cm^2 flasks and cultured in growing medium. After 3-4 days in culture, growing medium was removed and replaced with 50 ml of basal organoid medium. The medium was harvested after 1 week of incubation and collected into 50 ml Falcon tubes. The tubes were centrifuged at 500x g for 5 min to spin down non-adherent cells, and the supernatant was filtered through a 0.2 μm filter under vacuum. The R-spondin 1 supernatant was frozen in small aliquots. Samples were kept at -80º C for long-term storage or -20º C for short-term storage.

2.1.6 RIMS mounting medium

To prepare refractive index matching solution (RIMS), 40 g of Histodenz (Sigma #D2158) were dissolved in 30 ml PBS with 0.1% Tween-20 (Sigma #P2287) and 0.01% (w/v) sodium azide (VWR chemicals #103692k), resulting in a final concentration of 88% Histodenz w/v. The solution pH was adjusted to 7.5 with NaOH . Upon immunofluorescence staining, samples were incubated in RIMS overnight before microscopical analysis [152].

2.1.7 Sporozoite medium

DMEM (Life Technologies, Gibco #31966) containing containing 1% GlutaMAX supplement (Life Technologies, Gibco #35050), 1% sodium pyruvate (Life Technologies, Gibco #11360), 100 U/ml penicillin and 100 mg/ml streptomycin (Life Technologies, Gibco #15140).

2.2 Mice

The mouse work was carried out at Babraham Institute (BI) in accordance with the animals Scientific Procedures Act 1986, EU Directive 2010/63/EU and the Babraham Research Campus Animal Welfare and Ethic Review Body, under Home Office Project Licenses 80/2488 and 70/9073. Unless otherwise stated, all animals were maintained under pathogen free conditions and received standard food pellets and autoclaved sterile water *ad libitum*. For details on the mice strains used please refer to Table 2.1.

Mice were bred in a C57BL/6 background at the Babraham Institute Animal Facilities under specific pathogen-free conditions. Mice were housed in standard cages, maximum of five per cage, in a temperature-controlled room and under a twelve-hour light/dark cycle. Wild-type C57Bl/6 female mice, aged 6-12 weeks old, were used to derive intestinal organoids from intestinal crypts. *In vivo* experiments were performed on both male and female mice, sex- and age-matched. Animals were 8-15 weeks old.

Table 2.1 Transgenic mice details

Strain name	Abbreviation	Description
C57BL/6Babr	WT	
$Rag2^{tm1Fwa}$	$Rag2^{-/-}$	Due to the total inability to initiate V(D)J rearrangement, these mice fail to generate mature T or B lymphocytes [153].
$Tcra^{tm1Mom}$	TCR$\alpha^{-/-}$	The thymus of these mice is devoid of $CD4^+CD8^-$ and $CD4^-CD8^+$ cells. Normal numbers of $CD4^+CD8^+$ and $CD4^-CD8^-$ cells are retained [154].
TCRd-c^{tm1Mom}	TCR$\delta^{-/-}$	These mice show complete loss of T cells bearing TCR$\gamma\delta$ chains in adult lymphoid and epithelial organs. There is a normal development of the TCR$\alpha\beta$ T cells [155].
$Il2rg^{tm1Cgn}$	Il2r$\gamma^{-/-}$	The Il2r$\gamma^{-/-}$ show a 10-fold reduction in the absolute number of T and B cells and a complete depletion of NK cells and Peyer's Patches. Additionally, the development of gut-associated intraepithelial lymphocytes is also diminished [156].
$Il15ra^{tm1Ama}$	$Il15r^{-/-}$	The $Il15r^{-/-}$ are lymphopenic due to decreased proliferation and homing of IL15Rγ lymphocytes to peripheral lymph nodes. There is a depletion of NK cells, NKT cells, $CD8^+$ T lymphocytes and TCR$\gamma\delta$ intraepithelial lymphocytes [157].
$Il7r^{tm1Imx}$	$Il7r^{-/-}$	$Il7r^{-/-}$ mice show a reduced thymic and splenic lymphoid cellularity in both B and T cell compartments. The $Il7r^{-/-}$ phenotype resembles human IL2rγ deficiency. [158]

2.3 *Eimeria spp.*

2.3.1 Oocyst isolation and sporozoite purification

Sporozoites were purified as described before [159]. Briefly, *E. vermiformis* or *E. falciformis* oocysts, stored in 2.5% w/v potassium dichromate ($K_2Cr_2O_7$), were pelleted the desired number of oocysts in 50 ml Falcon tubes. Samples were washed three times with water to remove $K_2Cr_2O_7$, sterilised and re-suspended in sodium hypochlorite (NaOCl) solution (Sigma #425044). After this step, all the work was performed under sterile conditions. Oocysts were floated at 1100x *g* for 10 min at room temperature. The upper 10 ml supernatant, which contained the oocysts, was recovered with a 10 ml pipette and transferred to a new tube. The flotation step was repeated and oocysts were washed in sterile MilliQ water. Sporulation was scored microscopically, using a Fuchs-Rosenthal chamber, and isolated oocysts were stored over-night in 5 ml sterile MilliQ water at 4º C.

Oocysts walls were digested in 0.4% pepsin (AppliChem #A4289,0025), pH 3, at 37º C for 2 to 3 hours. Digestion was monitored microscopically until the oocyst wall was thin and wrinkled. The oocysts were washed with PBS, the supernatant was decanted and the pellet was mixed with 50 μl PBS. An equal volume of sterile glass beads (diam. 0.5 mm) was added and the sample was vortexed at 2700 rpm for 1.5 sec. This step was monitored microscopically until the majority of sporocysts was released from the oocysts, while sporozoites were kept enclosed. To induce excystation of sporozoites, 0.1 g/ml of trypsin (AppliChem #A4148) and 0.1 g/ml sodium tauroglycocholate (Fisher Chemical #S/6960148) were added to the parasites that had been re-suspended in sporozoites medium. The sample was incubated at 37º C for approximately 20 min. Digestion was monitored microscopically and, once it was completed, free sporozoites were purified in sterile conditions by passage through a DE-52 cellulose (Whatman) anion exchange chromatography column. For that, a 20 ml serynge was filled with autoclaved nylon wool (Robbins) up to the 5 ml mark. The nylon

wool was then soaked in 1% glucose-PBS. Next, the previously washed DE-52 cellulose was added and the column was calibrated with 50 ml of 1% glucose-PBS. Then, the sporozoites-containing medium was added to the column, which was further washed with 150-200 ml of 1% glucose-PBS. Sporozoites were pelleted and re-suspended in 1% glucose-PBS and kept at room temperature. Sporozoite concentration was determined microscopically using an Improved Neubauer chamber.

To determine sporozoite viability, a solution of 30 μg/ml of fluorescein diacetate (FDA)-PBS was freshly prepared and kept protected from light until used. In a separate tube, 10 μl of sporozoite suspension was mixed with 5 μl of the pre-prepared FDA solution and 5 μl of ethidium bromide (EtBr). A 7 μl droplet was mounted on a slide and at least 100 sporozoites were counted. Red FDA-stained sporozoites were classified as dead.

2.3.2 *Eimeria spp.* propagation

The natural life cycle of *Eimeria spp.* was maintained by continuous passages of the parasite oocysts in female C57BL/6 mice, and was performed every 3 to 4 months. Oocysts of the previous passage, stored in $K_2Cr_2O_7$ at 4° C, were washed in water, sterilised and floated with NaOCl (as described in 2.3.1). The recovered oocysts were quantified using a McMaster counting chamber. Eight to 12-week-old animals were orally infected with 1000 sporulated *E. vermiformis* or 50 sporulated *E. falciformis* oocysts in 100 μl water. All animals were weighed daily to monitor for weight loss during the course of infection. Infected animals were maintained on sand during the peak days of infection, specifically day 9 to 12 for *E. vermiformis* or 8 to 10 for *E. falciformis*, and faeces were collected daily. Faecal samples were dissolved in water and, after soaking for a minimum of 4 hours at room temperature, were suspended in 4% $K_2Cr_2O_7$ to a final concentration of 2.5%.

The samples were kept at room temperature with air supply and monitored for sporulation. Once a minimum of 70% sporulated oocysts had been reached, usually after 6-7 days for *E. vermiformis* or 3-4 days for *E. falciformis* oocyst stocks were stored at 4°C.

2.3.3 *E. vermiformis* infection

Oocysts of the previous passage, stored in $K_2Cr_2O_7$ at 4°C, were washed in water, sterilised and floated with NaOCl. The recovered oocysts were quantified using a McMaster counting chamber. Animals were infected by oral gavage with 100 *E. vermiformis* sporulated oocysts diluted in tap water. At day 7 post infection (just before the patency period starts), mice were caged singly and bedding was replaced by sand. Faeces were collected daily from day 8 until the end of the patency period and animals were monitored for weight loss.

2.3.4 Statistical analysis

No statistical methods were use to determine group size. All experiments were performed with four to six mice per group, and representative data are shown as mean (± SD) for two independent experiments unless stated otherwise. For the comparison of cumulative oocysts between groups, a non-parametric *t*-test with Welch's correction was performed. A two-way ANOVA test was used for statistical analysis of oocysts and weight-loss kinetics. Statistical analysis was performed using Graphpad Prism 7. Statistical significance was defined as P<0.05. * $P < 0.05$ ** $P < 0.01$ *** $P < 0.001$

2.4 Cell Culture

2.4.1 Crypt isolation and organoid cell culture

The crypt suspension was constantly kept at 4° C during the following protocol. Mouse proximal small intestines were isolated and their luminal contents removed. The intestines were opened longitudinally, washed twice with PBS, and cut into 3-5 mm fragments that were further washed with PBS by pipetting the fragments up and down five times. The supernatant was discarded and replaced with fresh PBS. This washing step was repeated approximately eight times. Crypts were isolated from the intestinal fragments by incubation for 30 min at 4° C in PBS containing 2 mM EDTA. After incubation, EDTA medium was removed and the intestinal fragments were gently washed in PBS. The samples were re-suspended in PBS in a final volume of 20 ml. Seven successive supernatant fractions were collected upon vigorous shaking of the intestinal suspension. The tissue composition of each fraction was determined microscopically. Fractions that showed an abundant villus concentration were discarded (typically, fraction 1 and sometimes fraction 2). The remaining crypt-containing fractions were filtered through a 70 μl cell strainer (Fisher Scientific #08-771-2), pooled into two 50 ml Falcon tubes and centrifuged at 500x *g* for 5 min.

The following work was carried out under sterile conditions. Isolated crypts were re-suspended in basal organoid medium and centrifuged at 300x *g* for 3 min. The pelleted crypts were re-suspended in 50% matrigel (VWR International #734-1100). Droplets of 50 μl were plated in the centre of each well of a pre-warmed 24-well plate. After matrigel polymerisation at 37° C (approximately 10-15 min), 500 μl of complete organoid medium was slowly added against the wall of each well. Organoids were incubated at 37° C, 7% CO_2. Medium was renewed every 2-3 days and intestinal organoids were passaged every week.

2.4.2 Small intestine organoid passage

Every 7-9 days, small intestine organoids were passaged using a 1:2 or 1:3 dilution. The medium was discarded and organoid droplets were washed in ice-cold PBS. After matrigel disruption, organoids were collected into a 50 ml Falcon tube and broken into smaller fragments by passaging five times through a 25G needle. Organoids were washed in PBS and centrifuged at 300x *g* for 3 min. Organoids were re-suspended in 50% matrigel and 50 μl droplets were plated in the centre of each well of a pre-warmed 24-well plate. After matrigel polymerisation at 37º C (approximately 10-15 min), 500 μl of complete organoid medium was slowly added against the wall of each well. Organoids were incubated at 37º C, 7% CO_2. Medium was renewed every 2-3 days until the following passage.

2.5 Microscopy

2.5.1 Immunofluorescence

For each time point, medium was removed and the well was washed with 200 μl of PBS. Organoids were fixed using 10% formaldehyde (Sigma-Aldrich #F8775) in PBS for 20 min at room temperature. Fixation disrupts the matrigel droplet while organoids remain attached to the bottom of the well or cover slip. If, after 20 min incubation, there was visible matrigel, samples were washed with PBS and fresh 10% formaldehyde-PBS was added for an additional 20 min. Upon fixation, organoids were washed twice in PBS for 5 min or overnight. Organoids were permeabilised with 1% Triton X-100 (Sigma-Aldrich #T8787) in PBS for 20 min and blocked with blocking buffer [2% BSA (Sigma-Aldrich #A7030) and 1% Triton X-100 in PBS] for 1 hour. Primary antibodies were diluted in blocking buffer, and samples were incubated for 2 hours at room temperature (for details refer to Table 2.2). After washing with PBS, secondary antibodies (AF488 goat anti-rabbit IgG #A11008 life technologies,AF 488 rabbit anti-mouse #A27023 life technologies) were diluted 1:1000 and incubated with the samples for 45 min at room temperature. Organoids were washed twice in PBS for 5 min. Samples were mounted and preserved in RIMS medium.

Table 2.2 Primary antibodies

Cell type	Antigen	Host	Supplier	Cat number	Dilution
Goblet cells	Muc 2	Rabbit polyclonal	Santa Cruz	Sc-15334	1:250
Paneth cells	LyzozymeC	Rabbit polyclonal	Abcam	Ab2408	1:250
Paneth/Proliferating cells	Sox9	Rabbit polyclonal	Millipore	AB5535	1:250
Enterocytes	Chromogranin A	Mouse monoclonal	Dako	M0869	1:250
Eimeria spp.	Eimeria serum	Rabbit polyclonal	Prof. Richard Lucius	NA	1:2000

2.5.2 Quantification of organoid growth

Images of the organoid cultures were taken, using the wide-field Zeiss Microbeam, with a magnification of 50x. Stitching image tiles generated a "whole-droplet" view. Matrigel offers a three-dimensional support for organoid growth. As a consequence, when imaging live organoids, which are displayed in different z planes, it was challenging to get all the organoids in focus. Every image was taken in the z plane that showed the highest number of organoids in focus. A total of 35 images was acquired per droplet (5x7), with 10% overlap, and images were combined using ZEN software (Zeiss).

Phenotype characterisation

To evaluate the outcome of the distinct organoid treatments, I investigated their impact on organoid growth. Organoids were characterised phenotypically based on their number of buds. Thus, they were classified into four groups: (i) cysts, (ii) organoids with less than 3 buds, (iii) organoids with 3 to 6 buds and (iv) organoids with more than 6 buds The quantification of the different organoid types was performed with Fiji software (using the Cell Counter plugin). Absolute numbers were exported and converted into percentage of that were further plotted and analysed in GraphPad Prism 6.

Area characterisation

Additionally, organoid surface growth was quantified using Fiji software. Pixel to µm conversion was set in accordance with the microscope specifications.

2.5.3 Statistical analysis

No statistical methods were used to predetermine sample size. All experiments were performed at least twice with multiple replicates per condition, and sample material coming from

at least two different mice. *In vitro* experiments that were technical failures, such as cultures that did not grow or autofluorescence induced by undigested matrigel were not included for analysis. All data are mean (± SD). For the comparisons of two groups, a non-parametric *t*-test with Welch's correction was performed. Statistical significance was defined as $P<0.05$. For kinetics, linear-regression was determined. Statistical analysis was performed using Graphpad Prism 7. * $P<0.05$, ** $P<0.01$, *** $P<0.001$.

2.6 Molecular biology

2.6.1 RNA isolation

Organoid RNA was extracted using the RNeasy extraction kit (Qiagen #74104) according to the manufacturer's instructions. In detail, at each time point, medium was removed and each well was washed once with PBS. Organoids were lysed in the well by adding 300 μl of RLT (lysis) buffer. They were stored at -80º C until RNA isolation. Lysates were thawed at 37º C in a water bath and vortexed at maximum speed during 1 min for sample homogenisation. To each tube, 350 μl of 70% ethanol were added. Samples were homogenised by pipetting, transferred to a spin column placed in a 2 ml tube and spun down at 10,000x *g* for 30 sec. The flow-through was discarded, 700 μl of RW1 buffer was added and samples were spun down at 10,000x *g* for 30 sec. The flow-through was discarded and 500 μl of RPE buffer was added and samples were spun down at 10,000x *g* for 30 sec. The last step was repeated, but this time samples were spun down for 2 min. The 2 ml tube was exchanged and samples were spun down at 15,000x *g* for 1 min, to completely dry the membrane. The spin column was placed in a fresh 1.5 ml tube and 30 μl RNase-free water was added to each membrane. The samples were incubated for 3-5 min at room temperature and then were spun down at 13,000x *g* for 1 min. The spin column was discarded. RNA concentration and purity was determined using a sample-retention system, NanoDrop (Thermo Scientific). Samples were stored at -80º C.

2.6.2 cDNA synthesis

The RNA was converted to cDNA using the Quantitect Reverse Transcription kit (Qiagen #205311) according to the manufacturer's instructions. In detail, 100 ng of RNA were mixed with RNase-free water until a final volume of 12 μl. Then, 2 μl of the DNA wipeout was

added to the RNA and incubated for 2 min at 42° C. Samples were placed on ice and the reverse transcriptase mix was prepared as follows:

Table 2.3 cDNA synthesis

Reagent	Volume per sample
Quantiscript Reverse Transcriptase	1 μl
Quantiscript RT 5x buffer	4 μl
RT Primer mix	1 μl
Total volume	6 μl

The reverse transcriptase mix was added to the "gDNA wipeout" tubes. The samples were spun down. In the thermocycler, samples were incubated at 42° C for 15 min, followed by an incubation at 95° C for 3 min to inactivate Quantiscript Reverse Tanscriptase. Finally, cDNA was diluted 1:10 by adding 180 μl milliQ water and stored at -20° C.

2.6.3 Real-time PCR

Real-time PCR was performing using SYBRgreen. For Platinum SYBRgreen qPCR super Mix UGD (Invitrogen #165505-7) the mastermix was prepared as follows:

Table 2.4 Real-time PCR mastermix

Reagent	Volume per sample
Master mix	10 μl
Quantitect primer assay	1 μl
Water	1 μl
Total volume	12 μl

According to a pre-defined layout, 12 μl of the mastermix were added to the wells of a 96-well plate together with 8 μl of the cDNA. Technical duplicates were run for each sample. The 96-well plate was sealed with transparent microseal (Biorad) and spun down for 30 sec at 300x g. Data were acquired on BioRad thermocyclers. For protocol details refer to Table 2.5.

Table 2.5 RT-PCR program for Platinum SYBR Green qPCR SuperMix

Step	Temperature	Time
1	50º C	2 min
2	95º C	2 min
3	95º C	5 sec
4	60º C	30 sec
repeat steps 3 and 4 for 40-45 times		
5	95º C	10 sec

2.6.4 Statistical analysis

Each value obtained is an average of three independent biological replicates, and the experiment was performed twice for each biological repeat. The relative gene expression was calculated using the comparative Ct method. Array genes were normalised to the average value of the housekeeping gene *hprt*.

Chapter 3

Regulation of the immune response against *E. vermiformis*

3.1 Introduction

Intestinal epithelial barrier disruption can lead to bacterial translocation and predisposes the host to inflammation. The cellular mechanisms that ensure barrier protection and healing in response to intestinal damage remain poorly understood. Accumulating evidence suggests that innate lymphoid cells (ILCs) contribute to the maintenance of the intestinal barrier function through epithelial cell activation and proliferation in response to tissue damage [160]. This is of particular importance for intestinal barrier homeostasis after infection. Specifically, it has been shown that ILC1s and ILC3s respond to different pathogens, such as *Listeria monocytogenes* and *Toxoplasma gondii* [84, 85].

In this chapter, I will use *E. vermiformis* as a model of mouse infection, to study the contribution of ILCs in a context of site-specific intestinal inflammation. It is well established that interferon (IFN)-γ-producing $CD4^+$ T cells are crucial in the immunoprotection against *E. vermiformis* primary infections. Moreover, $CD8^+$ T cells are also implicated, but to a lesser extent [133, 135]. Moreover, it has been shown that low NK cell activity relates with

greater susceptibility to infection, possibly due to their cytolytic activity or secretion of IFN-γ [132, 161, 162]. However, the contribution of the different ILC subsets to the resolution of infection is still unclear.

To investigate the role of ILCs in the context of *E. vermiformis* infection, I used mice bearing different combinations of genetic modifications affecting genes important to the immune system. The susceptibility of mice to infection can be reliably evaluated through the quantification of the number of oocysts shed. Symptoms of severe infection can include diarrhoea; however, *E. vermiformis* infection is self limiting, therefore even immunocompromised animals are able to clear infection within 3 weeks.

3.2 The effect of *E.vermiformis* dose on infection severity

E. vermiformis is a causative agent of coccidiosis, which can lead to weight loss and intestinal inflammation, especially in immunocompromised animals. An important consideration for the study of immune responses to *E. vermiformis* is animal welfare; in order to minimise animal distress and suffering I started by performing a dose titration of the parasite. Sporulated *E. vermiformis* oocysts were isolated and administered by oral gavage to age- and sex-matched mice. To implement the new model of infection in the laboratory, I started by testing the pathogenicity of a newly established stock of *E. vermiformis*, which was further passaged every 3 months. This required an initial dose-ranging study to optimise the initial dose of *E. vermiformis* infection (Figure 3.1).

Based on descriptions in different studies, four doses of infection were tested: 250, 500, 1,000 or 2,000 *E. vermiformis* sporulated oocysts were given to 5 mice per group. Weight-loss was monitored. At day 6 post-infection, mice were single caged and the total number of shed oocysts was determined daily. The doses of 250 and 500 *E. vermiformis* oocysts led to a lower parasite production compared to 1,000 or 2,000 oocysts (Figures 3.1A and 3.1C). In terms of absolute numbers of shed parasites, patency (time over which oocyst release occurs) or weight loss, no differences were seen between the doses of 1,000 and 2,000 *E. vermiformis* oocysts, indicating that a plateau was reached at a dose of infection of 1,000 sporulated *E. vermiformis* oocysts (Figures 3.1A and 3.1C). This could be due to the 'crowding effect', as it has been previously described for *E. maxima* and *E. praecox* chicken infections. Johnson and colleagues investigated if the fecundity of the parasites decreases as the dose of infection increases [163]. The authors showed that the interaction between the availability of intestinal enterocytes and immune responses contributed to the observed crowding effect [163].

Additionally, no significant differences in the patency duration or weight loss were observed among the dose range tested (Figures 3.1B and 3.1D). Therefore, an initial dose of 1,000 sporulated *E. vermiformis* oocysts was used in the following experiment.

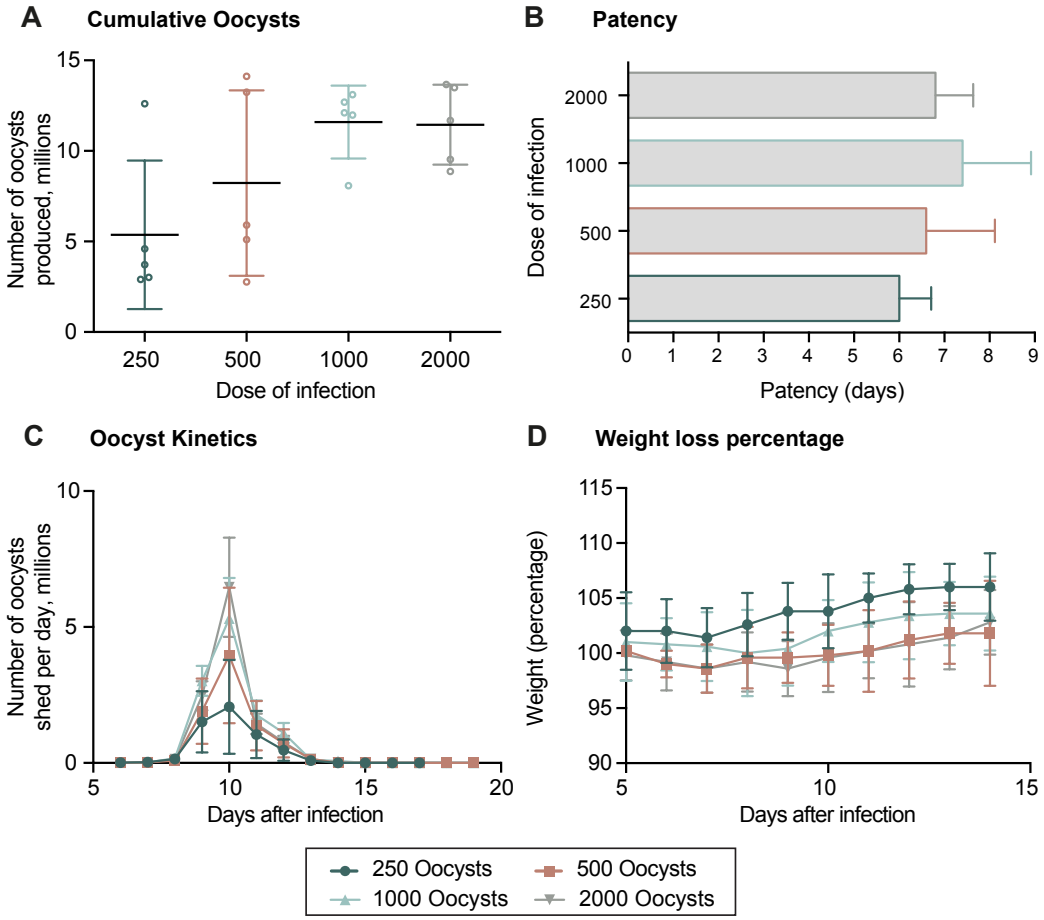

Fig. 3.1 The effect of *E.vermiformis* dose on infection severity

WT mice were infected with 250 (green), 500 (orange), 1,000 (blue) or 2,000 (grey) sporulated *E. vermiformis* oocysts. (A) Cumulative oocyst count. (B) Patency in days. (C) Oocyst kinetics during infection patency. (D) Percentage body weight loss. Data shown are mean (± SD) of five mice per group.

3.3 Immunocompromised mice are highly susceptible to *E. vermiformis* infection

Knowing that the activation of B and T cells is crucial in order to limit *E. vermiformis* primary infection [133, 135], I decided to test the pathogenicity of the recently established *E. vermiformis* stock in an immunocompromised mouse model, the Rag2$^{-/-}$ mouse. As Rag2$^{-/-}$ mice fail to develop mature B or T lymphocytes [153], I hypothesised that if my *E. vermiformis* stock had been successfully passaged, Rag2$^{-/-}$ would be highly susceptible to infection. Therefore, WT and Rag2$^{-/-}$ mice were infected with 1,000 *E. vermiformis* oocysts. Weight loss was monitored. At day 6 post infection, mice were single caged and the total number of shed oocysts was determined daily. Rag2$^{-/-}$ mice were reported by the institute veterinary to developed a severe intestinal inflammation and some animals died due to severe infection, even though, no more than 10% weight loss was observed (data not shown). This was a surprising result, as 1,000 *E.vermiformis* oocysts is a dose of infection widely used in immunodeficient mice across different groups without reports of fatal consequences.

In response to this observation, WT and Rag2$^{-/-}$ mice were challenged with a lower initial dose of 100 sporulated *E. vermiformis* oocysts (Figure 3.2). This infection dose was kept unchanged during the experimental designs that followed. As expected, Rag2$^{-/-}$ mice were significantly more susceptible to *E. vermiformis* infection than WT animals, displaying significant increases in the number of shed oocysts and the patency duration (Figures 3.2A to 3.2C). Even though these differences were clearly evident, they were not associated with major weight loss, as Rag2$^{-/-}$ lost less than 5% of their initial weight throughout the infection (Figure 3.2D). These data showed that, as previously described, the control of *E. vermiformis* primary infection is dependent on a T and/or B cell immune response.

In addition, from a pratical point of view, these results validate the successful propagation of the newly acquired *E. vermiformis* stock.

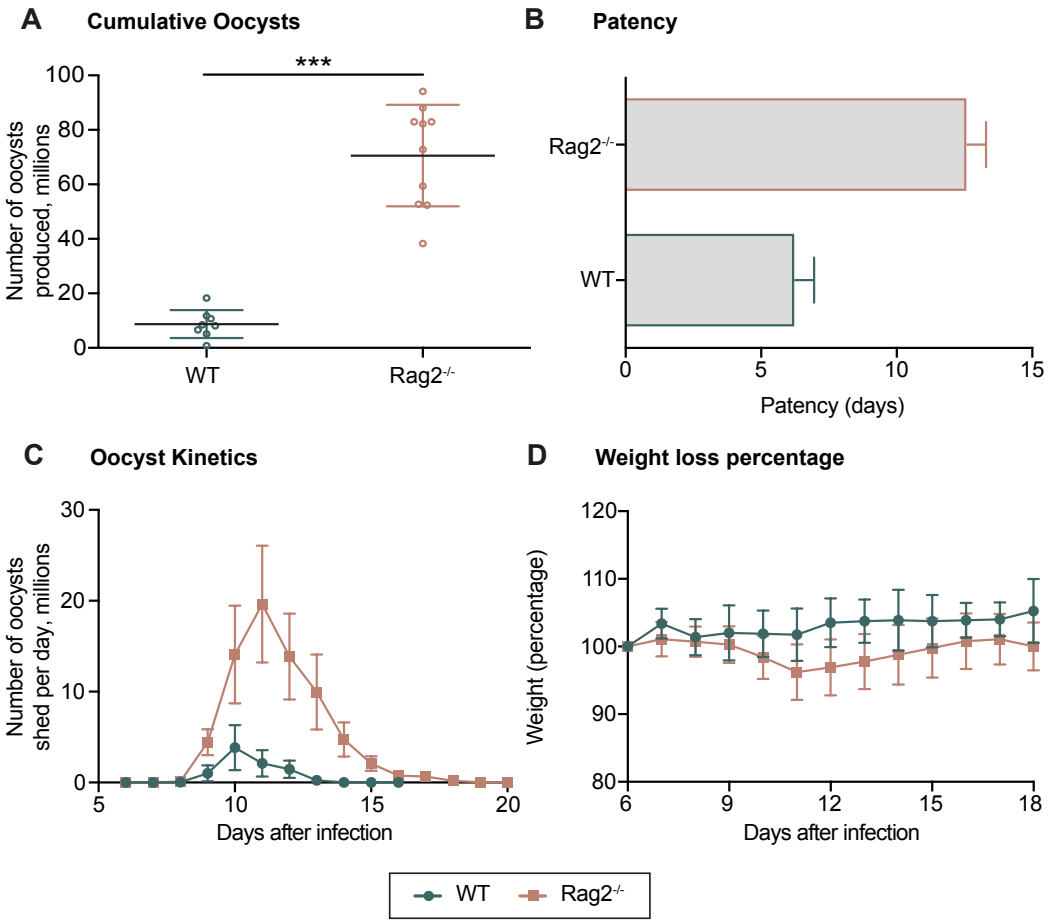

Fig. 3.2 Development of *E. vermiformis* pathology in WT and Rag2$^{-/-}$ mice

WT (green) or Rag2$^{-/-}$ (orange) mice were infected with 100 sporulated *E. vermiformis* oocysts. (A) Cumulative oocyst count. (B) Patency in days. (C) Oocyst kinetics during infection patency. (D) Percentage body weight loss. Data shown are mean (± SD) of five mice per group. Data are pooled from two independent experiments.

Having established an *in vivo* model for *E. vermiformis* infection, and using different knock-out mouse models, I next investigated how different host cell subsets mediate intestinal immunity against infection.

3.4 $\alpha\beta$ T cells are essential for the immune response against *E. vermiformis*

As described by Rose and colleagues and Smith and coworkers [133, 135] T cells are crucial for the immune response against *E. vermiformis*. Knowing that Rag2$^{-/-}$ mice are highly susceptible to infection, I wanted to further dissect the contribution of T cells in the context of *E. vermiformis* infection. It is known that T cells can be divided into two groups accordingly to the T cell receptor (TCR) that they express: $\alpha\beta$ T cells or $\gamma\delta$ T cells.

In this section I will address the contribution of $\alpha\beta$ T cells in the context of *E. vermiformis* infection. For that a TCR$\alpha^{-/-}$ mouse model was used. The thymus of TCR$\alpha^{-/-}$ mice contains normal numbers of CD4^{-}CD8^{-} and CD4^{+}CD8^{+} thymocytes but it is typically devoid of CD4^{+}CD8^{-} and CD4^{-}CD8^{+} cells. WT and TCR$\alpha^{-/-}$ were infected with 100 sporulated *E. vermiformis* oocysts and weight loss was monitored. At day 6 post infection, mice were single-caged and the total number of shed oocysts was determined daily (Figure 3.3). The results showed that in comparison with WT, TCR$\alpha^{-/-}$ mice have a small but significant increase in the cumulative number of parasites shed, although not as pronounced as seen in Rag2$^{-/-}$ mice (Figure 3.3A). There was also an increase in the duration of the patency in TCR$\alpha^{-/-}$ mice (Figure 3.3B), yet no differences in weight loss were observed (Figure 3.3D). The data suggests that $\alpha\beta$ T cells are required to limit *E. vermiformis* infection. This result is in agreement with the work of Roberts and colleagues, that established that $\alpha\beta$ T cells have a protective role against both primary and secondary *E. vermiformis* infections [127], but the difference between TCR$\alpha^{-/-}$ and Rag2$^{-/-}$ suggests that other components of the immune system are involved in protection.

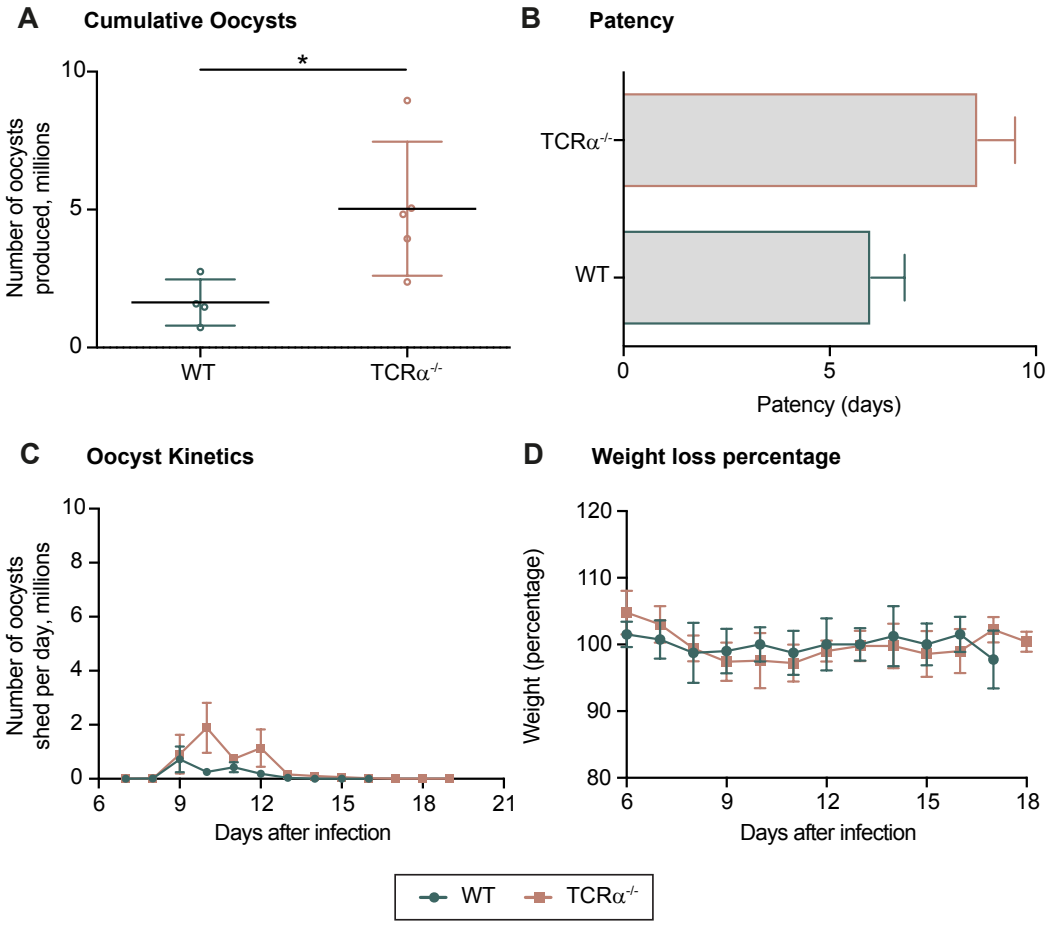

Fig. 3.3 Development of*E. vermiformis* pathology in WT and TCR$\alpha^{-/-}$ mice

WT (green) or TCR$\alpha^{-/-}$ (orange) mice were infected with 100 sporulated *E. vermiformis* oocysts. (A) Cumulative oocyst count. (B) Patency in days. (C) Oocyst kinetics during infection patency. (D) Percentage body weight loss. Data shown are mean (± SD) of five mice per group.

3.5 $\gamma\delta$ T cells are not essential for the control of *E. vermiformis* replication

Having established that $\alpha\beta$ T cells confer immunoprotection against *E. vermiformis* infection, I decided to investigate the contribution of $\gamma\delta$ T cells. To address this question, a TCR$\delta^{-/-}$ mouse model was used. These mice display deficient $\gamma\delta$ TCR expression in all adult lymphoid and epithelial organs, while there is normal development of the $\alpha\beta$ T cell lineage.

WT and TCR$\delta^{-/-}$ mice were infected with 100 sporulated *E. vermiformis* oocysts and weight-loss was monitored. At day 6 post-infection, mice were single caged and the total number of shed oocysts was determined daily (Figure 3.4). These results showed no significant differences between *E. vermiformis*-infected TCR$\delta^{-/-}$ and WT mice, in terms of oocyst output or kinetics, patency or weight loss (Figure 3.3). Nonetheless, a smaller non-significant trend showed an increase in TCR$\delta^{-/-}$ cumulative oocysts and day 10 of kinetics, when compared to the WT control (Figures 3.3A and 3.3C).

As shown before [127, 136], the data suggest that $\gamma\delta$ T cells are not crucial mediators in the control of *E. vermiformis* infection. OkHowever, Roberts and colleagues described an important role for $\gamma\delta$ T cells in the regulation of the immunopathology against *E. vermiformis*, since TCR$\delta^{-/-}$ mice displayed weight loss and gastrointestinal haemorrhage [127]. These symptoms were not observed in my experiments with TCR$\delta^{-/-}$ mice, but this could be explained by the different doses of *E. vermiformis* infection. Whereas mice in my experiments were infected with 100 oocysts, in Roberts' studies an infection dose of 1000 sporulated *E. vermiformis* oocysts was used [127]. Thus, further studies would be required to obtain a fuller picture of the regulatory contribution of $\gamma\delta$ T cells for the immunoprotection against *E. vermiformis* infection.

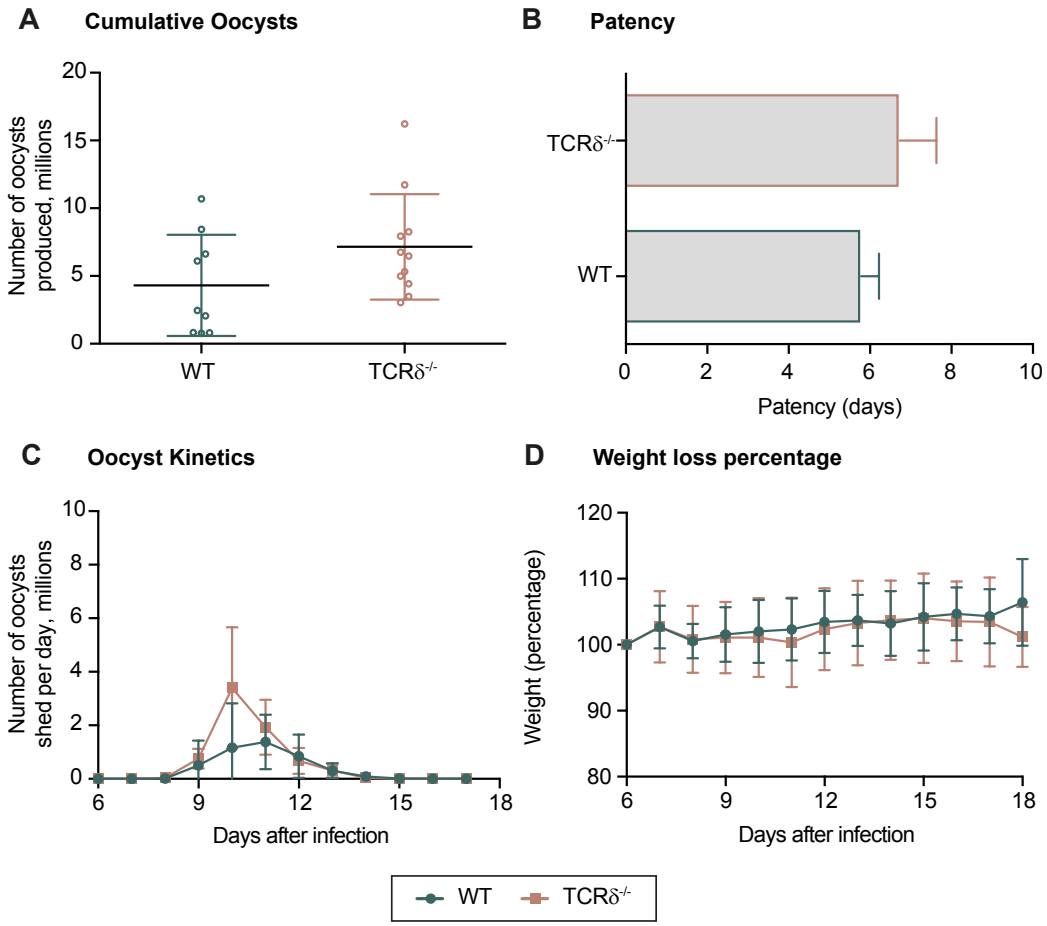

Fig. 3.4 Development of *E. vermiformis* pathology in WT and TCR$\delta^{-/-}$ mice

WT (green) or TCR$\delta^{-/-}$ (orange) mice were infected with 100 sporulated *E. vermiformis* oocysts. (A) Cumulative oocyst count. (B) Patency in days. (C) Oocyst kinetics during infection patency. (D) Percentage body weight loss. Data shown are mean (± SD) of five mice per group. Data are pooled from two independent experiments.

3.6 The contribution of ILCs to the host immune response to *E. vermiformis*

After clarifying the contribution of the different T cell subsets, the role of ILCs in the host protection against *E. vermiformis* was investigated. ILCs have been classified into three main groups based on their functional characteristics and similarity to T helper (T_H) cell subsets [73]. Thus, group 1 ILCs are defined by their ability to produce of IFNγ, and can be divided into two subgroups: natural-killer (NK) cells and ILC1s. Group 2 ILCs are able to produce T_H2 cell-associated cytokines, including interleukin (IL)-5 and IL-13. Finally, group 3 ILCs, characterised by the ability to produce T_H17 cell-associated cytokines, including IL-22 and IL-17, can be divided into 3 subgroups: NCR^+ILC3, NCR^-ILC3 or LTi cells [73].

All ILCs derive from a common lymphoid progenitor and depend on the common cytokine receptor γ-chain (a component of six different interleukin receptors: IL-2R, IL-4R, IL-7R, IL-9R, IL-15R and IL-21R) for their development and maintenance. With the exception of NK cells, which require IL-15 for their development, ILCs depend on IL-7 for their development and maintenance [73].

Thus in this section, an $Il2r\gamma^{-/-}$, $Il15r^{-/-}$ or $Il7r^{-/-}$ mouse model will be used alone or in combination with a $Rag2^{-/-}$ background to study the role of ILCs in the context of *E. vermiformis* infection.

3.6.1 The impact of Il2rγ signalling on immunoprotection against *E. vermiformis*

I started by analysing how the lack of Il2Rγ signalling on a Rag2-sufficient or -deficient background would impact the immune response against *E. vermiformis*. In addition to other cytokines, Il2rγ signalling is a component of the receptors for IL-7, and IL-15, which are essential for the development of ILCs. As a result, Il2r$\gamma^{-/-}$ mice lack NK cells and Peyer's patches. Their gut-associated ILCs are severely diminished and they show a reduction in the absolute numbers of lymphocytes. However, they are capable of developing some mature splenic B and T cells [156].

WT, Il2r$\gamma^{-/-}$, Rag2$^{-/-}$ and Il2r$\gamma^{-/-}$Rag2$^{-/-}$ mice were infected with 100 sporulated *E. vermiformis* oocysts and their weight loss was monitored. At day 6 post infection, mice were caged singly and the total number of shed oocysts was determined daily (Figure 3.5). As shown before, *E. vermiformis*-infected Rag2$^{-/-}$ were significantly more susceptible to infection than the WT control. Interestingly, this difference was mitigated in the Il2r$\gamma^{-/-}$Rag2$^{-/-}$ mice (Figure 3.5A and 3.5C). Additionally, no significant differences were observed in the output of *E. vermiformis* oocysts between Il2r$\gamma^{-/-}$ and WT control (Figure 3.5A). Il2r$\gamma^{-/-}$, Il2r$\gamma^{-/-}$Rag2$^{-/-}$ and Rag2$^{-/-}$ mice had equally longer patency periods when compared to the WT control (Figure 3.5B). Finally, the results showed no significant differences in weight-loss between the groups (Figure 3.5D).

Altogether, these data suggest a role for Il2Rγ signalling in the susceptibility to infection of immunocompromised mice. However, these data are insufficient to extract definitive conclusions.

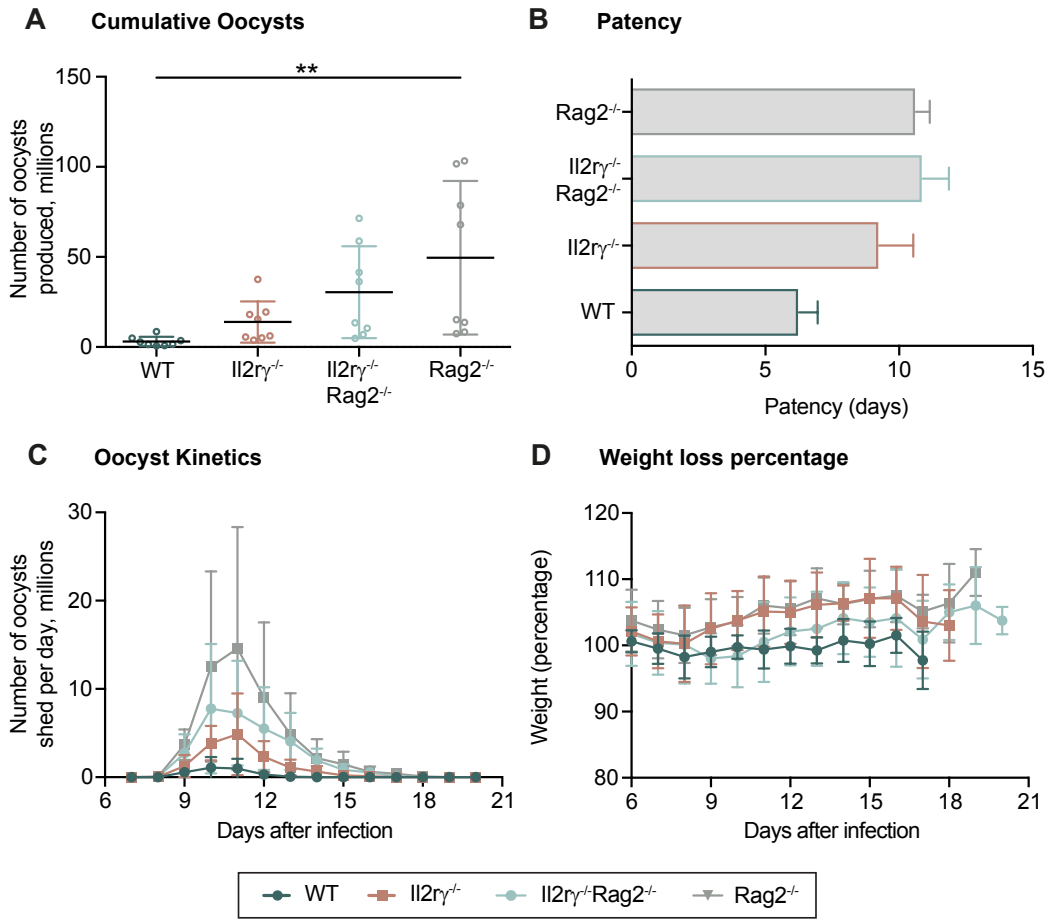

Fig. 3.5 Development of *E. vermiformis* pathology in WT, Il2r$\gamma^{-/-}$, Il2r$\gamma^{-/-}$Rag2$^{-/-}$ and Rag2$^{-/-}$ mice

WT (green), Il2r$\gamma^{-/-}$ (orange), Il2r$\gamma^{-/-}$Rag2$^{-/-}$ (blue) or Rag2$^{-/-}$ (grey) mice were infected with 100 sporulated *E. vermiformis* oocysts. (A) Cumulative oocyst count. (B) Patency in days. (C) Oocyst kinetics during infection patency. (D) Percentage body weight loss. Data shown are mean (± SD) of four mice per group. Data are pooled from two independent experiments. ** P<0.01.

3.6.2 Impact of Il15r signalling on immunoprotection against *E. vermiformis*

Given the pleiotropic role of IL-15 in immune development and function, Il15r$^{-/-}$ mice show a lymphopenic profile as a result of decreased proliferation and homing of lymphocytes to peripheral lymph nodes. Severe reduction in the absolute numbers of NK and NKT cells, TCR$\gamma\delta$ intraepithelial lymphocites and CD8^{+} cells are also observed [157]. Knowing that the contributions of $\gamma\delta$ T cells or CD8^{+} cells are not detrimental for immunoprotection against *E. vermiformis* primary infections [127, 133], the Il15r$^{-/-}$ mouse model might shed light on NK involvement in the immune response against this pathogen.

Therefore, WT, Il15r$^{-/-}$, Rag2$^{-/-}$ and Il15r$^{-/-}$Rag2$^{-/-}$ mice were infected with 100 sporulated *E. vermiformis* oocysts and their weight loss was monitored. At day 6 post infection, mice were caged singly and the total number of shed oocysts was determined daily (Figure 3.6).

With a more pronounced trend than Il2r$\gamma^{-/-}$Rag2$^{-/-}$, Il15r$^{-/-}$Rag2$^{-/-}$ show an intermediate susceptibility to *E. vermiformis* infection when compared with the Rag2$^{-/-}$ or WT controls (Figures 3.6A and 3.6C). No differences in absolute numbers of shed oocysts were observed between Il15r$^{-/-}$ and WT mice (Figure 3.6A). Higher oocyst outputs from Rag2$^{-/-}$ or Il15r$^{-/-}$Rag2$^{-/-}$ mice seem to correlate with a longer patency (Figure 3.6B). There were no significant differences in weight loss among the different groups (Figure 3.6D).

The results suggest a role for Il15R signalling in the susceptibility to *E. vermiformis* infection of immunodeficient mice. Nonetheless, further research is required to determine whether if the phenotype observed is due to NK cells and to further investigate how NK cell activation impacts on the immune response against *E. vermiformis* infection.

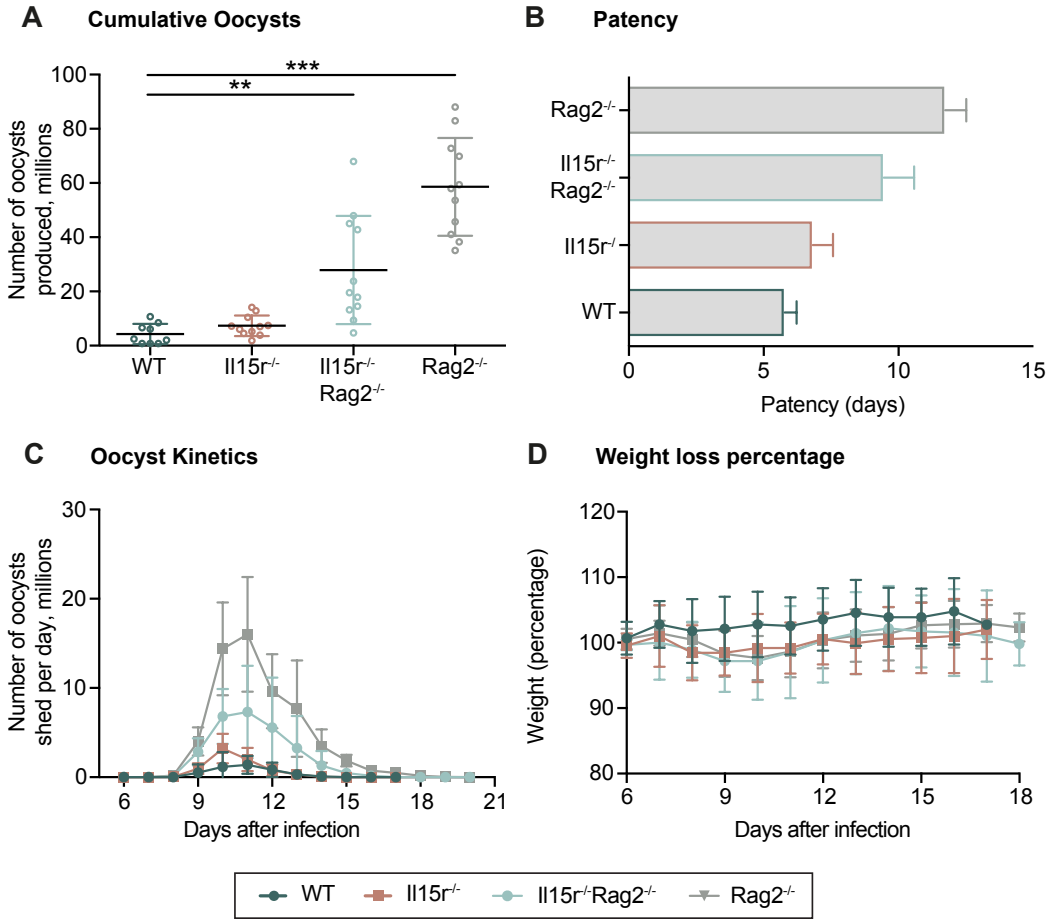

Fig. 3.6 Development of *E. vermiformis* pathology in WT, Il15r$^{-/-}$, Il15r$^{-/-}$Rag2$^{-/-}$ and Rag2$^{-/-}$ mice

WT (green), Il15r$^{-/-}$ (orange), Il15r$^{-/-}$Rag2$^{-/-}$ (blue) or Rag2$^{-/-}$ (grey) mice were infected with 100 sporulated *E. vermiformis* oocysts. (A) Cumulative oocyst count. (B) Patency in days. (C) Oocyst kinetics during infection patency. (D) Percentage body weight loss. Data shown are mean (± SD) of four or five mice per group. Data are pooled from two independent experiments. ** P<0.01 *** P<0.001.

3.6.3 Impact of Il7r signalling on immunoprotection against *E. vermiformis*

To investigate the possible roles of the remaining ILC populations (groups 1 to 3, with the exception of NK cells), an Il7r$^{-/-}$ mouse model was used. Il7r$^{-/-}$ mice display normal development of NK cells, but lack $\gamma\delta$ T cells and show a reduction of $\alpha\beta$ T cells [164]. Importantly, Il7r$^{-/-}$ mice have a severe reduction in the absolute number of ILCs [165].

WT, Il7r$^{-/-}$, Rag2$^{-/-}$ and Il7r$^{-/-}$Rag2$^{-/-}$ mice were infected with 100 sporulated *E. vermiformis* oocysts and their weight loss was monitored. At day 6 post infection, mice were caged singly and the total number of shed oocysts was determined daily (Figure 3.7)

Interestingly, the comparison of *E. vermiformis*-infected Rag2$^{-/-}$ mice with Il7r$^{-/-}$Rag2$^{-/-}$ mice showed a similar pattern to that observed for the Rag2$^{-/-}$ to Il2r$\gamma^{-/-}$Rag2$^{-/-}$ comparison. Particularly, Il7r$^{-/-}$Rag2$^{-/-}$ mice show an increased resistance to *E. vermiformis* infection compared with Rag2$^{-/-}$ (Figures 3.7A and 3.7B). No differences in parasite loads were seen between WT and Il7r$^{-/-}$ (Figures 3.7A and 3.7B). As seen before, patency duration seemed to be longer in the groups that show higher cumulative oocysts output (Figure 3.7A and 3.7B). No significant differences were observed between the groups in terms of weight loss (Figure 3.7D).

As previously discussed for Il2r$\gamma^{-/-}$ and Il15r$^{-/-}$ mice, there also seems to be an adverse effect induced in immunocompromised mice by Il7R signalling. Further research would be required to study how the different ILCs play a role in the observed phenotype.

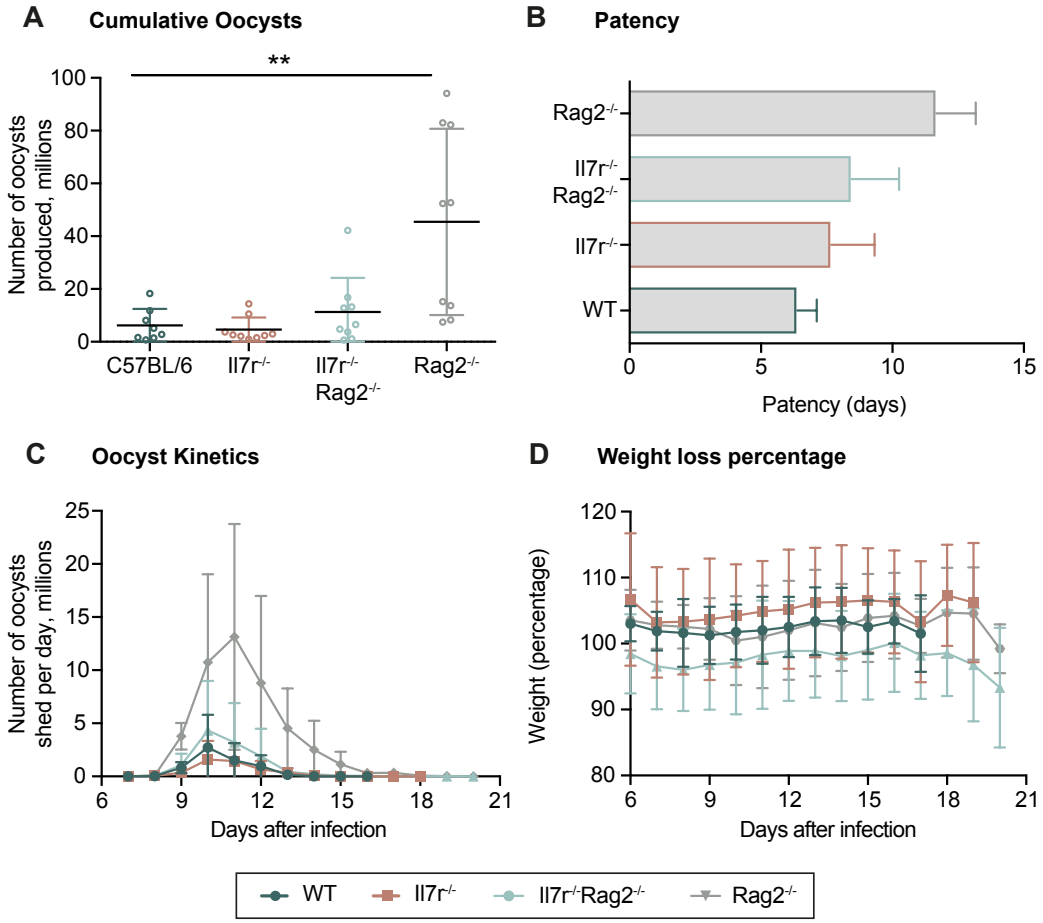

Fig. 3.7 Development of *E. vermiformis* pathology in WT, Il7r$^{-/-}$, Il7r$^{-/-}$Rag2$^{-/-}$ and Rag2$^{-/-}$ mice

WT (green), Il7r$^{-/-}$ (orange), Il7r$^{-/-}$Rag2$^{-/-}$ (blue) or Rag2$^{-/-}$ (grey) mice were infected with 100 sporulated *E. vermiformis* oocysts. (A) Cumulative oocyst count. (B) Patency in days. (C) Oocyst kinetics during infection patency. (D) Percentage body weight loss. Data shown are mean (± SD) of four or five mice per group. Data are pooled from two independent experiments. ** P<0.01.

3.7 Discussion

In order to study host-pathogen interactions at the intestinal epithelial barrier, I decided to use *E. vermiformis* as an infectious model to induce site-specific intestinal inflammation. *E. vermiformis* is known to infect the ileum and jejunum [166] and infection can be initiated via the natural route by oral gavage. Following infection, the resistance or susceptibility of mice can be reliably quantified by enumeration of shed oocysts into the faeces and by the length of the patent period (time over which oocyst release occurs).

First, a titration of the initial dose of infection was performed (Figure 3.1). Interestingly, no differences in the absolute number of oocysts or oocyst production kinetics were seen between an initial dose of 1000 or 2000 *E. vermiformis* oocysts, suggesting that the intensity of infection reached a plateau. Moreover, no differences were seen in the patency duration and no weight loss was registered. Therefore it was decided to proceed with the experimental work using a 1000 sporulated *E. vermiformis* as the infection dose. However, this dose of infection proved to be inappropriate when using immunocompromised mice. Although these did not show severe weight loss, they succumbed to infection around day 8/9. Post-mortem analysis of intestinal pathology, performed by the Babraham institute veterinary, revealed a highly inflamed intestine (data not shown). Due to the different susceptibilities of mice, several authors adjust infection dose accordingly [127, 135, 137]. Therefore, in the experiments that followed I infected mice with 100 sporulated *E. vermiformis* oocysts.

Data were pooled from independent experiments for presentation in my figures. As a consequence, the data sometimes showed big spreads. Even though age- and sex-matched animals were infected with the same dose of sporulated *E. vermiformis* oocysts, we also observed, at times, a big data spread within the same group. Data spread could also be induced by the researcher while performing gavage. However, because *E. vermiformis* stocks were passaged *in vivo*, their potency inevitably varies between inocula and with storage over time.

Secondly, because *E. vermiformis* was brought to Babraham from Prof. Richard Lucius - Humboldt Universität zu Berlin, after successfully passage of the stock received, I wanted to evaluate how the infection induced by the parasite would compare to what is described in the literature. It is well established that primary immune responses against *E. vermiformis* are IFN-γ-induced and $CD4^+$ T cell-dependent [133, 126, 134]. Consequently, immunocompromised mice display high susceptibility to *E. vermiformis* infection as shown by Schito and colleagues using SCID mice [167]. Therefore, my first experimental design consisted in assessing how $Rag2^{-/-}$ immunocompromised mice responded to *E. vermiformis* infection. As expected, my results showed that $Rag2^{-/-}$ mice are more susceptible than the WT controls (Figure 3.2). These results were in accordance with what has been previously described [167], indicating that T and/or B cells are required for protection against *E. vermiformis* infection. However, as referred to before, it is known that T cells play a crucial role in immunity against primary infection with *E. vermiformis*. Thus, to clarify the involvement of T cells in the immune response against *E. vermiformis*, I utilised $\alpha\beta$ T cell- or $\gamma\delta$ T cell-deficient mice (Figures 3.3 and 3.4).

Even though I observed a slight increased susceptibility to *E. vermiformis* infection in the $TCR\alpha^{-/-}$ mice, my data confirmed previous reports [127, 135] showing that $\alpha\beta$ T cells are important contributors for immunoprotection against *E. vermiformis* infection (Figure 3.3). Differences in the $TCR\alpha^{-/-}$ susceptibility of the animals used in my study and the ones used by other authors [127, 135] could be related with the different background of the transgenic animals that were used or the differences in the mice housing, which consequently impact their microbiota, as showed in studies in my lab (data not published) and by different authors [168, 169]. These microbiota differences play an important role in the induction, priming and function of the intestinal immunity, consequently being able to impact the immune response against infections, such as *E. vermiformis* [170–172].

can impact the intestinal immune surveillance sensibility and thus impact the mice response to infection.

On the other hand, $\gamma\delta$ T cells, which are commonly abundant within the intestinal epithelium, did not showed a effective clearance of infection. However, it has been reported that, in the context of *E. vermiformis* infection, $\gamma\delta$ T cells are increased after infection and support the activation of other lymphoid cells in the absence of $\alpha\beta$ T cells [137]. More importantly, it has been described that mice lacking $\gamma\delta$ T cells display an excessive intestinal damage, which can be related to a failure in the regulation of the $\alpha\beta$ T response [127]. Thus, more studies would be required to study an immunomodulatory role for $\gamma\delta$ T cells in response to *E. vermiformis* at the small intestine epithelial barrier.

In this chapter, my goal consisted of addressing the contribution of ILCs in the context of site-specific intestinal inflammation. It it known that in the colon and caecum, during *E. falciformis* infection, Depletion of ILCs (Thy1.2) does not increase pathology (like seen in Rag2$^{-/-}$Il2r$\gamma^{-/-}$) but led to a slight increase in oocyst production (Jörg Stange communication, data not publish).

E. vermiformis infection of Il15r$^{-/-}$ or Il7r$^{-/-}$ mice, which lack NK cells or ILCs, respectively, showed an effective clearance of the pathogen, compared to the WT control, including a comparable patency time (Figures 3.6A, 3.6B, 3.7A and 3.7B). Interesting results were obtained when mice bearing combine deficiencies for interleukin receptor components and Rag2 were tested. Deficiencies in the interleukin receptors appeared to ameliorate the severe infection seen in Rag2 deficiency alone. This suggests that ILCs are important regulators of intestine homeostasis. ILC3s comprise the largest population of ILCs in the intestine, specifically NCR^{+} ILC3s, which are able to produce IL-22 [77, 173]. In turn, IL-22 plays an important role in the maintenance of the intestinal epithelial barrier, being required for epithelial cell activation and proliferation in response to intestinal damage [160, 79].

It has been reported that ILCs are capable of responding to apicomplexan pathogens, such as *Toxoplasma gondii* [84]. Additionally, several reports have shown that ILCs may have a detrimental impact on the intestinal pathology induced after infection. For example, an abnormal increase in the absolute number of NCR^- ILC3s in the ileum and colon of Crohn's patients has been reported, suggesting a role for these cells in the pathophisiology of intestinal inflammation, through cytokine production, cell recruitment and organisation of the inflammatory tissue [86]. Furthermore, ILC1s are also known to be increased in the inflamed intestinal mucosa of Crohn's disease patients, which is associated with disease severity [174].

Additionally, similar findings shown in Figure 3.5, less inflammation was observed in the airway of $Il2r\gamma^{-/-}Rag2^{-/-}$ than in $Rag2^{-/-}$ in response to protease-induced ling inflammation. The authors showed that ILC2 engraftment into $Il2r\gamma^{-/-}Rag2^{-/-}$ led to an increase in airway inflammation [175].

Altogether, these reports strongly suggest that, in an unregulated environment, ILCs can induce an aggravation of immunopathologic effects during an inflammatory response. Further studies would be required to identify which ILCs populations are involved in the intestinal immune response against *E. vermiformis* and how they contribute to the pathology observed in immunocompromised animals.

A remote possibility to explain why $Il2r\gamma^{-/-}Rag2^{-/-}$, $Il15r^{-/-}Rag2^{-/-}$ or $Il7r^{-/-}Rag2^{-/-}$ are less susceptible to infection than $Rag2^{-/-}$ could be related to developmental requirements that *E. vermiformis* may have. Restricting the access *E. vermiformis* to certain factors could limit parasite development. For example, it is known that the development of sexual stages is dependent on tryptophan, a metabolite produce by the microbiota [176]. However, to my knowledge, there are no reports so far on the dependence of *E. vermiformis* on factors produced by immune cells.

Chapter 4

Eimeria spp.-infected small intestine organoids as a model of infection

4.1 Introduction

Coccidiosis, a disease that affects many vertebrates worldwide, can be caused by *Eimeria spp.* In this chapter, I describe *Eimeria spp.* and their use as a model of infection, as they present several advantages for the study of host-pathogen interactions. Firstly, as an apicomplexan parasite, *Eimeria spp.* are closely related to human pathogens such as *T. gondii*, *Plasmodium spp.* or *Cryptosporidium spp.* [177, 139]. Secondly, infection by *Eimeria spp.* is site-specific and it is limited to the intestinal epithelium. In this context, the intestinal epithelium provides a barrier against harmful agents, including parasites. Loss of intestinal barrier function may ultimately lead to systemic inflammation or remote organ failure.

To investigate host-pathogen interactions at the intestinal site, the laboratory in which I have worked has explored the use of mouse *E. vermiformis* or *E. falciformis* as models of *in vitro* infection. Due to the complexity of their life cycles, which comprise asexual (schizogony) and sexual (gamatogony) stages, the *in vitro* study of these parasites has been limited to the use of cell lines which allow sporozoite development up to their first schizogony

[147, 110]. To try to overcome this limitation, I have explored the use of three-dimensional organoids, generated from mouse intestinal crypts.

In 2009, Sato and colleagues reported the establishment of the first long-term *in vitro* cultures of intestinal organoids derived from human biopsies or mouse intestinal crypts [16]. According to the authors, these three-dimensional organoids display the main characteristics of the intestinal epithelial layer, including their biological organisation as crypt- and villus-like epithelial domains. Containing specialised epithelial intestinal cells, including stem cells, organoids are capable of self-renewal for more than a year [16]. Moreover, given this self-renewal ability, the organoid model can be applied to the study of organogenesis, regenerative medicine or tumorigenesis.

In this chapter, I describe the establishment and characterisation of a stable organoid culture model, suitable for the study of host-pathogen interactions. Even though *Eimeria spp.* infect and replicate mostly in enterocytes [134], the complexity of the organoid culture will potentially provide additional signals from neighbouring cells as well as structural organisation cues, such as cellular polarisation, which might be of importance for the progression of the *E. vermiformis* or *E. falciformis* life cycles.

Little is known about the maintenance of tissue integrity during intestinal epithelial infection. The successful establishment of this organoid model will allow the investigation of host-pathogen interactions at the intestinal epithelial barrier and dissection of the signalling mechanisms employed by site-specific epithelial cells in the triggering of an immune response and/or maintenance of intestinal homeostasis.

4.2 Characterisation of small intestine organoids

Based on the protocol described by Sato and colleagues [16], the small intestine organoid model was successfully established. In this section, I shall characterise the preparation, growth and behaviour of small intestine organoids.

After crypt isolation, organoids were seeded in 50% matrigel and cultured in complete organoid medium, which contains the required factors for crypt growth, namely EGF, R-Spondin and Noggin. These cells were described as passage 0 (Figure 4.1). Crypts rapidly organised into spherical organoids (first seen at 4 hours post-seeding, data not shown), and from one day post-seeding, organoids grew in a stereotypical manner. During passage 0, organoids developed mostly on the edges of the matrigel droplet, possibly due to the high and non-specific cellular content that had been seeded and started to die, which was highly concentrated in the middle of the droplet (Figure 4.1). Medium was changed at day 2 and organoids were passaged at day 3 or 4 post crypt seeding. From passage 1 onwards, cellular debris was washed away and the culture became organoid specific (Figure 4.1). Intestinal organoids grew faster and at a consistent rate among different passages, compared to passage 0.

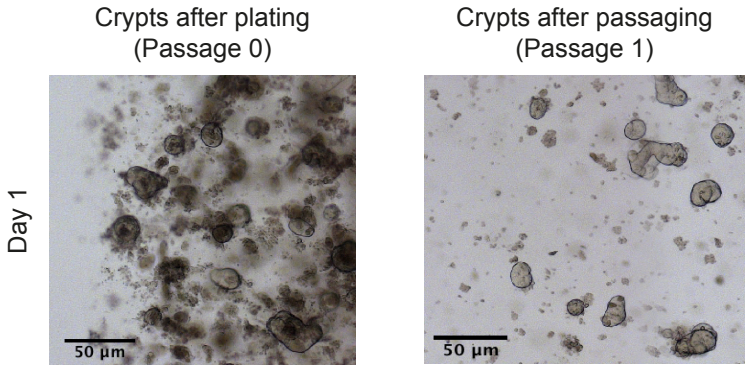

Fig. 4.1 Small intestine organoids: primary culture

Small intestinal crypts were isolated and cultured in 50% matrigel (left). After 3 to 4 days, organoids were passaged and kept in culture for 7 to 10 days (right). Image representations were taken 1 day after seeding. Scale bar = 50 μm

In detail, after passage, small intestine organoids organised into spherical structures. Within a day, the lumen sealed and the organoids grew into multi-budded structures that seemed roughly double in size every 24 hours (Figure 4.2). Additionally, due to continuous budding events and epithelial turnover, the organoid lumen starts to fill with dead cells and as a consequence gets darker at day 4 or 5 post-passage (Figure 4.2).

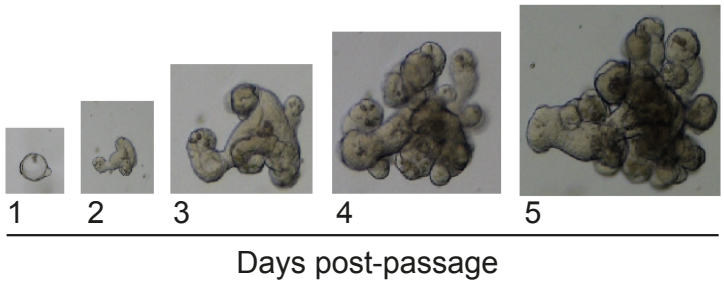

Fig. 4.2 Small intestine organoid growth

Representative images showing the progress of organoid growth. Images were taken every 24 hours from day 1 to day 5 after passage.

To further validate this *in vitro* small intestine organoid model I investigated the presence of specific specialised epithelial cell types within the cultured organoids. For that, 3 to 4 day old organoids were stained in order to identify $Lgr5^{+}$ cells (Sox9), Paneth cells (lysozyme C), enteroendocrine cells (chromogranin A) and goblet cells (Sox9, mucin 2) (Figure 4.3). Small intestine organoids showed positive staining for all markers, indicating that they encompass all the mentioned specialised cells types. $Lgr5^{+}$ cells, identified by the positive $Sox9^{high}$ staining, were consistently localised at the base of the organoid crypts (Figure 4.3A). Similarly, Paneth cells, identified by positive lysozyme C staining, were also localised at the base of the crypts (Figure 4.3B). The same was observed for enteroendocrine cells, stained for chromogranin A (Figure 4.3C). Goblet cells were specifically stained with anti-mucin 2 antibody, however, they also expressed $Sox9^{low}$. These were spread along the crypt and villous domains of the small intestine organoid (Figure 4.3D). Staining for F-actin with

phalloidin and cell nuclei with DAPI revealed that organoids were organised in a single cell layer (Figure 4.3).

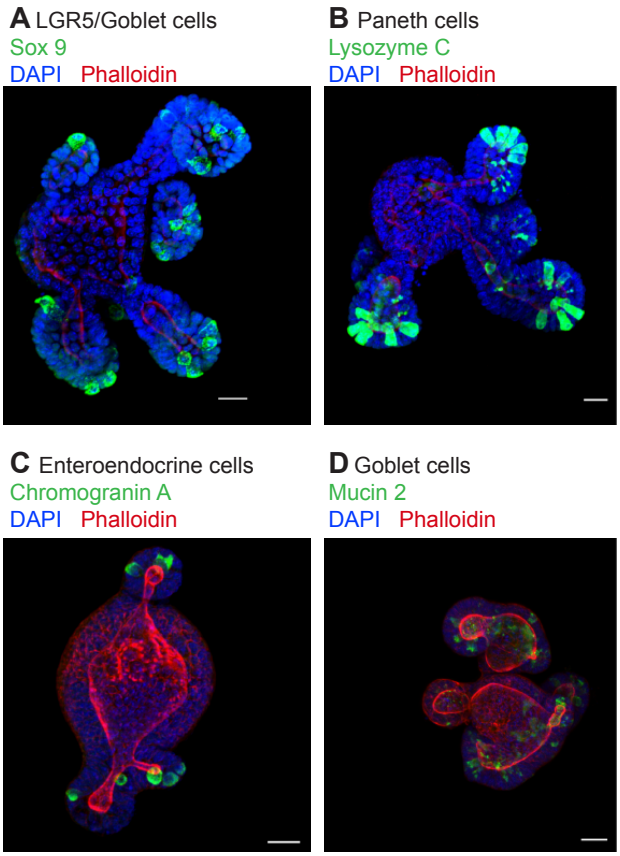

Fig. 4.3 Small intestine organoids: cellular characterisation

Immunofluorescence staining of (A) $Sox9^+$ LGR5+ cells and $Sox9^+$ goblet cells, (B) Lysozyme C^+ Paneth cells, (C) Chromogranin A^+ enteroendocrine cells and (D) Mucin 2^+ goblet cells. DAPI, blue and Phalloidin, red. Scale bar = 30 µm

Altogether, the results showed that small intestinal organoids are complex structures with close parallels to their *in vivo* counterparts. By displaying self-renewing capabilities and a close resemblance to the *in vivo* crypt-villi architecture, they present many advantages for the study of host-pathogen and cell-cell interactions.

4.3 Optimisation of small intestine organoid culture conditions

As stated earlier, the organoid model I established was based on the method described by Sato and colleagues [16]. Nonetheless, in order to achieve a more efficient culture system for the study of infection at the intestinal epithelial barrier, I decided to optimise some of the culture parameters, starting with the matrigel density.

4.3.1 Optimisation of matrigel concentration

Matrigel, a commercial formulation, contains proteins essential for the development of organoids, as laminin; moreover, it provides a structural scaffold for the three-dimensional growth of organoids. Knowing this, I decided to test increasing concentrations of matrigel, ranging from 20% to 90%. Organoids were passaged and the same cellular suspension was divided into four tubes. The organoids were then re-suspended in 20%, 50%, 70% or 90% matrigel, respectively. Small intestine organoid growth was recorded every 24 hours by bright field imaging and organoid surface area (Figure 4.4) or phenotype (Figure 4.5) was determined using Fiji software.

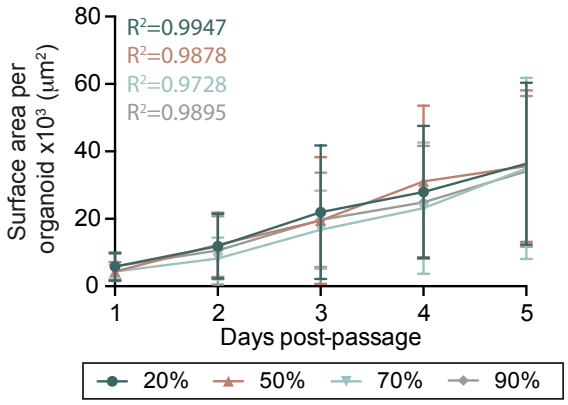

Fig. 4.4 Small intestine organoids surface area: optimisation of the matrigel concentration

Small intestine organoids were seeded in 20% (green), 50% (orange), 70% (blue) or 90% (grey) matrigel. The surface area of 100 organoids from two technical replicates was determined. Mean (± SD) and linear regression were plotted. Data are representative of two independent experiments.

Independently of the matrigel concentration, small intestine organoids displayed an exponential growth over 5 days in culture. Organoid surface area was similar among the different conditions tested (Figure 4.4).

Next, based on the number of buds, small intestine organoids were classified into 4 groups: (i) cysts (no buds); (ii) organoids with 1 or 2 buds; (iii) organoids with 3 to 6 buds; (iv) organoids with more than 6 buds (Figure 4.5).

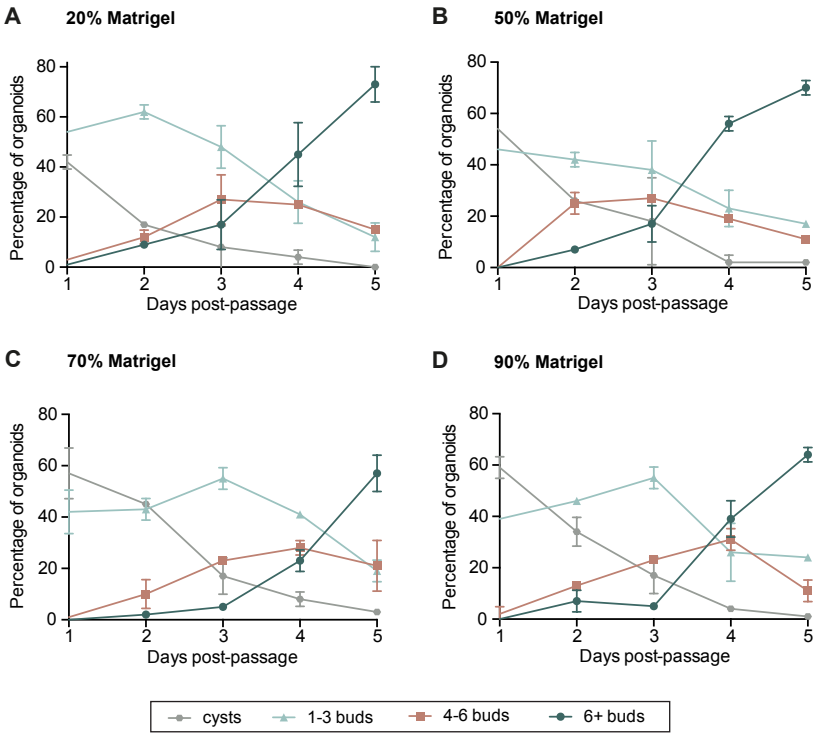

Fig. 4.5 Phenotypical characterisation of small intestine organoids: optimisation of the matrigel concentration

Small intestine organoids were seeded in 20%, 50%, 70% or 90% matrigel. For each condition, 100 organoids were classified as follows: cysts (grey); organoids with 1 or 2 buds (blue); organoids with 3 to 6 buds (orange); organoids with more than 6 buds (green). The results are presented as mean (± SD). Data are representative of two independent experiments.

As expected, the results showed a reduction in the number of cysts over time, whereas the number of multi-budded organoids increased (Figure 4.5). Specifically, at day 1 post-passage, small intestine organoids that were seeded in 20% matrigel showed 42% of cysts and 54% of organoids with 1 to 2 buds. However, at day five no cysts could be found and only 12% of organoids showed a phenotype with 1 to 2 buds. In contrast, the number of organoids with more than 6 buds increased from 1% to 73% from day 1 to day 5 post-passage (Figure 4.5A; Supplementary Table A.1). The same trend was observed when organoids were seeded in higher concentrations of matrigel. (Figure 4.5; Supplementary Tables A.2, A.3 and A.4).

Nonetheless, from day 3 post-passage, there was a sharp increase in the number of organoids with more than 6 buds for all tested conditions (Figure 4.5).

In conclusion, these data sets showed no major differences in the development of organoids under different concentrations of matrigel. However, at day five post-passage, multi-budded organoids organoids seeded in 20% matrigel displayed large dark centres and the majority of their lumina had burst (Figure 4.6A). Organoids seeded in 50%, 70% or 90% matrigel presented dark centres but generally their lumina had not burst and their morphology was distinct (Figure 4.6).

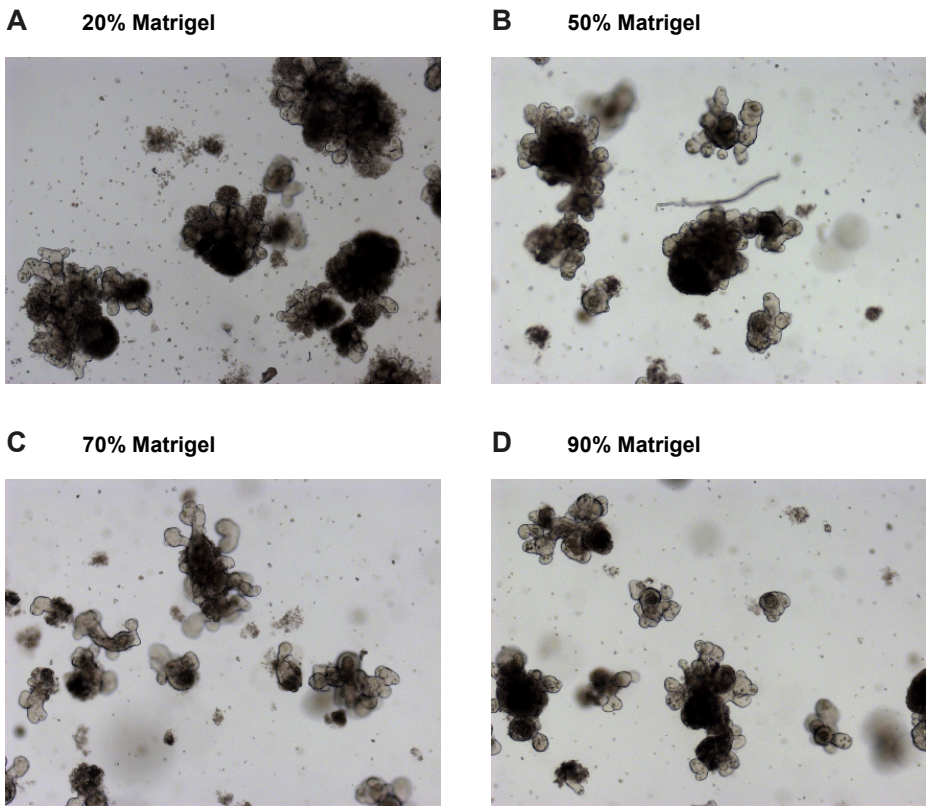

Fig. 4.6 Small intestine organoids: optimisation of the matrigel concentration

Representative brightfield images of 5 day old small intestine organoids seeded in (A) 20%, (B) 50%, (C) 70% or (D) 90% matrigel. Images are representative of two independent experiments.

4.3.2 Optimisation of R-spondin 1 supernatant concentration

R-spondin 1 plays an important role in maintaining a 'stemness' profile in intestinal epithelial cells, and therefore it is a crucial growth factor for the maintenance of small intestine organoids. Having established the small intestine organoid culture system using recombinant human R-spondin 1, a R-spondin 1 producing cell-line, 293T-HA-RspoI-Fc, was acquired (from Calvin Kuo, Stanford Univ., USA). The use of R-spondin 1 supernatant would allow me to expand the small intestine organoid cultures while reducing the cost associated with it. In order to transition from the recombinant human R-spondin 1 to the R-spondin 1 supernatant, a series of tests were performed to ensure that the properties of the small intestine organoids remained unaltered. Therefore, organoids were seeded in 50% matrigel and the complete organoid medium supplemented with 10% or 20% R-spondin 1 supernatant. As described before, organoids were imaged every 24 hours, from day 1 to day 5 post-passage. The organoid area and phenotype were determined using Fiji software (Figure 4.7).

The data showed no differences in the organoid surface area in organoids grown using R-spondin supernatant compared to those growing using recombinant R-spondin (Figure 4.7A). Furthermore, no differences were observed in the organoid development over time, as the phenotypes of small intestine organoids grown in 10% or 20% R-spondin 1 supernatant were identical to each other. Additionally, organoids had comparable dark centres, which could be an indication that cell turnover is also similar (Figure 4.8). Finally, small intestine organoids have also exhibited all the major specialised epithelial cells populations: stem cells, Paneth cells, goblet cells and enteroendocrine cells (data not shown).

These results suggest that small intestine organoids seeded in 500 ng/ml of recombinant human R-spondin 1 and 10% or 20% R-spondin 1 supernatant are comparable. Thus, unless stated otherwise, in the experiments that follow, all small intestine organoid cultures were supplemented with 10% R-spondin 1 supernatant.

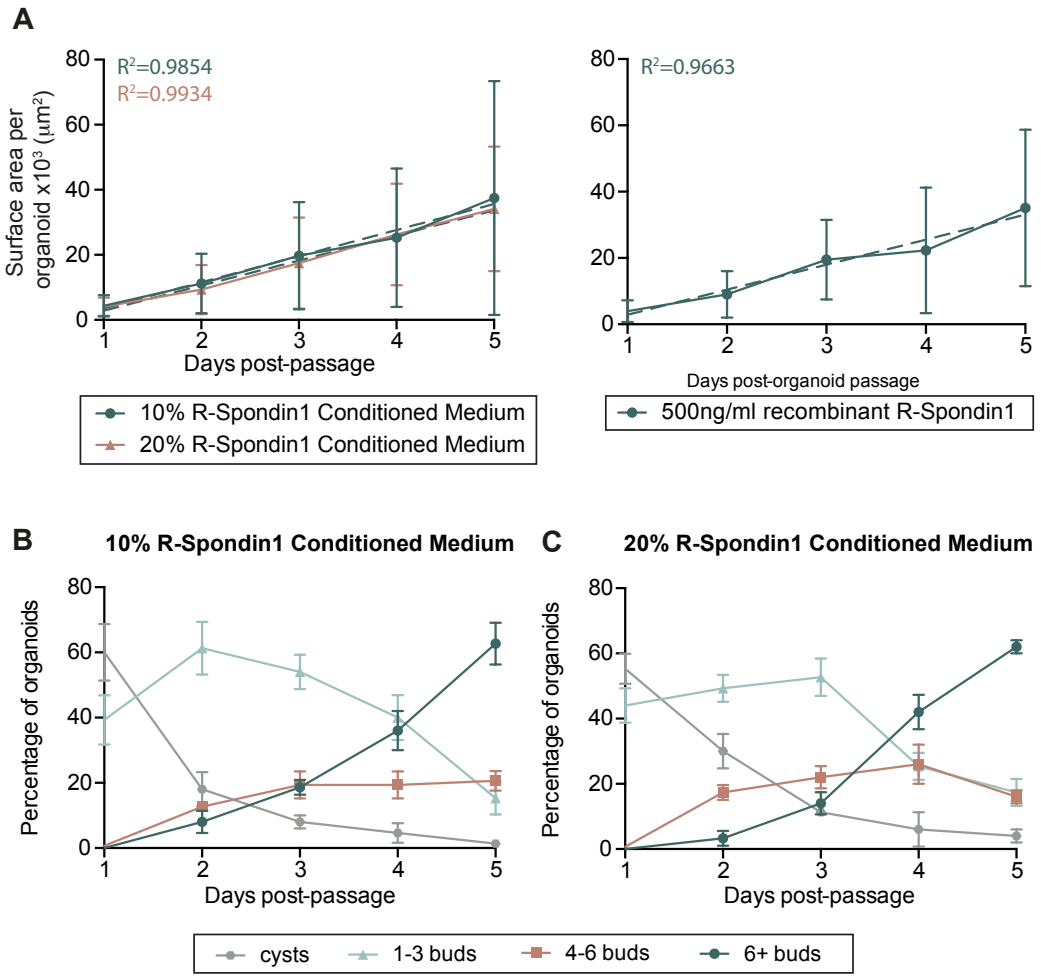

Fig. 4.7 Phenotype characterisation of small intestine organoids: optimisation of R-Spondin 1 supernatant concentration

(A) Small intestine organoids were seeded in 10% (green) or 20% (orange) R-Spondin 1 supernatant. The surface area of 150 organoids from three technical replicates was determined. Mean (± SD) and linear regression were plotted. (B-C) Small intestine organoids were seeded in 10% or 20% R-Spondin 1 supernatant. For each condition, 150 organoids were classified as follows: cysts (grey); organoids with 1 or 2 buds (blue); organoids with 3 to 6 buds (orange); organoids with more than 6 buds (green). Results are expressed as mean (± SD). Data are representative of two independent experiments.

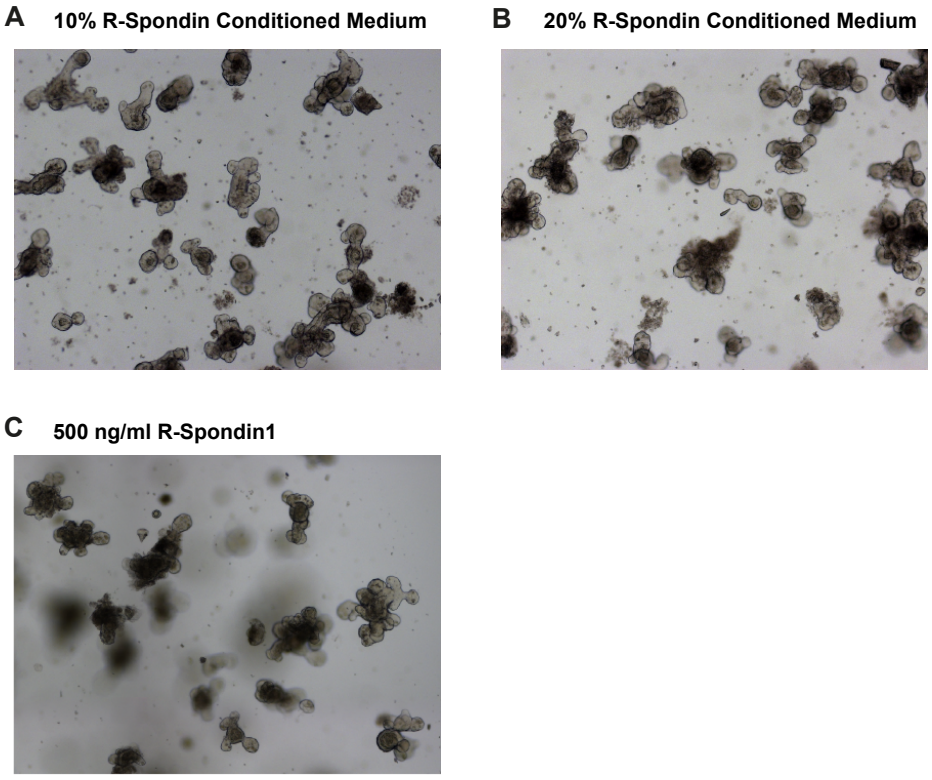

Fig. 4.8 Small intestine organoids: optimisation of the R-spondin 1 supernatant concentration

Representative brightfield images of 4 day-old small intestine organoids seeded in (A) 10% R-spondin 1 supernatant (B) 20% R-spondin 1 supernatant (C) 500 ng/ml of human recombinant R-spondin 1. Images are representative of two independent experiments.

4.4 Establishment of an *Eimeria spp.*-infected small intestine organoid model

As shown in the previous chapter, at day 3 or 4 post-passage, organoids show a crypt-villi three-dimensional structure, in which the major specialised intestinal epithelial cells are represented. Thus, to use organoids as a recipient model for parasite infection, I let them grow for at least 3 days post-passage. To establish the co-culture protocol, *E. vermiformis* was used as an infectious agent. Small intestine organoids would be expected to provide *E. vermiformis* environment for infection matched to its natural intestinal site, as *E. vermiformis* is known to specifically infect the lower 2/3 of the small intestine *in vivo* [129][178].

For all the tested protocols, *E. vermiformis* sporozoites were freshly isolated on the infection day, and their viability was higher than 90%. Our first protocol was based on those described by Rose *et al.* and Stange *et al.* [147, 110]. Thus, 100,000 *E. vermiformis* sporozoites were added per well to 3 to 4 day-old small intestine organoids (Figure 4.9A). After 4 hours of incubation, the sporozoite-containing medium was removed, organoids were washed with PBS and fresh complete organoid medium was added to the wells (Figure 4.9B). *E. vermiformis*-infected small intestine organoids were fixed at 4 and 21 hours post-infection, stained and analysed by immunofluorescence.

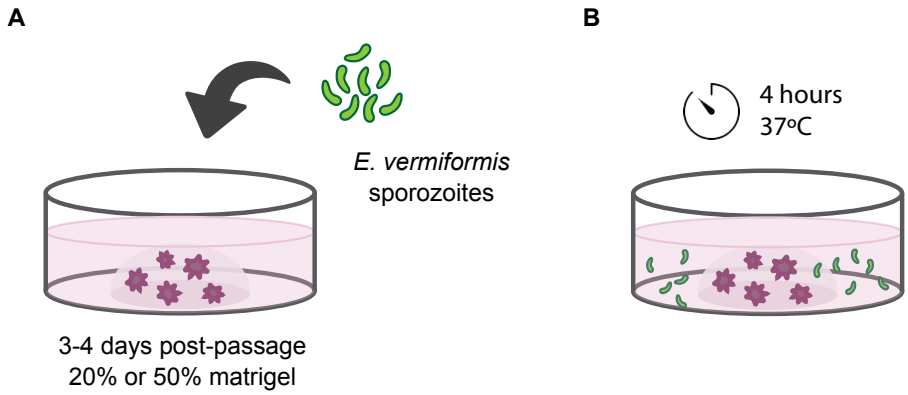

Fig. 4.9 *E. vermiformis*-infected small intestine organoids: Protocol 1

Even though there were occasional organoids infected at 4 hours post-incubation, there were consistently no intracellular parasites at 21 hours post-incubation. Since *E. vermiformis* successfully invades cell lines with this protocol, the lack of infection of small intestine organoids led us to hypothesise that motile *E. vermiformis* sporozoites were incapable of effectively moving through the scaffold of the matrigel, which, typically, is not present in the two-dimensional cell cultures. In order to overcome this limitation, we repeated the same protocol, however this time we seeded small intestine organoids in 20% matrigel, for comparison with 50% matrigel (Figure 5.1). *E. vermiformis*-infected small intestine organoids were fixed at 4 and 21 hours, stained and analysed by immunofluorescence.

The results obtained with small intestine organoids seeded in 20% or 50% matrigel were very similar. Infected organoids seeded in 20% matrigel showed an occasional invasion of 1 to 2 organoids per well, mostly the ones located at the edge of the matrigel droplet. Nevertheless, no infected organoids were seen at 21 hours post-incubation.

We wanted to investigate further the hypothesis that matrigel is limiting the accessibility of *E. vermiformis* sporozoites to the small intestine organoids. It is known that, besides providing structural support for growth, matrigel also contains proteins that are crucial for the development of the organoids. In order to avoid complete matrigel deprivation to the small intestinal organoids, in the next protocol I recovered and washed 3 to 4 days-old small intestine organoids (Figures 4.10A and 4.10B), which were then seeded on the top of a 'thin' matrigel layer, that had been previously polymerised for 15 minutes at 37º C. This polymerisation step was designed to allow organoids to remain on top of the matrigel layer, thus diminishing the sinking effect. This approach would allow the organoids to be in direct contact with both the matrigel and the parasite. Subsequently, 100,000 *E. vermiformis* sporozoites per well were mixed with fresh complete organoid medium and added to the top of the organoids (Figure 4.10C). Medium was renewed after 4 hours (Figure 4.10D). *E.*

vermiformis-infected small intestine organoids were fixed at 4 and 21 hours, stained and analysed by immunofluorescence.

The data showed that after 4 hours of incubation, organoids seeded on the top of the matrigel layer had lost their structure and were becoming flat. At 21 hours post-infection, both infected and non-infected organoids were dead.

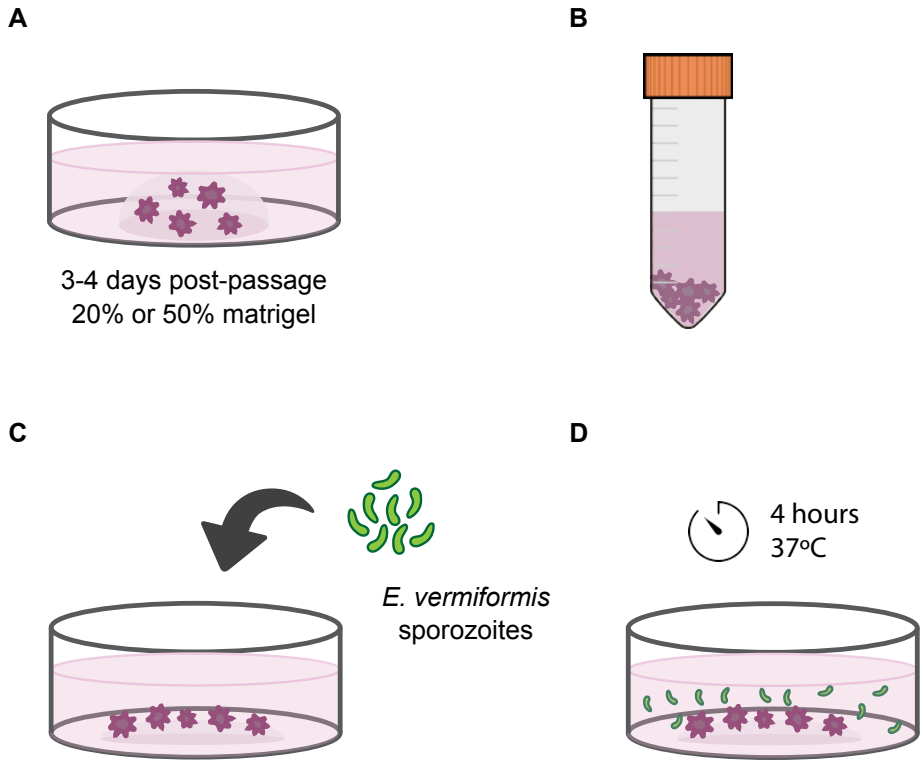

Fig. 4.10 *E. vermiformis*-infected small intestine organoids: Protocol 2

To explore further the hypothesis that matrigel is restricting the access of *E. vermiformis* sporozoites to the small intestine organoids, we injected 100,000 *E. vermiformis* sporozoites into the matrigel droplet, hence increasing the chance of close contact between the parasite and the host cells. This experiment was performed with 3 to 4 day-old small intestine organoids seeded in 20% or 50% matrigel, to test different matrigel resistance and fluid retention (Figure 4.11). This technique proved to be quite challenging, as the injectable volume of sporozoite suspension without disrupting the matrigel droplet was limited to less than 50 μl. *E. vermiformis*-infected small intestine organoids were fixed at 4 and 21

hours, stained and analysed by immunofluorescence. Still, it was observed that the infection efficiency had not been improved. The results, together with the reproducibility issues that arose from the technical challenges of the protocol, motivated me to identify a more suitable option.

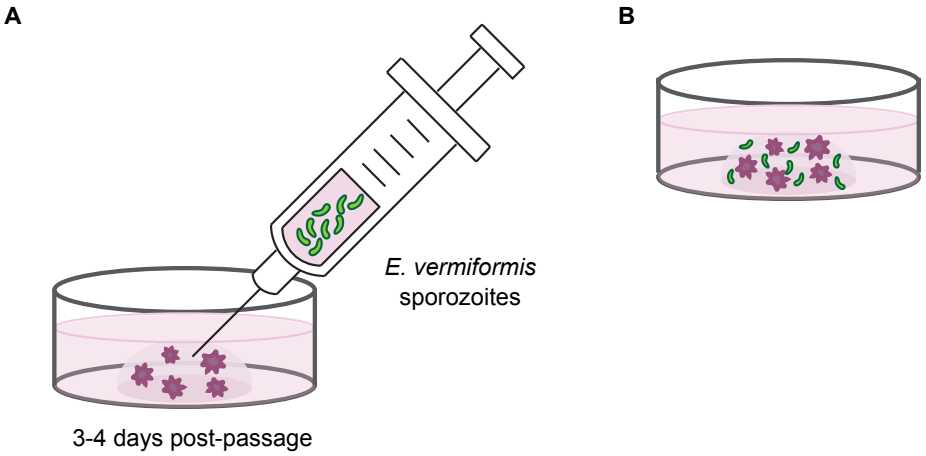

Fig. 4.11 *E. vermiformis*-infected small intestine organoids: Protocol 3

Next, I decided to completely isolate small intestine organoids from the matrigel and, in the absence of matrigel, submit the organoid suspension to a short incubation in complete medium with *E. vermiformis*. I recovered 3 to 4 day-old small intestine organoids which were incubated in cell recovery solution (BD Biosciences #354253) for 1 hour, on ice, to completely digest the matrigel. Organoids were washed and resuspended in complete organoid medium containing *E. vermiformis* sporozoites, plated in a 6 well-plate and incubated for 30 minutes at 37º C (Figure 4.12).

Following the 30-minute incubation, most of organoids were dead, including the non-infected controls. Thus, we concluded that organoid death was induced by the lack of matrigel.

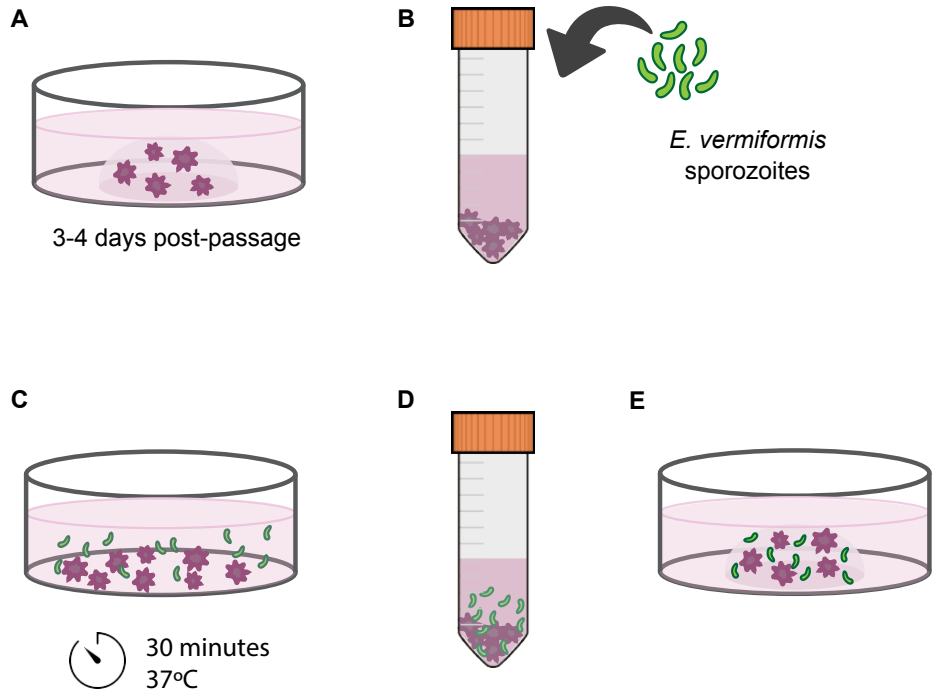

Fig. 4.12 *E. vermiformis*-infected small intestine organoids: Protocol 4

We then tried two additional approaches: i) injecting *E. vermiformis* sporozoites into the lumen of the organoids or ii) optimising the previous protocol, by submitting organoids to *E. vermiformis* infection in the absence of matrigel for a shorter period of time.

Injecting *E. vermiformis* sporozoites directly into the lumen of the small intestine organoids would mimic the *in vivo* conditions of infection. Physiologically, sporozoites are discharged into the lumen of the small intestine and attach to the epithelial cells through their apical side [146]. Microinjection with commercially available needles was not possible, as the sporozoites are 15 μm in length, which is bigger that the largest diameter available. Therefore, we used a FemtoJet with custom-made needles. Organoids were seeded on a coverslip post-passage. A coverslip carrying 6 to 7 day-old organoids was placed under a microscope, allowing us to trace the position of the needle in relation to the organoid. Approximately 7-9 *E. vermiformis* sporozoites were injected into the lumen of each organoid and at least 10 organoids were infected per coverslip (Figure 4.13). After injection, the organoids kept their structural organisation even though their lumens were slightly expanded.

E. vermiformis-infected small intestine organoids were fixed at 4 and 21 hours, stained and analysed by immunofluorescence.

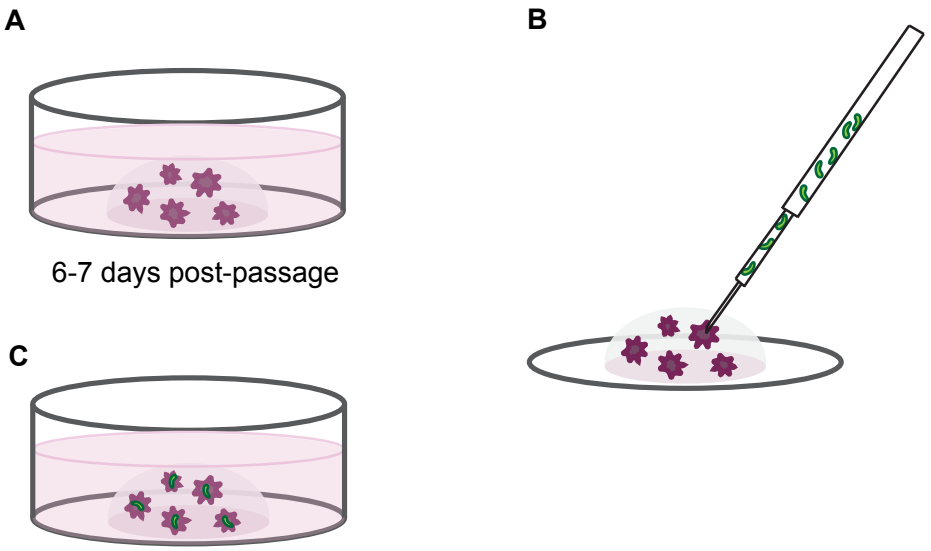

Fig. 4.13 *E. vermiformis*-infected small intestine organoids: Protocol 5

My analysis protocol was not suitable for organoids older than 6 days. After 6 days in culture, small intestine organoids can grow up to 200 μm in diameter and their lumens become dense. Even though RIMS medium was used as a clearing solution, the increase in the depth of the field gained was not sufficient to scan the whole organoid. Nevertheless, I proceeded with my analysis, even though the readout was slightly compromised. However, no infected organoids could be observed.

Due to the potential failure of infection, the technical complexity of the protocol and the limitations in the read-out and analysis, I decided to use a different approach.

Simultaneously with the protocol previously described, I had attempted to optimise the infection protocol in the absence of matrigel. Thus, 3 to 4 day-old small intestine organoids were recovered and homogenised by repeated aspiration with a 21 G needle (Figure 4.14A and 4.14B). By doing so, the matrigel scaffold was disintegrated while the organoids were slightly broken in order to expose their lumen. Then, organoids were washed in PBS until no traces of matrigel were observed, resuspended in basal medium containing *E. vermiformis*

sporozoites and incubated at 37°C for 5 min (Figure 4.14C). Upon incubation, infected organoids were washed, resuspended in 50 % matrigel and seeded into 8-well ibidi slides. After a 15-min incubation to allow matrigel polymerisation, 250 μl of complete organoid medium was added to each well (Figure 4.14D). *E. vermiformis*-infected small intestine organoids were fixed at 4, 21 and 45 hours, stained and analysed by immunofluorescence.

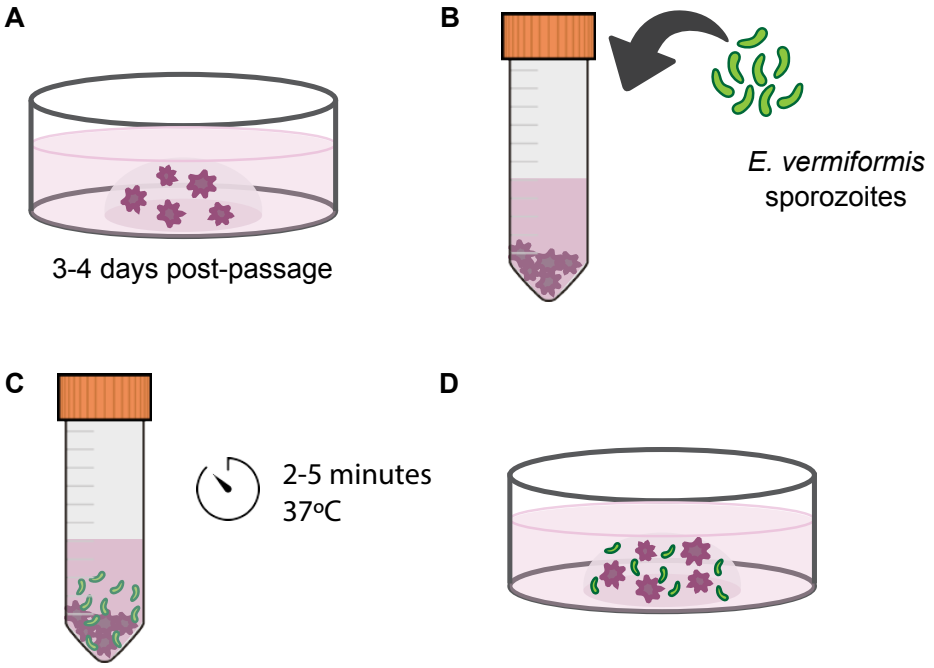

Fig. 4.14 *E. vermiformis*-infected small intestine organoids: Protocol 6

Immunofluorescent analysis showed that following this time point, at least 50% of the small intestine organoids were infected with *E. vermiformis* sporozoites at 4 hours post-infection. Even though the ratio of infection is lower at 21 or 45 hours post-infection than at 4 hours post-infection, organoids remain infected, showing progression of *E. vermiformis* development into first generation schizonts. *E. vermiformis* life cycle progression in small intestine organoids will be further described later in this chapter.

Altogether, these observations indicate that the presence of matrigel limits the invasion capacity of *E. vermiformis* sporozoites presumably by restricting their access to the small intestine organoids. To further understand how to increase the *E. vermiformis* infection

efficiency and how to manipulate the established infection model, I next performed a series of experiments to study different protocol variables.

4.5 Optimisation of small intestine organoid and *E. vermiformis* co-culture

Having established a reproducible protocol to study interactions between *E. vermiformis* and intestinal epithelial cells, I went on to investigate and optimise the different variables of the protocol.

4.5.1 Optimisation of small intestine organoid size prior to infection

I started by analysing how the initial size of the small intestine organoids influences the effectiveness of invasion by sporozoites and subsequent infection. For that, I recovered 3 to 4 day-old organoids that were divided into two cell suspensions, one of which was homogenised with a 21 G needle and the other with a 25 G needle, in both cases attached to a 20 ml syringe. The syringe was filled and emptied three times with the organoid suspension. As expected using a 25 G needle, organoids were broken into considerably smaller fragments when compared to the homogenised product of a 21 G needle. These two cell suspensions were incubated with 100,000 *E. vermiformis* sporozoites per 100 organoids for 5 minutes, washed and resuspended in 50% matrigel and 25 μl droplets of suspension were then plated. *E. vermiformis*-infected small intestine organoids were fixed at 4 and 21 hours post incubation, stained and the efficiency of infection was quantified by immunofluorescence. As described before, the use of a 21 G needle to homogenise organoids prior to infection maintains the organoid structural organisation while exposing its lumen. This seems to be favourable to an effective *E. vermiformis* infection. In contrast to this observation, when we used a 25 G needle, organoids were broken into small fragments, sometimes single cells, consequently leading to a considerable reduction in the number of viable organoids. Thus, this was proved to be an inefficient approach, as only occasional organoids were infected at 4 hours post-infection and infected organoids were not observed at 21 hours post-infection (data

not shown). These results suggest that a 21 G needle homogenises organoids to an optimal experimental size, allowing for an effective *E. vermiformis* infection and a quick organoid recovery from the stress induced by the incubation step in the absence of matrigel. Therefore, unless stated otherwise, organoids were homogenised with a 21 G needle in the following experiments.

4.5.2 Optimisation of small intestine organoid co-culture time

One of the key variables in the successful establishment of *E. vermiformis* infected organoids is the co-culture incubation period. This step is of crucial importance, as organoids will be under stress due to the lack of matrigel. Thus, we evaluated the impact of different incubation times, both at the level of organoid distress and infection efficiency. After being homogenised, 3 to 4 days-old small intestine organoids were incubated at 37º C in a ratio of 100,000 *E. vermiformis* sporozoites to 100 organoids. These were incubated for 5 or 10 minutes and time points were collected at 4, 21 and 45 hours post infection. Samples were analysed by immunofluorescence (Figure 4.15).

The data showed that at 4 and 21 hours both the number of intracellular *E. vermiformis* per organoid (Figure 4.15A) and the percentage of infected organoids (Figure 4.15B) were higher when organoids were incubated with *E. vermiformis* sporozoites for 10 minutes. However, these differences were no longer seen at 45 hours post-infection. Given that a longer incubation period without matrigel induces higher levels of stress to the organoids, it was determined that during the subsequent experiments the incubation period would be restricted to 5 minutes.

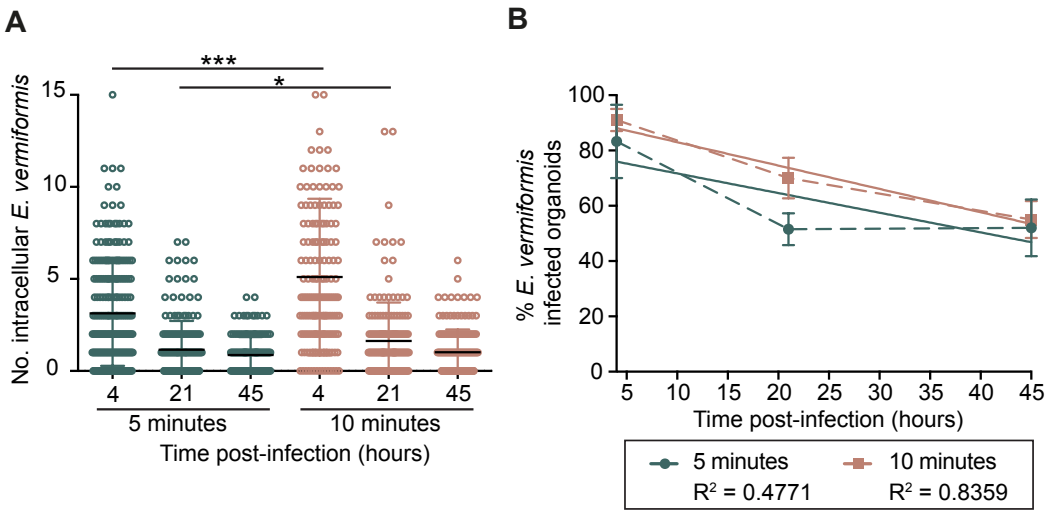

Fig. 4.15 *E. vermiformis* sporozoite invasion is influenced by the duration of the incubation period but without impact on long-term infection efficiency

Small intestine organoids were recovered at day 3 post-passage and were incubated with *E. vermiformis* sporozoites for 5 (green) or 10 (orange) minutes in basal medium at 37°C. Infected organoids were seeded in 25 μl droplets of 50% matrigel and cultured in complete organoid medium. (A) The number of intracellular *E. vermiformis* sporozoites per organoid was quantified by immunofluorescence at 4, 21 and 45 hours post-infection. Scatter plots display mean (± SD). Significance was determined by unpaired *t* test with Welch's correction. (B) The percentage of infected organoids was also determined. Mean (± SD) and linear regression were plotted. * P<0.05 *** P<0.0001. Data pooled from 2 independent experiments.

4.5.3 Optimisation of the initial infection dose of *E. vermiformis*

To further optimise our intestinal epithelial infection model, I investigated if reducing the ratio of *E. vermiformis* sporozoites to organoids would be beneficial. The first approach consisted in studying the impact of a initial dose of *E. vermiformis* infection of 12,500 or 25,000 sporozoites to 100 small intestine organoids (Figure 4.16). Compared to the initial ratio of infection, these initial doses of infection represented decreases of 87.5% and 75%, respectively. Due to the considerably lower number of parasites, I decided to test how an incubation period of 5 or 10 minutes would impact the outcome of the experiment

(Figure 4.16). *E. vermiformis*-infected small intestine organoids were fixed at 4 and 21 hours post-incubation, stained and the infection efficiency was quantified by immunofluorescence.

The data showed that even with an initial dose of *E. vermiformis* infection of 12,500 or 25,000, the incubation period does not lead to significant differences in the outcome of infection (Figure 4.16A and 4.16B). Additionally, it was observed that an initial dose of *E. vermiformis* infection of 12,500 *E. vermiformis* sporozoites to 100 organoids led to 0-10% infected organoids at 45 hours post-infection. (Figure 4.16C). In contrast, with an initial dose of *E. vermiformis* infection of 25,000 sporozoites to 100 organoids, it was observed that 52-60% of organoids were infected, with an average of 1.09 *E. vermiformis* sporozoites per organoid at 4 hours post-infection (Figure 4.16B and 4.16D). However, at 21 and 45 hours post-infection, the average number of parasites per organoid drops significantly from 1.09 to 0.31 and 0.46 (Figure 4.16B), respectively, accompanied by a decrease in the percentage of infected organoids to 26-34% (Figure 4.16D). Because there is a decrease in both the number of parasites per organoid and the percentage of organoids infected from 4 to 21 hours post infection, and because the infection seems to stabilise at 45 hours, which corresponds to the *E. vermiformis* first generation schizonts, it is safe to assume that at this stage the *E. vermiformis* infection is well established. Thus, I decided to employ 45 hours post-infection as a reference time point for the effectiveness of infection.

It was intended to apply this model to study how different proteins impact the small intestine organoids responses to infection, and this could involve either limiting or exacerbating the outcome of infection. In order to see both effects I decided to further optimise the infection dose of *E. vermiformis* sporozoites to small intestine organoids and aim for 50% of infected organoids at 45 hours post-infection. As shown before in Figure 4.16D, an initial dose of *E. vermiformis* of 25,000:100 would give a maximum of 34% infected organoids at 45 hours post-infection. Therefore, I tested higher doses of *E. vermiformis* infection, specifically 100,000 or 200,000 *E. vermiformis* sporozoites to 100 small intestine

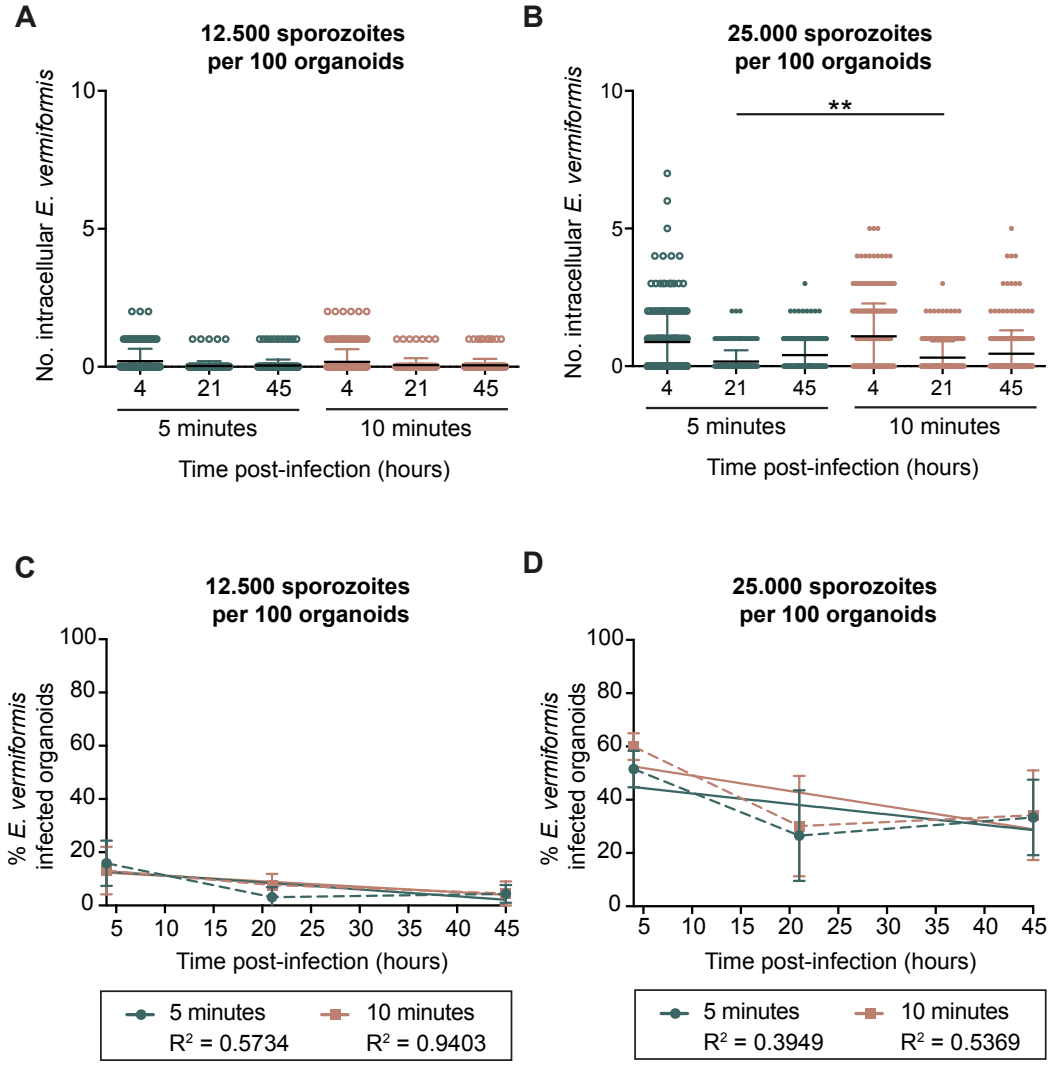

Fig. 4.16 *E. vermiformis* infection efficiency is impacted by the initial co-culture ratio of sporozoites per organoids

Small intestine organoids were recovered at day 3 post-passage and co-cultured with 12,500 (A, C) or 25,000 (B, D) *E. vermiformis* sporozoites per 100 organoids for 5 (green) or 10 (orange) minutes in basal medium at 37° C. Infected organoids were seeded in 25 μl droplets of 50% matrigel and cultured in complete organoid medium. The number of intracellular *E. vermiformis* sporozoites per organoid was quantified by immunofluorescence at 4, 21 and 45 hours post-infection (A, B). Scatter plots display mean (± SD) Significance was determined by unpaired *t* test with Welch's correction. The percentage of infected organoids was also determined (C, D). Mean (± SD) and linear regression were plotted. ** P<0.01. Data were pooled from 2 independent experiments.

organoids (Figure 4.17). *E. vermiformis*-infected small intestine organoids were fixed at 4, 21 and 45 hours post-incubation, stained and the infection efficiency was quantified by immunofluorescence.

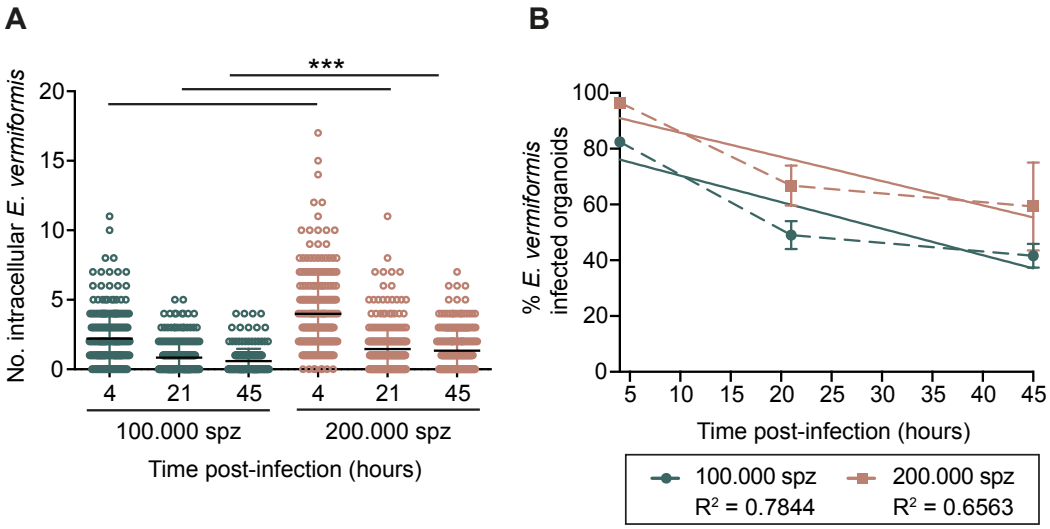

Fig. 4.17 *E. vermiformis* infection efficiency is impacted by the initial co-culture ratio of sporozoites per organoids

Small intestine organoids were recovered at day 3 post-passage and then co-cultured with 100,000 (green) or 200,000 (orange) *E. vermiformis* sporozoites per 100 organoids for 5 minutes in basal medium at 37° C. Infected organoids were seeded in 25 μl droplets of 50% matrigel and cultured in complete organoid medium. (A) The number of intracellular *E. vermiformis* sporozoites per organoid was quantified by immunofluorescence at 4, 21 and 45 hours post-infection. Scatter plots display mean (± SD). Significance was determined by unpaired *t* test with Welch's correction. (B) The percentage of infected organoids was also determined . mean (± SD) and linear regression plotted. *** P<0.001. Data were pooled from 2 independent experiments. spz = sporozoites

The results showed a correlation between a higher initial dose of *E. vermiformis* and the number of sporozoites per organoid. In particular, 200,000 *E. vermiformis* sporozoites to 100 organoids led to significantly higher numbers of parasites per organoid, across all time points, when compared to a 100,000:100 ratio (Figure 4.17A). This was accompanied by a higher percentage of organoids infected over time (Figure 4.17B).

As observed with lower initial doses of *E. vermiformis* infection, there was a significant decrease in the number of parasites per organoid from 4 to 21 hours post-infection (Figure

4.17A), which correlates with a decrease in the percentage of infected organoids (Figure 4.17B).

Based on my aim to get 50% infected organoids at 45 hours post-infection, we decided to use an initial infection dose of *E. vermiformis* of 100,000 sporozoites to 100 organoids in the following experiments. This would provide a baseline to enable the observation of susceptibility or protective differences induced by different treatments.

4.5.4 Optimisation of the culture medium for *E.vermiformis* invasion

Next, I decided to investigate whether the presence of Penicillin-Streptomycin (P/S) in the culture medium was limiting the invasion ability of the *E. vermiformis* sporozoites. Therefore, employing the previously established protocol, 100,000 *E. vermiformis* sporozoites per 100 organoids were incubated for 5 minutes at 37° C in the presence or absence of P/S (Figure 4.18).

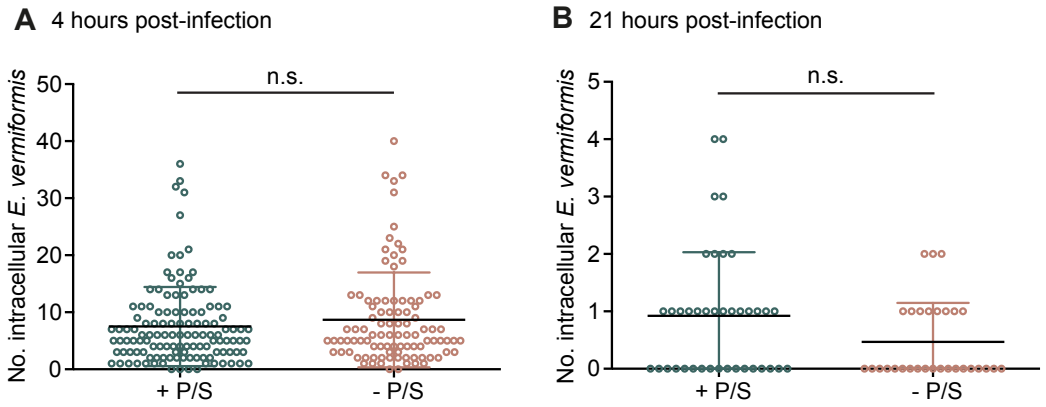

Fig. 4.18 P/S does not impact *E. vermiformis* infection efficiency

Small intestine organoids were recovered at day 3 to 4 post-passage and co-cultured with 100,000 *E. vermiformis* sporozoites per 100 organoids for 5 minutes in basal medium at 37° C in the presence (green) or absence (orange) of P/S. Infected organoids were seeded in 25 μl droplets of 50% matrigel and cultured in complete organoid medium. The number of intracellular *E. vermiformis* sporozoites per organoid was quantified by immunofluorescence at 4 (A) and 21 (B) hours post-infection. Scatter plots display mean (± SD). Significance was determined by unpaired *t* test with Welch's correction. n.s. = non-significant. Data pooled from 2 independent experiments.

The data show no significant differences in the number of intracellular parasites per organoid between the infected organoids cultured in the presence or absence of P/S, either at 4 or 21 hours post-infection (Figure 4.18A and 4.18B). Also, no differences in the percentage of infected organoids were observed (data not shown). Altogether, these results led to the conclusion that the use of P/S in culture does not influence the ability of *E. vermiformis* to infect small intestine organoids. Therefore, in the following experiments, P/S was added to the culture medium.

4.6 Asexual development of *E. vermiformis in vitro*

After testing major protocol variables (Section 4.5), it was decided to keep *E. vermiformis* infected small intestine organoids in culture for 7 days. This time corresponds to the *in vivo* pre-patent period: specifically it refers to the *E. vermiformis* life cycle development, from the point at which a sporulated oocyst is ingested by the mouse until its release as an unsporulated oocyst. Because infected organoids were kept in culture for a week, complete organoid medium was renewed every 2 to 3 days. *E. vermiformis*-infected small intestine organoids were fixed at 4, 21, 45, 69, 96, 117 and 141 hours post-incubation, stained and analysed by immunofluorescence.

It was observed that *E. vermiformis* sporozoites invaded small intestine epithelial cells at 4 hours post-infection. As observed *in vivo* [129], the intracellular sporozoites are randomly localised in the crypts or villi sections of the small intestine organoid (Figure 4.19A).

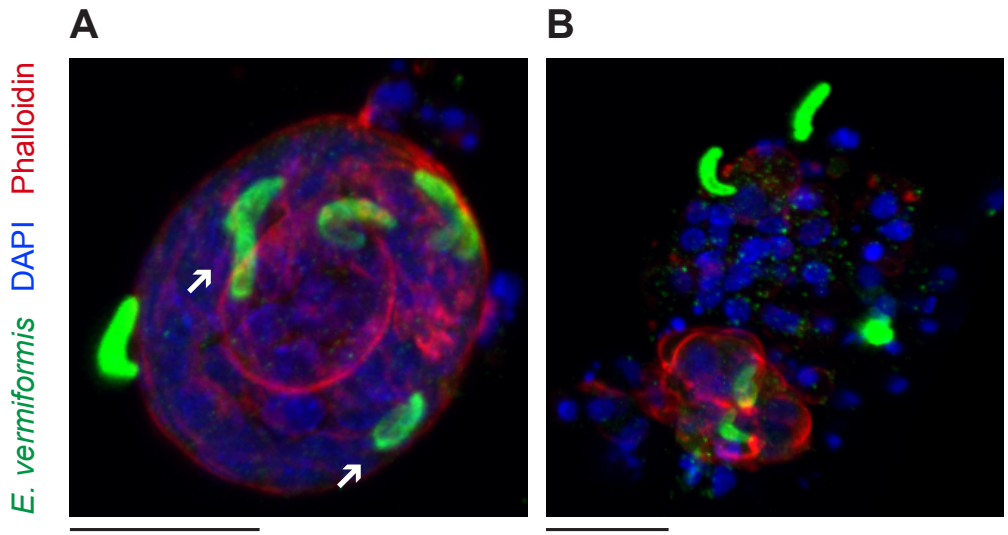

Fig. 4.19 *E. vermiformis*-infected organoids (4 hours post-infection)

Immunofluorescence z-stack of 1 μm slices of *E. vermiformis*-infected small intestine organoids. (A) Small intestine organoid infected with *E. vermiformis* sporozoites. Intracellular sporozoite starts to fold back onto itself (white arrows). (B) Dysmorphic small intestine organoid infected with *E. vermiformis* sporozoites. Scale bar = 30 μm. Figures are representative of at least three independent experiments.

Frequently, I could also observe organoids that were dysmorphic, possibly due to the stress induced during the infection (Figure 4.19B). These were often infected by multiple *E. vermiformis* sporozoites. However, these dysmorphic organoids seemed to die, possibly as a consequence of infection.

It was observed that, at 21 hours post-infection, endogenous parasites push the nuclei above, below or to the side of the cell, while sporozoites start to fold back onto themselves. In multi-budded organoids, we observed that sporozoites are mostly located at the crypt sites (Figure 4.20A). As shown before, there was a decrease in the number of intracellular parasites compared to the previous time point (Figure 4.20B).

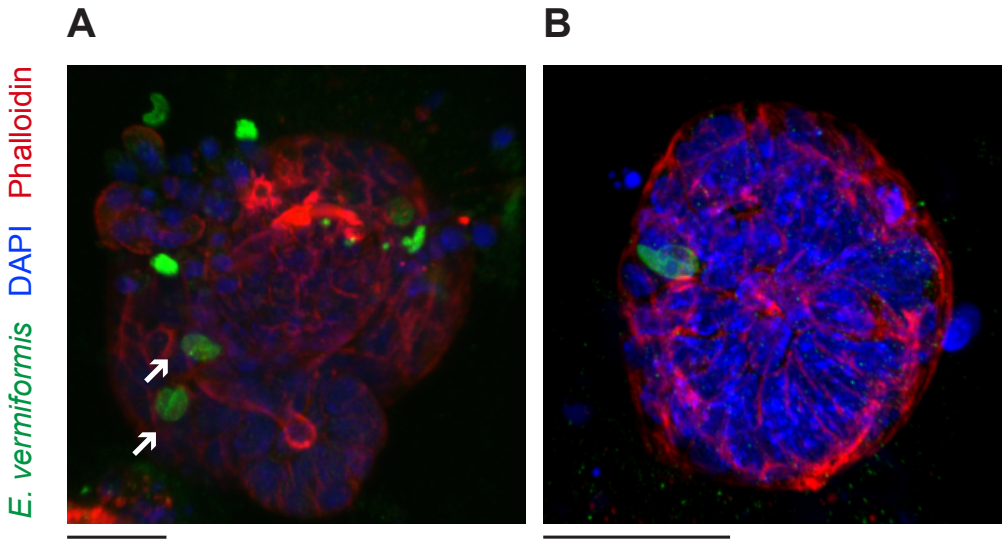

Fig. 4.20 *E. vermiformis*-infected organoids (21 hours post-infection)

Immunofluorescence z-stack of 1 μm slices of *E. vermiformis*-infected small intestine organoids. (A) Sporozoite were fold back onto themselves (white arrows) (B) *E. vermiformis* sporozoite folding back onto itself with a prominent central nucleus. Scale bar = 30 μm. Figures are representative of at least three independent experiments.

In vitro, *E. vermiformis* schizonts were observed at 45 hours post-infection (Figure 4.21). These were consistently located at the crypt sites of the small intestine organoids. Schizonts were multinucleated and found in different levels of maturation, typically only one schizont per organoid bud.

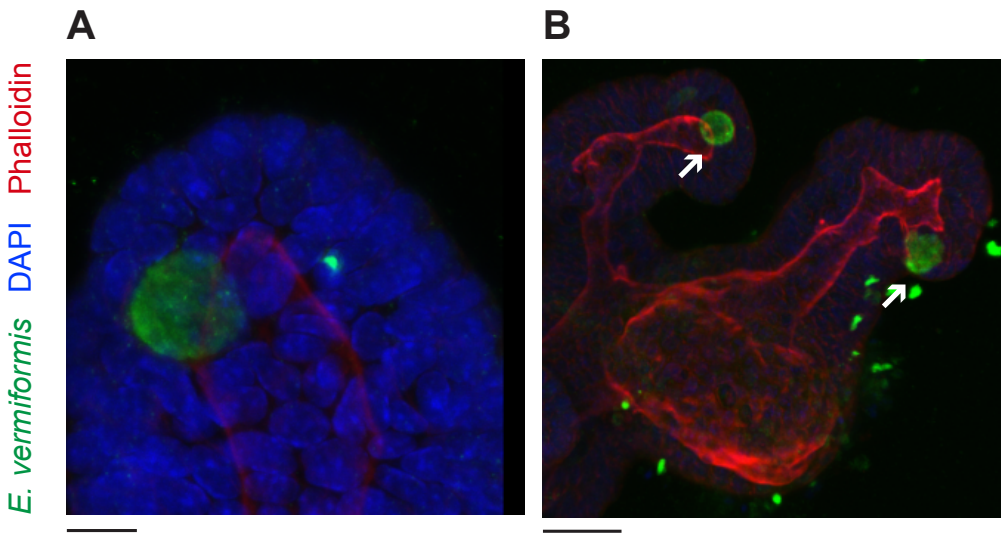

Fig. 4.21 *E. vermiformis*-infected organoids (45 hours post-infection)

Immunofluorescence z-stack of 1 μm slices of *E. vermiformis*-infected small intestine organoids. (A) Immature *E. vermiformis* schizonts (B) *E. vermiformis* are localised at the crypt site of the organoids (white arrows). Scale bar = 30 μm. Figures are representative of at least three independent experiments.

At 69 hours post-infection, we occasionally observed the first generation of merozoites, which were small and curved (Figure 4.22A). These are motile and capable of re-infecting in neighbouring epithelial cells to further evolve into second generation schizonts. These are typically organised in clusters and mostly localised at the crypt site of the small intestine organoids (Figure 4.22A). The nuclei in immature schizonts were randomly arranged, whereas in mature ones they were bigger and aligned around the periphery of the schizont (Figure 4.22B).

At 96 hours post-infection, second generation schizonts were bigger, multinucleated and mostly matured (Figure 4.23). Again, schizonts were clustered in the organoid crypts.

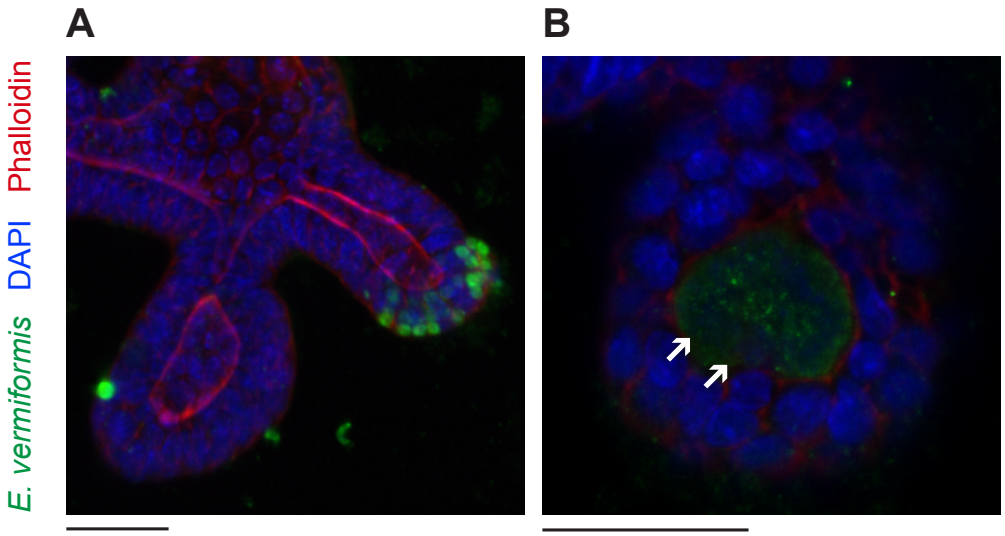

Fig. 4.22 *E. vermiformis*-infected organoids (69 hours post-infection)

Immunofluorescence z-stack of 1 μm slices of *E. vermiformis*-infected small intestine organoids. (A) Second generation *E. vermiformis* schizonts clustered at the crypt site of the organoid. (B) *E. vermiformis* mature schizont show nuclei aligned around its periphery (white arrows). Scale bar = 30 μm. Figures are representative of at least three independent experiments.

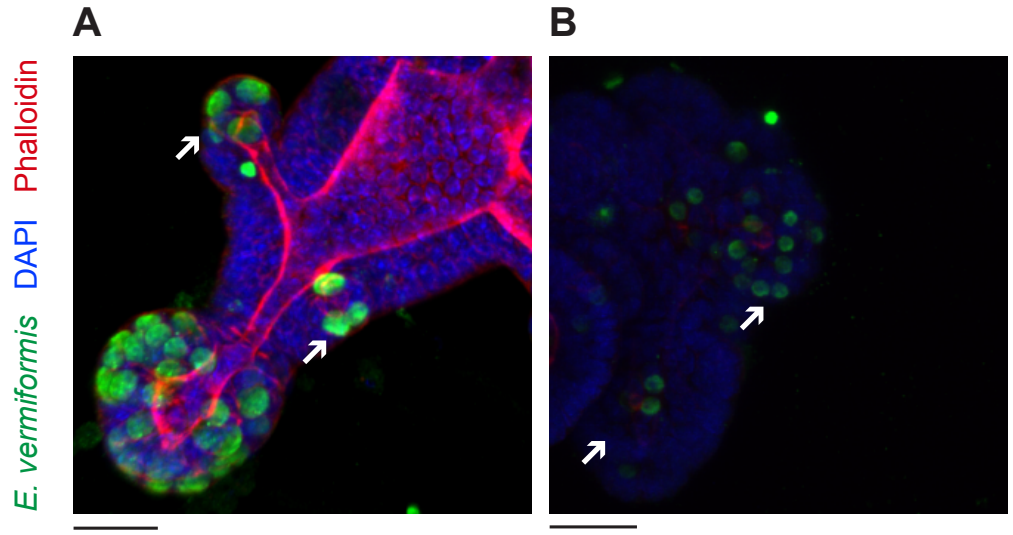

Fig. 4.23 *E. vermiformis*-infected organoids (96 hours post-infection)

Immunofluorescence z-stack of 1 μm slices of *E. vermiformis*-infected small intestine organoids. (A and B) Second-generation *E. vermiformis* schizonts are clustered at the crypt site of the organoids (white arrows). Scale bar = 30 μm. Figures are representative of at least three independent experiments.

Interestingly, at 117 hours post-infection, mature schizonts encompassing well defined merozoites were still observed. In some cases, these schizonts were observed outside the organoid, in the matrix (Figure 4.24A). Moreover, the second generation of *E. vermiformis* merozoites were observed (Figure 4.24B), which were considerably longer than the ones observed at 69 hours. These were mostly localised in the matrix and even though they are known to be motile and capable of infecting neighbouring cells, after 117 hours I could not detect the presence of intracellular parasites in the small intestine organoids.

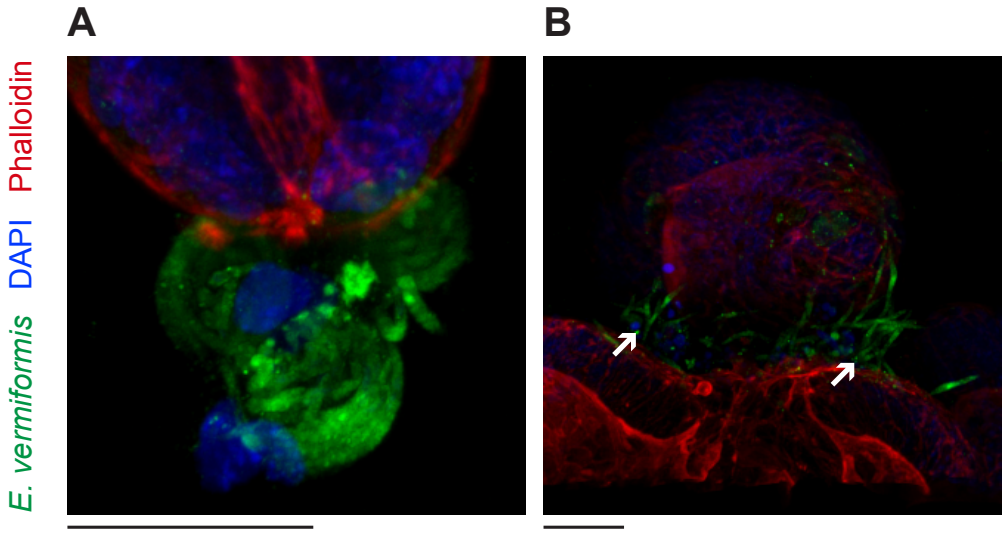

Fig. 4.24 *E. vermiformis*-infected organoids (117 hours post-infection)

Immunofluorescence z-stack of 1 μm slices of *E. vermiformis*-infected small intestine organoids. (A) Mature second generation *E. vermiformis* extracellular schizonts. (B) Second-generation *E. vermiformis* merozoites (white arrows). Scale bar = 30 μm. Figures are representative of at least three independent experiments.

Altogether, these data show that *E. vermiformis* sporozoites were able to infect small intestine organoids epithelial cells and successfully replicate at least two rounds of asexual development.

4.7 Optimisation of the initial infection dose of *E. falciformis*

Having established a reliable system to study asexual stages of *E. vermiformis* infection *in vitro*, I asked whether the same protocol would work with a different *Eimeria spp.*, specifically *E. falciformis*, which *in vivo* infects epithelial cells from the colon and caecum.

Variables of the protocol that are directly related to reducing organoid stress, such as the organoid stage of development, the homogenisation process and the time of incubation, were kept as previously defined. Specifically, 3 to 4 day-old organoids were recovered and homogenised with a 21 G needle; the co-incubation period of *E. falciformis* with small intestine organoids was kept under 5 minutes. Thus, I proceeded with the optimisation of the initial infection dose of *E. falciformis* to small intestine organoids, and the study of P/S influence in the process of *E. falciformis* invasion.

Three *E. falciformis* doses of infection were tested, specifically 500, 2,500 or 5,000 sporozoites per 100 small intestine organoids, in the presence or absence of P/S (Figure 4.25). After a 5 minute incubation at 37º C, infected organoids were washed and plated in 50 % matrigel. *E. falciformis*-infected small intestine organoids were fixed at 4 and 21 hours post-incubation, stained and infection efficiency was quantified by immunofluorescence.

As I had observed for *E. vermiformis*, there were no significant differences when *E. falciformis* infected organoids were cultured in the presence or absence of P/S (Figure 4.25A to 4.25F). So, for the subsequent experiments, P/S was added to the culture medium.

Moreover, the data showed that an initial dose of infection of 2,500 and 5,000 sporozoites per 100 organoids led to approximately 50% of infected organoids at 4 hours post-infection, in contrast to what was observed with 500 sporozoites, where there were only about 20% of infected organoids (Figures 4.25A, 4.25C and 4.25E). The course of *E. falciformis* infection from 4 to 21 hours post infection followed the same decay pattern as it was observed for *E. vermiformis* infection, both in terms of number of parasites and the percentage of infected organoids (Figures 4.25A to 4.25D). Exceptionally, this trend was not observed

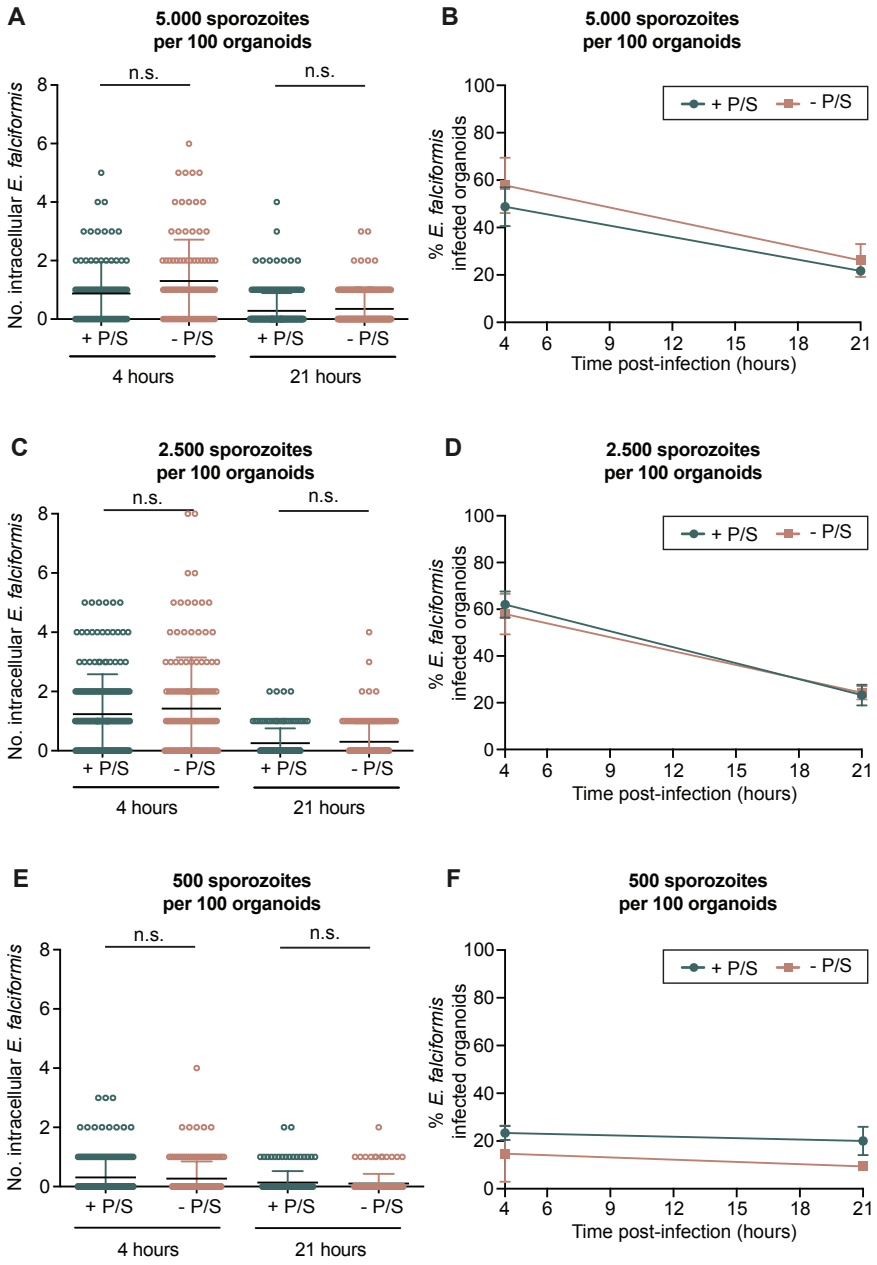

Fig. 4.25 *E. falciformis* infection efficiency is impacted by the initial co-culture ratio of sporozoites per organoids

Small intestine organoids were recovered at day 3 or 4 post-passage and co-cultured with 5,000 (A, B), 2,500 (C, D) or 500 (E, F) *E. falciformis* sporozoites per 100 organoids for 5 minutes, in basal medium, at 37°C, in the presence (green) or absence (orange) of P/S. Infected organoids were seeded in 25 μl droplets of 50% matrigel and cultured in complete organoid medium. (A, C, E) The number of intracellular *E. falciformis* sporozoites per organoid was quantified by immunofluorescence at 4 and 21 hours post-infection. Scatter plots represent mean (± SD). Significance was determined by unpaired *t-test* with Welch's correction. (B, D, F) The percentage of infected organoids was also determined. Mean (± SD) and linear regression were plotted. n.s. = non-significant. Data pooled from 2 independent experiments.

when infection was induced with 500 *E. falciformis* sporozoites per 100 organoids (Figure 4.25E and 4.25F). This was probably due to the low number of organoids infected from the start of the infection, which was also associated with a noticeable low number of parasites per organoid.

Interestingly, there is no significant differences between the results achieved with an initial dose of infection of 2,500 or 5,000 *E. falciformis* sporozoites to 100 organoids (Figure 4.25A to 4.25D). Higher concentrations were tested, however these led to organoid death (data not shown). Therefore, it seems that with 2,500 *E. falciformis* sporozoites per 100 organoids there is a plateau of the number of cells infected, as we see no significant increase when organoids are infected with 5,000 sporozoites. Since there were no microscopical differences that indicated a higher stress level induced in organoids by the highest concentration tested, compared with 2,500 sporozoites, an initial dose of 5,000 *E. falciformis* sporozoites per 100 organoids was used in the subsequent experiments.

4.8 The asexual development of *E. falciformis in vitro*

Having established the protocol for *E. falciformis* infection of small intestine organoids, I wanted to investigate the parasite's life cycle progression *in vitro*. For that, infected organoids were maintained in culture for at least 7 days, which corresponded to the *in vivo E. falciformis* pre-patent period [179]. Complete cell culture medium was renewed every 2 to 3 days. *E. falciformis*-infected organoids were fixed at 4, 32, 69, 93, 117, 140 and 230 hours post-incubation, stained and analysed by immunofluorescence.

After invading the small intestine organoids, *in vitro E. falciformis* sporozoites were rounding-up at 4 hours post-infection. As seen before, the stress induced by the protocol appeared to damage some organoids, inducing a dysmorphic morphology (Figure 4.26).

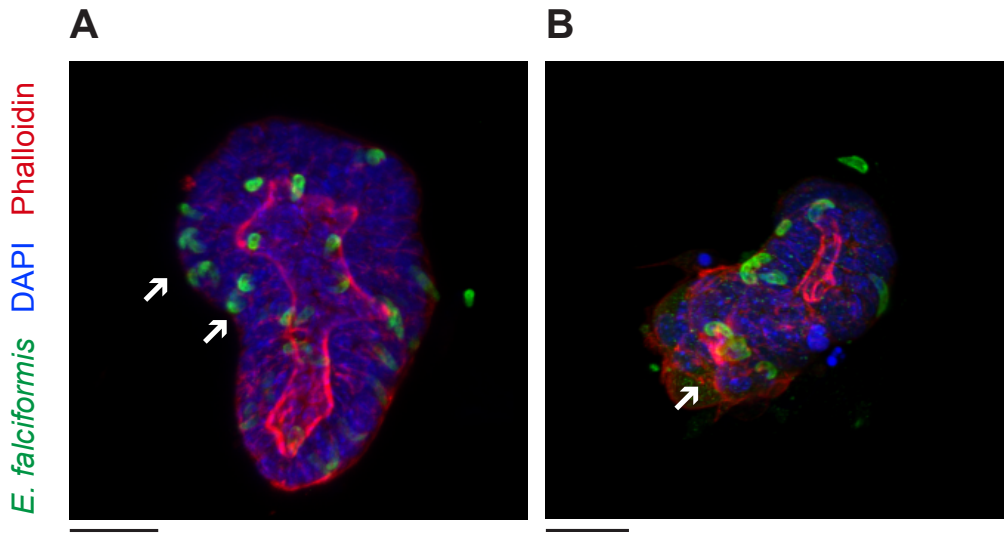

Fig. 4.26 *E. falciformis*-infected organoids (4 hours post-infection)

Immunofluorescence z-stack of 1 μm slices of *E. falciformis*-infected small intestine organoids. (A) Multiple intracellular sporozoites per small intestine organoid (white arrows). (B) Dysmorphic small intestine organoid (white arrow) infected with *E. falciformis* sporozoites. Scale bar = 30 μm. Figures are representative of at least three independent experiments.

At 32 hours post infection the first-generation trophozoites was observed, showing a central nucleus and two peripheral retractile bodies (Figure 4.27A). Additionally, and

knowing that *E. falciformis* development *in vivo* is not synchronous, first generation schizonts were also observed, with their nuclei aligned around the periphery of the schizont (Figure 4.27B). Moreover, all intracellular stages pushed the infected epithelial cell nucleus to the side (Figure 4.27B).

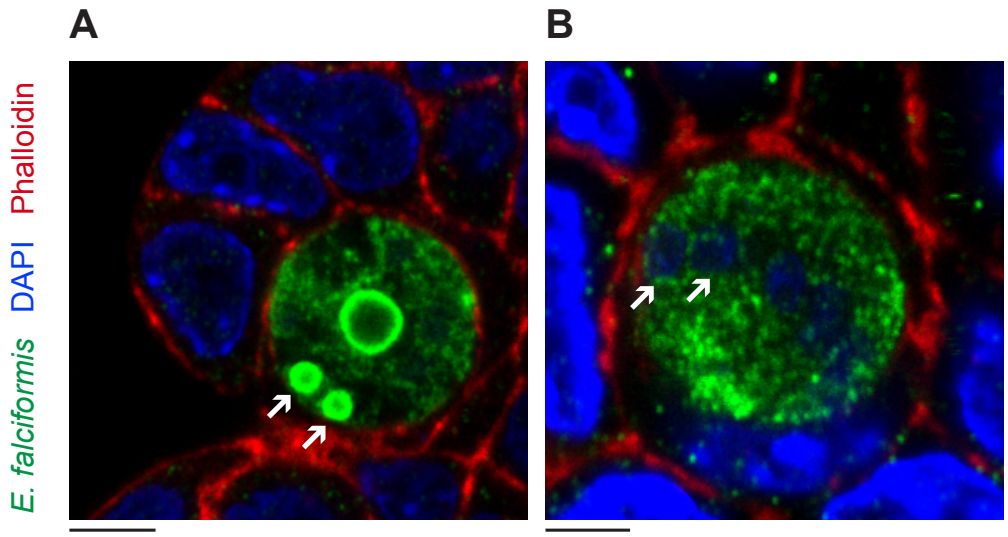

Fig. 4.27 *E. falciformis*-infected organoids (32 hours post-infection)

E. falciformis-infected small intestine organoids. (A) Cross-section showing an intracellular *E. falciformis* trophozoite with a central nucleus and two peripheral refractile bodies (white arrows). (B) Cross-section showing a first generation *E. falciformis* schizont with its nuclei centrally aligned (white arrows). Scale bar = 5 μm. Figures are representative of at least three independent experiments.

At 69 hours post-infection, multi-nucleated *E. falciformis* second generation schizonts were located mostly at the crypt site of small intestine organoids (Figures 4.28A and 4.28B). Mature *E. falciformis* schizonts consisted of merozoites closely packed and intertwined with each other. The merozoites' nuclei were located at the same level around the schizont. The schizonts started bursting out of the epithelial cells at 93 hours post-infection (Figure 4.29A). They were long, being about 20 μm in length. However, at this time point, mature second generation *E. falciformis* schizonts were still observed (Figure 4.29).

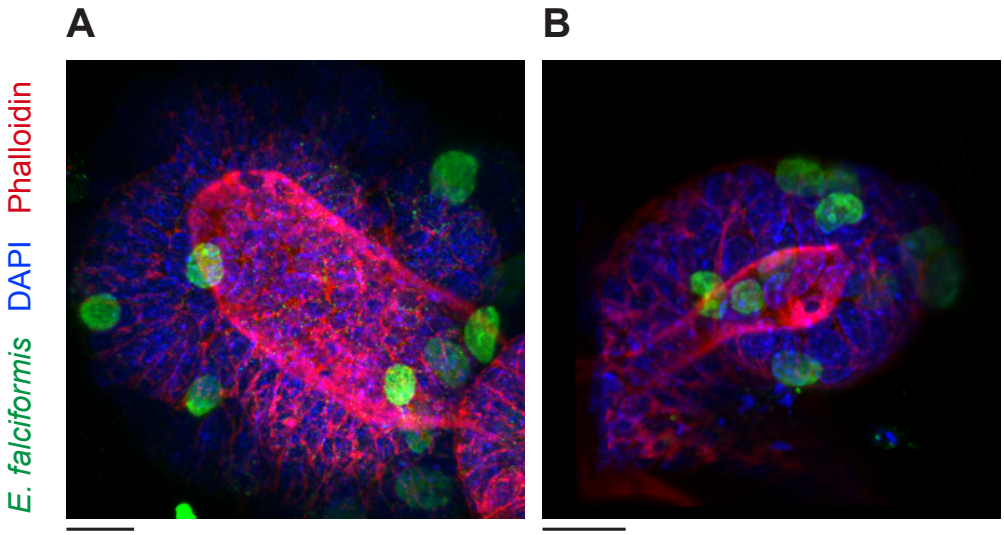

Fig. 4.28 *E. falciformis*-infected organoids (69 hours post-infection)

Immunofluorescence z-stack of 1 μm slices of *E. falciformis*-infected small intestine organoids. (A and B) Second generation *E. falciformis* schizonts. Scale bar = 10 μm. Figures are representative of at least three independent experiments.

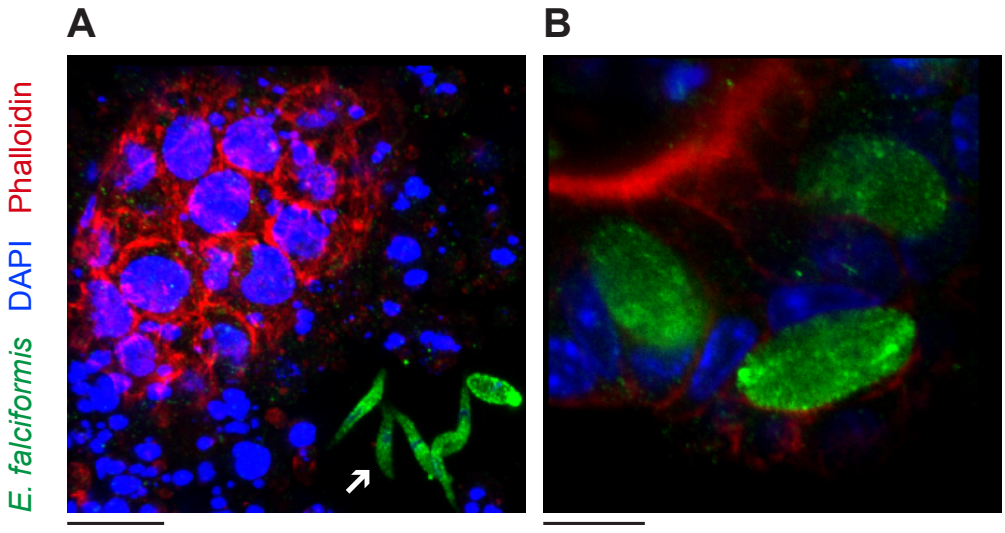

Fig. 4.29 *E. falciformis*-infected organoids (93 hours post-infection)

Immunofluorescence z-stack of 1 μm slices of *E. falciformis*-infected small intestine organoids. (A) Second generation *E. falciformis* merozoites (white arrow) (B) Mature *E. falciformis* schizonts. Scale bar = 5 μm. Figures are representative of at least three independent experiments.

At 117 hours post-infection I could observe what I hypothesise to be third generation schizonts, located at the crypt site of the small intestine organoids. These were round and smaller than the second generation ones. Also, the number of parasites per organoid decreases substantially (Figure 4.30).

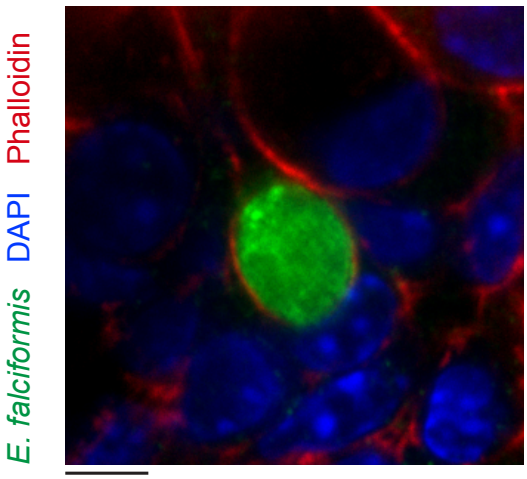

Fig. 4.30 *E. falciformis*-infected organoid (117 hours post-infection)

E. falciformis-infected small intestine organoid. Cross-section showing a mature *E. falciformis* schizont. Scale bar = 5 μm. Figures are representative of at least three independent experiments.

Interestingly, at 140 hours post-infection different *E. falciformis* stages were observed. There were second generation merozoites that were still visible in the matrix (Figure 4.31A). We also observed round schizonts, that probably correspond to the *E. falciformis* third round of asexual replication. They were mature and consisted of merozoites with their nuclei aligned in the centre of the schizont (Figure 4.31B). There were alongated and bigger schizonts, that possibly belong to the second generation (Figure 4.31C). Finally, merozoites, which were smaller in size when compared to the second generation ones that could belong to either first or third generation schizonts, were observed. Because the replication of *E. falciformis* is known to be asynchronous, it is difficult to distinguish the first from the third or the second from the fourth schizogony.

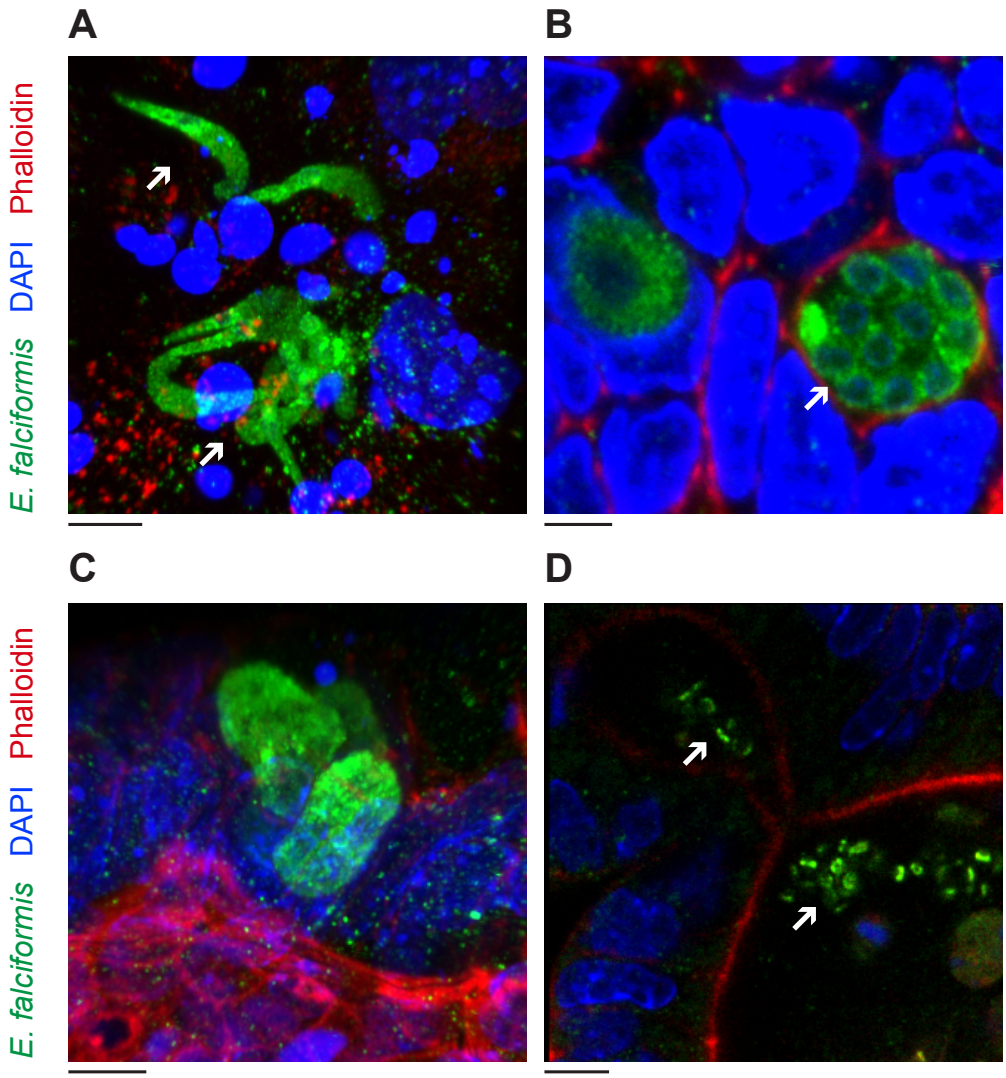

Fig. 4.31 *E. falciformis*-infected organoids (140 hours post-infection)

E. falciformis-infected small intestine organoids.(A) Z-stack of 1 μm slices. *E. falciformis* merozoites. (B) Cross-section showing a mature *E. falciformis* schizont. Encapsulated merozoites show their nuclei centrally aligned within the schizont. (C) Z-stack of 1 μm slices. Mature intracellular *E. falciformis* schizonts. (D) Cross-section showing *E. falciformis* sporozoites. Scale bar = 5 μm. Figures are representative of at least three independent experiments.

At 230 hours post-infection there was a sharp decrease in the number of intracellular parasite. *E. falciformis* schizonts could be observed, possibly third generation, at the crypt site of the small intestine organoids (Figure 4.32). However, I did not observe any of the *E. falciformis* sexual stages of development and, after this time point, no parasites were observed in the small intestine organoids.

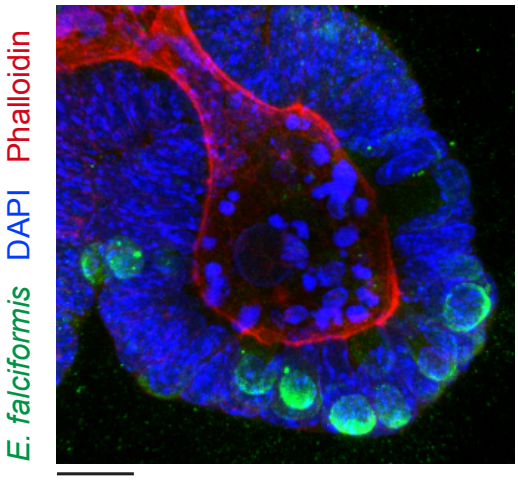

Fig. 4.32 *E. falciformis*-infected organoid (230 hours post-infection)

Cross-section of a *E. falciformis*-infected small intestine organoid. Immature *E. falciformis* schizont. Scale bar = 30 μm. Figures are representative of at least two independent experiments.

Altogether, data showed that using small intestine organoids as an *in vitro* infection model for *E. falciformis* allows to mimic its *in vivo* asexual development. However, this model is not sufficient to allow the study of *E. falciformis*' sexual development.

4.9 Discussion

To create an *in vitro* system able to meet the needs of *Eimeria spp.*, I started by establishing a small intestine organoid model. Based on the protocol described by Sato and colleagues [16], I was able to establish a stable primary cell culture of intestinal epithelial cells. These small intestine organoids showed self-renewing capabilities, and a crypt-villus architecture that closely resembled the gut histology. Furthermore, organoids showed an exponential growth after passage (Figure 4.4), a consequence of the continuous budding events which are reminiscent of crypt fission [180]. The continuous self-renewal of epithelial cells led to an accumulation of dying cells in the lumen. The presence of distinct specialised epithelial cells within the small intestine organoids was also confirmed. As previously described, Paneth cells constitute the niche for $Lgr5^+$ stem cells, and these were both localised at the designated "crypt sites" of the organoid (Figures 4.3A and 4.3B) [27, 16]. The presence of enteroendocrine and goblet cells was also confirmed (Figures 4.3C and 4.3D). Finally, F-actin and nuclear staining revealed a single epithelial cell layer (Figure 4.3).

Small intestine organoid cultures were kept for up to 6 months, as it has been previously shown that they are able to retain their characteristics for more than 8 months [16]. In order to understand better and manipulate the behaviour of small intestine organoids, I optimised the concentrations of matrigel and R-spondin1 in the culture system.

At the crypt base, there is an enrichment of laminin ($\alpha 1$ and $\alpha 2$), in accordance with which laminin-rich matrigel has proven to be of greater importance for the support of the intestinal epithelial growth [181][16]. To my knowledge, there have not been previous reports showing how different matrigel concentrations impact organoid growth. Thus, a titration of increasing doses of matrigel was performed. There were no differences in the organoid surface area among the different culture conditions (Figure 4.6). However, when organoids were cultured in 20% matrigel, at day 5 post-passage they showed large dark centres, which sometimes masked the whole organoid. Organoids generally burst and cellular debris was

found spread across the matrigel layer. This is possibly a consequence of limited access to laminin and other proteins essential for organoid growth, a result of a low concentration of matrigel.

Next, recombinant human R-spondin 1 was replaced by R-spondin 1 supernatant for economic reasons. No significant differences in architectural structure of the organoids were found between the enrichment of growth medium with human recombinant R-spondin 1 or the supernatant (Figure 4.8). Therefore, R-spondin 1 supernatant was used for the maintenance of organoid cultures and experimental work.

Having established a stable small intestine organoid culture, I started applying this model to the study of host-pathogen interactions.

Most observational studies with *Eimeria spp.* have, so far, been performed *in vivo*. In order to isolate the different variables involved in the immune response against *E. vermiformis* or *E. falciformis*, an *in vitro* model of infection using small intestine organoids was established. Many *Eimeria spp.* have been maintained in different cell culture systems and have shown varying degrees of development. For example it has been shown that *in vitro* development of *E. bovis* is sustained in bovine, human and porcine endothelial cell lines, bovine foetal gastrointestinal cells (BFGC), Madin-Darby bovine kidney (MDBK) cells, African green monkey kidney epithelial (Vero) cells [148], bovine colonic epithelial cells (BCEC) [149], bovine umbilical vein cells (BUVEC) and bovine spleen lymphatic endothelial cells (BSLEC) [150, 151]. These systems proved useful to study different properties of the parasite-host cell interactions, although the completion of the *E. bovis* life cycle *in vitro* has not been achieved.

In vitro culture models for the avian parasite *E. tenella* have also been thoroughly investigated. In 1998, Kelleher and Tomley described the first protocol for transient transfection of *E. tenella* sporozoites[182]. This protocol was further developed and transfected parasites were cultured in primary chicken kidney (PCK) cells. *E. tenella* showed completion of its endogenous development *in vitro* [144, 152].

Even though *Eimeria spp.* had been extensively studied, only a few studies reported the *in vitro* culture of *E. vermiformis* or *E. falciformis*. In 1977, Kelley and Youssef cultured *E. vermiformis* sporozoites in bovine kidney cells, Madin-Darby bovine kidney (MDBK) cells and primary cultures of whole mouse embryos. The authors described the *in vitro* development of first generation schizonts and merozoites [145]. Adam and colleagues, used MDBK or PK-15 cells for the study of *E. vermiformis* sporozoite invasion. The authors did not state, however, whether the parasites were able to progress though their life cycle [146]. Later, Rose and coworkers, described the development of *E. vermiformis* sporozoites into fully matured schizonts 45 hours after infection of murine fibroblast-like L-929 cell. The authors also replicated this result in rat epithelial-like cells (RATEC) but the parasite development was slower [147]. No further attempts at *E. vermiformis* development *in vitro* have been described. The study of *E. falciformis in vitro* is also documented. Stange and colleagues, infected mouse intestinal epithelial cell line CMT-93 cells with *E. falciformis* sporozoites and observed the *in vitro* completion of their first schizogony at 39 hours post-infection [110]. Altogether, it seems that *Eimeria spp.* can benefit from a cell culture system rich in different epithelial cell types, as shown with PCK cells for *E. tenella*. Therefore, in our studies, we used small intestine organoids, which encompass the main epithelial cell types found in the intestinal epithelium *in vivo*. Additionally, the organoid structural organisation mimics that present *in vivo*. In particular, cells are polarised towards the lumen of the organoid, and are organised into crypts and villi.

I successfully established an infection protocol for *E. vermiformis* and *E. falciformis* infected small intestine organoids. This has proven to be more efficient than using a two-dimensional cell culture system, as both *E. vermiformis* and *E. falciformis* were able to progress with their life cycle beyond their first schizogony.

Fist, I aimed at standardizing the size of organoids before subjecting them to infection. For that, a 25 G needle was used, which is employed for organoid passage, or a 21 G needle,

which would accommodate bigger organoids. The data showed that infection of organoids homogenised with a 25 G needle was not possible, as organoids were dead after a 5-minute incubation with *E. vermiformis* sporozoites. This could be related to a loss of their structural organisation, and as a consequence the organoids would no longer be fit for sporozoite invasion. Therefore, a 21 G needle was used to homogenise organoids prior to infection. Nonetheless, this step appeared to be of importance as it "opens" the organoid, allowing sporozoites access to their lumen which I hypothesise is a critical event for effective infection.

The data also suggest that matrigel limits the ability of sporozoite invasion, both for *E. vermiformis* and *E. falciformis*. As shown in Section 4.3.1, small intestine organoids were viable in low matrigel densities, down to 20%. However, even with 20% matrigel, organoids were not efficiently infected by the parasite. As merozoites seem not to have a motility problem in the presence of the matrigel, we hypothesised that the "opening" of the matrix scaffold is not the limiting factor. I could not exclude the possibility of sporozoite interaction with proteins present in the matrigel, which could misguide and alter the behaviour of the parasite, thus limiting invasion efficacy. Therefore, the solution consisted in a complete removal of the matrigel from the organoids followed by a short incubation with the *E. vermiformis* or *E. falciformis* sporozoites. This incubation period was optimised to minimise organoid stress induced by lack of matrigel since, as shown by the data, uninfected organoids were dead after 30 minutes' incubation in the absence of matrigel. Without the matrigel support, organoids cannot maintain their three-dimensional structure, which may compromise their physiological organisation and, consequently, their crypt-villi gradients of growth and development factors would also be disturbed. Additionally, without matrigel, organoids would have no access to proteins essential for their development which are exclusively present in the matrix. Hence, I limited the sporozoite-organoid incubation time to 5 minutes (Figure 4.10). Even though this protocol was used among different parasite batches, after each *E. vermiformis* or *E. falciformis* stock passage, the incubation time was tested and had to be

adjusted to between 2 and 5 minutes. Each batch optimisation took into account the invasion efficiency of the sporozoites and the damage induced to the small intestine organoids, thus enabling standardised start conditions among different parasite stocks.

Interestingly, the data shows that the initial infection dose required for an effective *E. vermiformis* infection is higher than for *E. falciformis*, as the organoids are generated from small intestine crypts, the target site of infection of *E. vermiformis*. This can be related with many factors. For example,we know that the colon does not have specialised Paneth cells, thus we can assume that there are some differences at the cellular level between the two intestinal regions. *In vivo*, these differences might give *E. falciformis* a greater challenge to invade cells, thus requiring a better adaptation from the parasite. Moreover, the colon has a protective thick mucus layer, so that the access to epithelial cells here is more difficult when compared to the access to epithelial cells from the small intestine. Again, *E. falciformis* could be better adapted to invade intestinal epithelial cells in adverse conditions.

One question that remains unanswered is why *E. falciformis* specifically infects caecum and colon *in vivo*, as *in vitro* it easily infects epithelial cells that mimic the cellular composition and structural organisation of the proximal small intestine epithelium.

The results showed that both *E. vermiformis* and *E. falciformis* sporozoites were able to develop *in vitro* beyond what has previously been described. Specifically, both species are able to progress though their first schizogony [147, 110].

According to the latest description of the *E. vermiformis* life cycle by Rose and Millard, *E. vermiformis* goes through three schizogonies before initiation of its sexual development [183]. *In vivo*, after 4 hours inoculation, intracellular *E. vermiformis* sporozoites were observed in both the tips of the villi and the crypts of Lieberkühn. However, from 8 to 24 hours post-inoculation the majority of the sporozoites were localised in the epithelial cells of the intestinal crypt [178, 183]. This observation could explain why there is a decrease in the number of parasites per intestinal organoid from 4 to 21 hours post-infection, assuming that

the remaining parasites are at the crypt site of the organoid. This is difficult to determine categorically as organoids are in their first stages of development, and their crypt sites (buds) are not very well defined.

In vivo, from 16 to 24 hours post-inoculation, the *E. vermiformis* sporozoite starts to fold back on itself [178, 183]. Similarly, in our culture system, I observed that the sporozoites started to round-off, and are often enlarged, at 21 hours post-infection (Figure 4.20).

At 48 hours post-inoculation some first generation schizonts have matured *in vivo* and contain 40-80 merozoites [183]. In my *in vitro* model, I was able to observe that most sporozoites had developed into schizonts at 45 hours post-infection. However, the confocal analysis did not have sufficient resolution to determine the number of enclosed merozoites (Figure 4.21). Additionally, I could still observe free first-generation merozoites at 69 hours post-infection (Figure 4.22 A).

As I observed *in vitro*, *in vivo* second-generation schizonts developed in the crypts and base of the villi (Figure 4.22). *In vivo*, their mature development was seen at 72 hours post-inoculation when they contained 50-70 merozoites [183]. *In vitro*, the maturation process of second-generation schizonts was seen only at 96 hours post-infection (Figure 4.23) and second-generation merozoites were only observed at 117 hours post-infection (Figure 4.24). *In vivo*, mature third generation schizonts were seen at 80 hours post-infection, and *E. vermiformis*' earliest mature gametocysts were seen at 168 hours post-inoculation [183]. However, I did not observe the development of these stages in the *in vitro* model of infection. This could result from many factors. First, organoids might no longer be fit for infection. As organoids were one week old when I observed second generation schizonts, their lumen is filled with debris and their growth starts to get compromised by the limited availability of matrigel proteins. I tried to passage the *E. vermiformis* infected organoids into fresh matrigel, both at 69 and 96 hours post-infection. However, even though the parasite is intracellular at this time points, I did not observe any infected cells after passage. Second,

the signals involved in the development of *E. vermiformis* are not very well understood and could be missing in the system. For example, it is known that *E. bovis* modulates the host cell LDL-cholesterol metabolism to increase its growth and success of replication from the first stages of development [184].

The life cycle of *E. falciformis* was described in detail by Mesfin and Bellamy, and shown to consist of four schizogonies followed by a gametogony [179]. *In vivo*, trophozoites were initially seen at 18 hours post-inoculation, with a clear definition of their retractile bodies and eccentric nuclei. Similarly, at 32 hours, I observed some trophozoites present in the small intestine organoids with an identical morphology (Figure 4.28A).

At 48 hours post-inoculation, a few mature first-generation schizonts were described *in vivo*. Their maturation peaked at 60-72 hours post-inoculation, together with the peak of first-generation merozoites [179]. In my *in vitro* model, immature first-generation schizonts were observed at 32 hours post-infection (Figure 4.28B). However, I missed the mature first generation schizonts as well as the first-generation merozoites.

E. falciformis immature second generation schizonts were observed *in vivo* at 72 hours post-inoculation [179]. The peak of maturation and merogony was observed at 96 hours post-inoculation. Merozoites were small and curved. Similarly, immature second-generation schizonts were observed at 69 hours post organoid infection (Figure 4.29), whereas maturation was seen at 93 hours post-infection (Figure 4.30). However, given that first and third generation merozoites are known to be long and slightly curved, with an average length of 15.5 μm [179], I believe that the merozoites that I occasionally observed at 93 hours post-infection belong to the first-generation (Figure 4.30B).

Mature third-generation schizonts were seen *in vivo* between 108 ad 120 hours post-inoculation [179]. However I could not tell if the schizonts observed *in vitro* at 117 hours post-infection belonged to the second or third generation (Figure 4.32).

E. falciformis fourth-generation schizonts were seen between 132 and 150 hours post-inoculation and were morphologically similar to those of the second-generation [179]. In contrast, I could no longer distinguish between the different stages of *E. falciformis* development *in vitro* (Figure 4.32). At 140 hours post-infection merozoites were observed that were long and slightly curved which, according to the *in vivo* descriptions, could be from the first or third-generation (Figure 4.32A). Additionally, I observed merozoites that were small and curved which could be from the second or fourth generation (Figure 4.32D). Several schizonts were also observed, with different shapes at different levels of maturation (Figure 4.32B and 4.32C). Gametogony stages were first seen *in vivo* at 144 hours post-inoculation [179]; however, they were not observed in my *in vitro* model. Some schizonts were observed at 230 hours post-infection but, after this time point, I could no longer see any *E. falciformis* development stages in the organoid. Again, the interruption of *E. falciformis* development could be related to the fitness of the organoid or lack of metabolites. For example, it is known that xanthurenic acid, a by-product of tryptophan catabolism, is a gametocyte-development factor and is crucial for *E. falciformis* development [176]. Nonetheless, supplementation of the culture medium of infected organoids with various concentrations of xanthurenic acid at different time points did not reveal any further parasite development. This could be an indication that *E. falciformis* gametocyte development is dependent on a combination of different favourable factors.

Even though I was not able to induce completion of *E. vermiformis* or *E. falciformis* life cycles *in vitro*, progress was made compared with previous efforts. Multiple schizogonies were achieved, possible due to the structural and cellular complexity of the small intestine organoid model. This represents a valuable tool for the study of host-pathogen interactions, notably the study of maintenance of the epithelial barrier integrity upon infection and the study of epithelial immunity.

Chapter 5

Intestinal epithelial response against *E. vermiformis* infection

5.1 Introduction

After the successful establishment of a small intestine organoid culture system suitable for the asexual development of *E. vermiformis* and *E. falciformis*, I decided to study how intestinal epithelial cell (IECs) activation can induce protection against *E. vermiformis* infection. Knowing that interferon (IFN)-γ plays a crucial role in immunoprotection against *E. vermiformis* [126], and knowing that intestinal epithelial homeostasis is regulated by IFN-γ [185], I started by investigating in detail how the presence of IFN-γ in the system might influence the host-*E. vermiformis* interactions. This analysis was complemented with the investigation of how various cytokines may play a role in the organoid protection against *E. vermiformis*.

The role of various cytokines, such as IFN-λ, interleukin (IL)-13, IL-17 and IL-22, in the maintenance or immunoprotection of the intestinal barrier after infection, are well-established.

IFN-λ production by epithelial cells is typically induced by protection of the intestine viral infections [186, 187]. Furthermore, it has been shown that, after viral infection epithelium is conferred by the synergistic action of IFN-λ and IL-22 signalling the activation of the transcription factor STAT1 and the induction of IFN-stimulated genes [188].

Besides its role in the regeneration of the intestinal epithelium, IL-13 is known to regulate the differentiation of goblet cells [189, 190]. Steenwinckel and colleagues showed that IL-13 overexpression is a driver of goblet cell hyperplasia. In addition, goblet cell hyperplasia induced by IL-23 or IL-9 overexpression leads to an increase in mucin expression regulated by IL-13-dependent pathways [19].

IL-17 has been implicated in the regulation of the immune response against *Eimeria ssp.*. It is known that the expression of IL-17A leads to a decrease in *E. tenella* oocyst shedding, through an induced impairment in the schizont formation and inhibition of the migration of infected cells [191, 192]. Furthermore, expression of IL-17A has also been implicated in the immune response against *E. falciformis*. It has been observed that an *in vitro* IL-17A-treated intestinal epithelial cell line has reduced parasite development [110].

IL-17 and IL-22 can synergise to induce innate immune responses in IECs. However, IL-17 is known to be an inflammatory cytokine whereas IL-22 induces a protective/regenerative response [193]. Nonetheless, IL-17 and IL-22 are known to act synergistically to enhance the production of antimicrobial peptides [194]. IL-22 has also been implicated in protection against *E. falciformis*. It has been shown that the expression of IL-22 leads to a significant reduction of *E. falciformis* development *in vitro* [110].

Given the important role of IFN-γ in protection against *E. vermiformis* infection, an IFN-λ, IL-13, IL-17 and IL-22 in the maintenance and protection of the intestinal epithelial barrier, I investigated how these cytokines contribute to the small intestine organoid response against *E. vermiformis* infection. Furthermore, I also performed a screen of the innate response cytokines that are produced by *E. vermiformis*-infected organoids.

5.2 Effect of IFN-γ on *E. vermiformis*-infected organoids

To study the immune activation of IECs, I used the previously established (Chapter 4) *E. vermiformis*-infected small intestine system. Immune control of *E. vermiformis* is mediated by IFN-γ *in vivo* [126, 135]. Furthermore, it has been shown that IFN-γ inhibits *E. vermiformis* growth in both fibroblasts and epithelial cells [147]. Therefore, I investigated how IFN-γ impacts *E. vermiformis* development in the small intestine organoid model.

5.2.1 IFN-γ stimulus leads to IEC activation

First, in order to have a better understanding of the behaviour of small intestine organoids in comparison with the *in vivo* intestinal epithelium, I analysed RNA sequencing data acquired by Middendrop and colleagues on small intestine organoids and small intestine villi or crypts (GEO: GSE53297) [195]. The FastQ raw data were mapped by TopHat to a reference genome, GRCm38 (mm10), into a BAM file. Data, including only unique alignments, were analysed on SeqMonk software. Besides confirming a high level of similarity of gene expression between organoids and the small intestine, data analysis showed specifically that organoids express the receptor for IFN-γ at a steady state (data not shown).

Second, I aimed to confirm if IEC signalling in small intestine organoids was triggered by IFN-γ treatment. As shown before, 3-day old organoids exhibited the presence of different specialised epithelial cells. Based on this result, infection with *E. vermiformis* was performed in 3 or 4 day-old organoids, as it has been shown that at this stage organoid development resembles the *in vivo* counterpart. Therefore, 3 and 5 day-old organoids were stimulated with 2 ng/ml of mouse recombinant IFN-γ, for 6 hours.

The expression of both *IDO1* and *CXCL9* is known to be regulated by IFN-γ and has been implicated in resistance against pathogens like *Toxoplasma gondii* [196, 197]. Thus, the relative expression of *Ido1* and *Cxcl9* was measured by RT-PCR and normalised against the non-treated control (Figure 5.1).

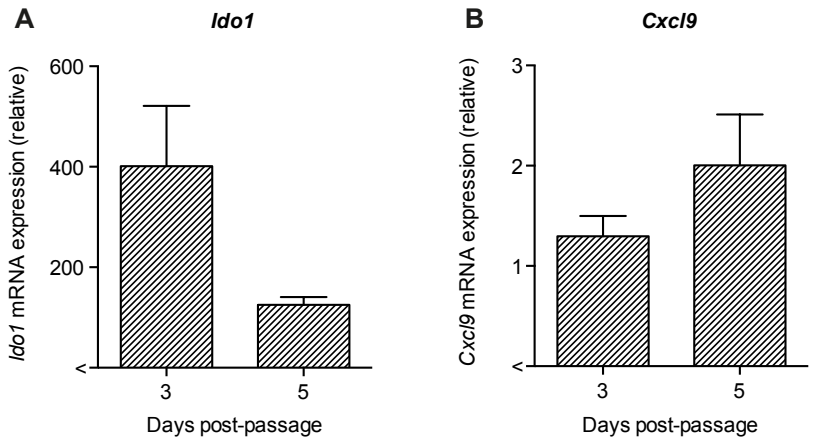

Fig. 5.1 IFN-γ-stimulated small intestine organoids

Three- or five- day old small intestine organoids were stimulated with 2 ng/ml of mouse recombinant IFN-γ for 6 hours. Technical triplicates were collected for each condition. Data is representative of gene expression levels, normalised to *Hprt*. Non-treated control = 1. Data are representative of two independent experiments.

The results showed that the relative expression of both *Ido1* and *Cxcl9* is increased after IFN-γ treatment of day 3 small intestine organoids. Additionally, the expression of both genes are equally increased in 5 day-old organoids, suggesting that organoids are responsive in a homogeneous way through their development.

5.2.2 IFN-γ treatment of *E. vermiformis*-infected organoids

Having established that organoids were responsive to treatment with mouse recombinant IFN-γ, I decided to submit *E. vermiformis*-infected organoids to IFN-γ treatment. Thus, as previously described, 3 to 4 day-old small intestine organoids were infected with *E. vermiformis* sporozoites and seeded in 50% matrigel. After matrigel polymerisation, complete organoid medium containing 0, 0.5 or 2 ng/ml of recombinant IFN-γ was added to the wells. To determine the effect of the treatment on the growth of the parasite, the number of intracellular *E. vermiformis* was determined for each condition at 4, 21 and 45 hours post-infection. Additionally, the percentage of infected organoids was calculated (Figure 5.2).

The results showed a significant increase in the number of intracellular parasites in the 0.5 ng/ml IFN-γ-treated organoids when compared to the non-treated control (Figure 5.2A). This effect was also observed at 4 hours post-infection in the organoids treated with 2 ng/ml IFN-γ (Figure 5.2A). However, no differences in the percentage of infected organoids were observed between the different conditions (Figure 5.2B). Again, as seen before (Section 4.6), the number of infected organoids decreased over time, which also related with a decrease in the percentage of infected organoids. This was observed for all conditions, independently of IFN-γ treatment (Figure 5.2).

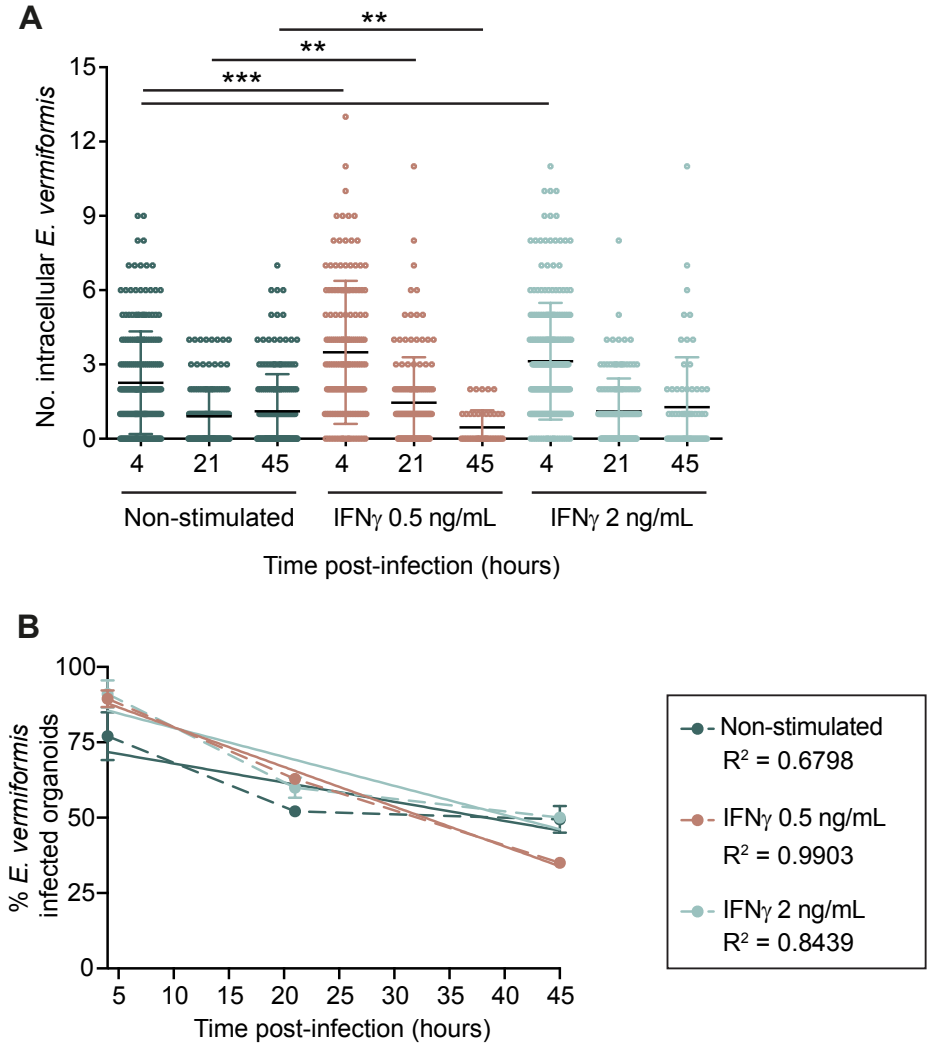

Fig. 5.2 IFN-γ-stimulated small intestine organoids after *E. vermiformis* infection

Three- to four- day old small intestine organoids were infected with *E. vermiformis* and treated with 0 (green), 0.5 (orange) or 2 ng/ml (blue) of mouse recombinant IFN-γ. (A) The number of intracellular *E. vermiformis* was determined at 4, 21 and 45 hours post-infection. Mean (± SD) and non-parametric *t*-test with Welch's correction was plotted. (B) Percentage kinetics of infected organoids. Mean (± SD) and linear regression was plotted. Data are representative of at least two independent experiments. N.S. = Non-stimulated **P < 0.01 ***P < 0.001.

In addition, microscopic analysis of *E. vermiformis*-infected organoids showed that despite the differences in the numbers of intracellular parasites, *E. vermiformis* development is not compromised. At 4 hours post-infection, multiple intracellular sporozoites were observed (Figures 5.3A to 5.3C) and, at 21 hours post-infection, *E. vermiformis* sporozoites started to fold back onto themselves (Figures 5.3D to 5.3F). At 45 hours post-infection, the first generation of schizonts was observed (data not shown).

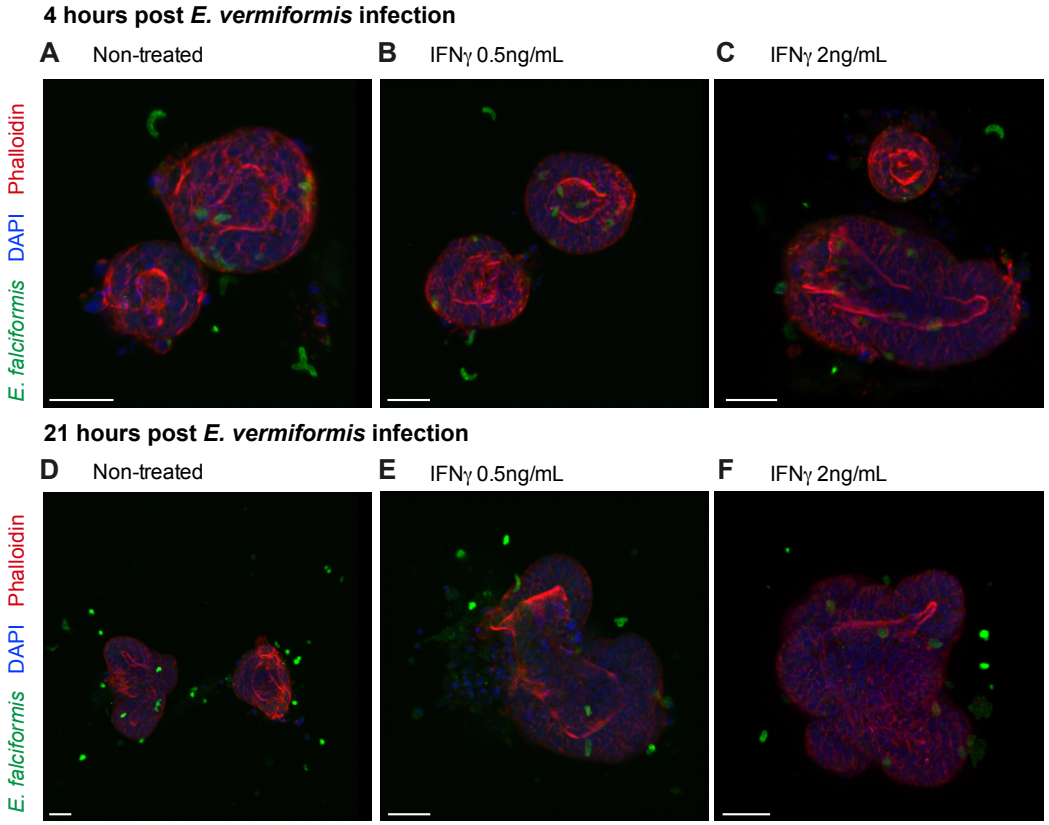

Fig. 5.3 Development of IFN-γ-stimulated small intestine organoids after *E. vermiformis* infection

Immunofluorescence z-stack of 1μm slices. *E. vermiformis*-infected small intestine organoids untreated (A, D), treated with IFN-γ0.5 ng/ml (B, E) or IFN-γ2 ng/ml (C, F), at 4 and 21 hours post-infection. Data are representative of at least two independent experiments. Scale bar = 30 μm.

5.2.3 *E. vermiformis* infection delays organoid development

In my microscopic analysis there were indications that IFNγ treatment was inducing a decrease in the total number of organoids in culture (Section 5.2.1). *E. vermiformis*-infected small intestine organoids were seeded among all conditions from a homogeneous cell suspension. Thus, the number of organoids seeded per well at the day of infection was comparable. Interestingly, IFN-γ-treated organoids, showed a sharp decrease in the total number of organoids in culture from 21 to 45 hours post-infection (Figure 5.4).

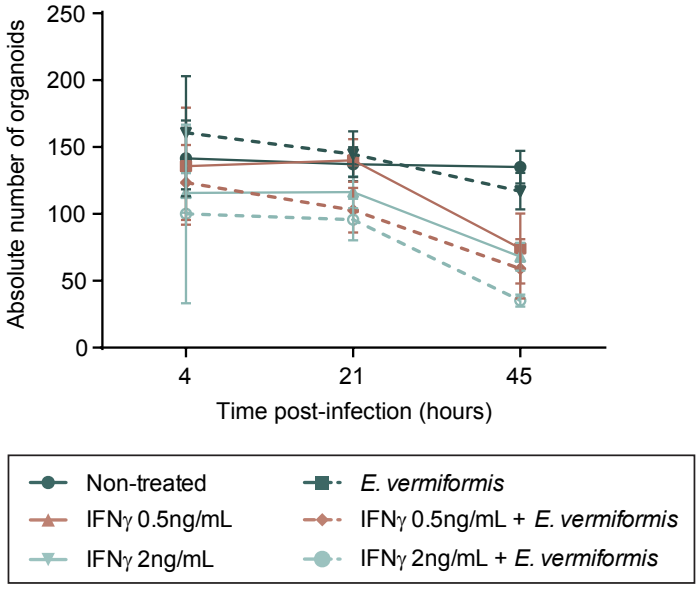

Fig. 5.4 Absolute number of *E. vermiformis*-infected organoids after IFN-γ treatment

Three- to four- day old small intestine organoids infected with *E. vermiformis* or non-infected controls were treated with 0 (green), 0.5 (orange) or 2 ng/ml (blue) of mouse recombinant IFN-γ. The absolute number of organoids was determined. Mean (± SD). Data are representative of at least two independent experiments.

This result suggested that IFN-γ had a detrimental effect on the viability of the small intestine organoids. To further evaluate the outcome of IFN-γ stimulation in both infected and non-infected small intestine organoids, their development was quantified based on their phenotype (Figure 5.5). Organoids were classified into four groups: (i) cysts, (ii) organoids with 1 to 2 buds, (iii) organoids with 3 to 6 buds and (iv) organoids with more than 6 buds.

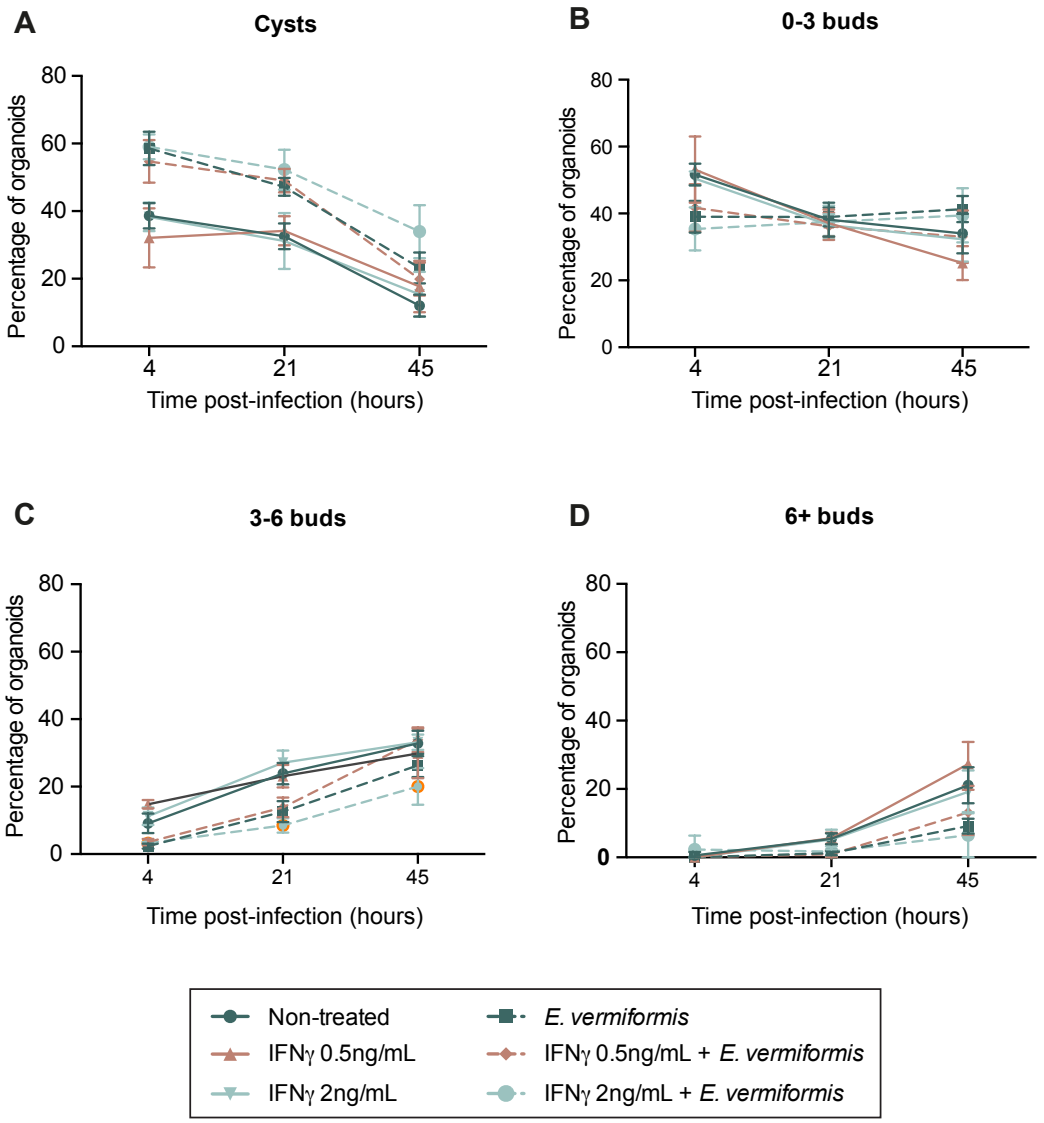

Fig. 5.5 Development of IFN-γ-stimulated small intestine organoids after *E. vermiformis* infection

Three- to four- day old small intestine organoids infected with *E. vermiformis* or non-infected controls were treated with 0 (green), 0.5 (orange) or 2 ng/ml (blue) of mouse recombinant IFN-γ. Organoids were classified in 4 groups: (A) cysts (B) organoids with 1 to 2 buds (C) organoids with 3 to 6 buds (D) organoids with more than 6 buds. Mean (± SD) was plotted. Data are representative of at least two independent experiments.

The data showed no developmental differences across the IFN-γ-treated organoids when compared to the non-treated controls. However, there was a consistent difference between the *E. vermiformis*-infected organoids when compared to the non-infected controls. *E. vermiformis*-infected organoids had a higher percentage of cysts over the time of infection (Figure 5.5A), accompanied by a lower number of multi-budded structures (Figures 5.5C and 5.5D). Altogether, the data suggest that *E. vermiformis* infection inhibits organoid development.

Organoid development inhibition and the decrease of the absolute number of organoids after infection, seemed to correspond to an increase in the number of burst organoids, observed by microscopy. Thus, I next quantified the number of organoids that were burst. To be considered a burst organoid, I defined two inclusion criteria: (i) being a multi-budded organoid and (ii) displaying an open lumen, which could be confirmed by Phalloidin immunofluorescence staining (Figure 5.6).

The analysis showed that at 21 and 45 hours post-infection, infected organoids display a higher number of burst organoids compared to the non-infected controls. Yet, this effect was intensified when infected organoids were treated with IFN-γ. Furthermore, at 45 hours post-infection, there was a distinct correlation between higher concentration of IFN-γ and a higher percentage of burst organoids, both in infected or non-infected organoids. Altogether, these data suggest that IFN-γ was having an adverse effect in the maintenance of organoid structure integrity.

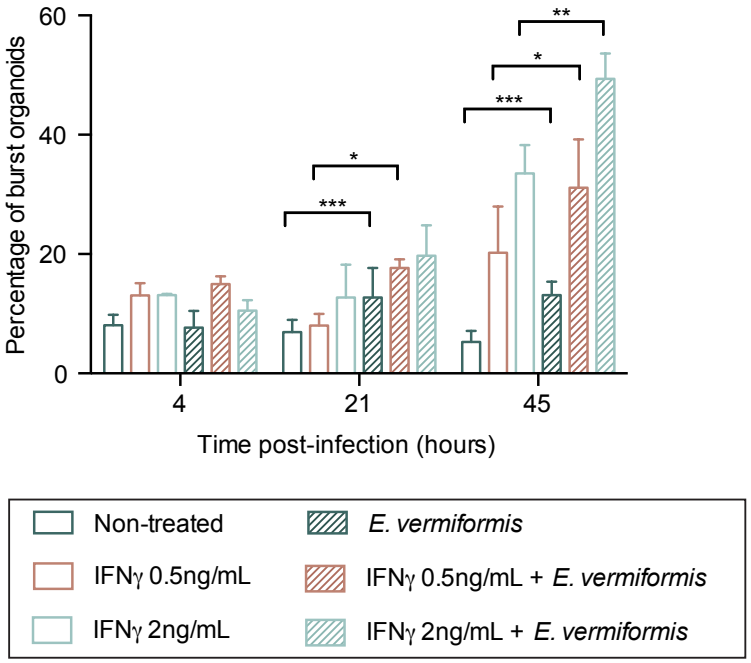

Fig. 5.6 Development of IFN-γ-stimulated small intestine organoids after *E. vermiformis* infection

Three- to four- day old small intestine organoids infected with *E. vermiformis* or non-infected controls were treated with 0 (green), 0.5 (orange) or 2 ng/ml (blue) of mouse recombinant IFN-γ. The number of burst organoids was determined. Mean ($\pm$ SD) and non-parametric *t*-test with Welch's correction was plotted. Data are representative of at least two independent experiments.

5.3 IL-13 activation of IECs leads to a decreased number of intracellular *E. vermiformis*

As previously described, it is well established that IFN-λ, IL-13, IL-17 and IL-22 play important roles in the maintenance and protection of the intestinal barrier. Therefore, in this section, small intestine organoids were infected with *E. vermiformis* and complete organoid medium was supplemented with 2 ng/ml of IFN-γ, IFN-λ, IL-13, IL-17 or IL-22. To quantify the effect of the cytokine treatment, the absolute number of intracellular parasites per organoid and the percentage of infected organoids was determined (Figure 5.7).

As seen before, *E. vermiformis* organoids treated with 2 ng/ml of IFN-γ showed a significant increase in the number of intracellular parasites at 4 hours post-infection. No differences were seen at 21 and 45 hours post-infection (Figure 5.7). Additionally, there were no differences in the number of intracellular parasites in the *E. vermiformis*-infected organoids treated with IFN-λ, IL-17 or IL-22, in comparison with the non-treated control (Figures 5.7C, 5.7G and 5.7I). However, in the case of IL-22, inconsistent results were obtained. A total of 4 experiments were performed, 2 of which showed no differences while the other 2 showed a significant decrease in the number of intracellular parasites at both at 4 and 21 hours post-infection (data not shown).´

Interestingly, treatment with 2 ng/ml of IL-13 led to a significant reduction of the number of intracellular *E. vermiformis* across all time points (Figure 5.7E).

Overall, no statical differences were observed in the percentage of infected organoids between the cytokine-treated conditions and the non-treated control (Figures 5.7B, 5.7D, 5.7F, 5.7H and 5.7J).

Altogether, the screening of the different cytokines suggested a role for IL-13 in epithelial protection against *E. vermiformis* infection. Moreover, the data obtained from IL-22-treated *E. vermiformis*-infected organoids suggest that IL-22 might also play a role in the interaction

between the epithelial cells and the parasite. However, further investigation would be required to confirm if and how IL-22 induces a protective effect against *E. vermiformis* infection.

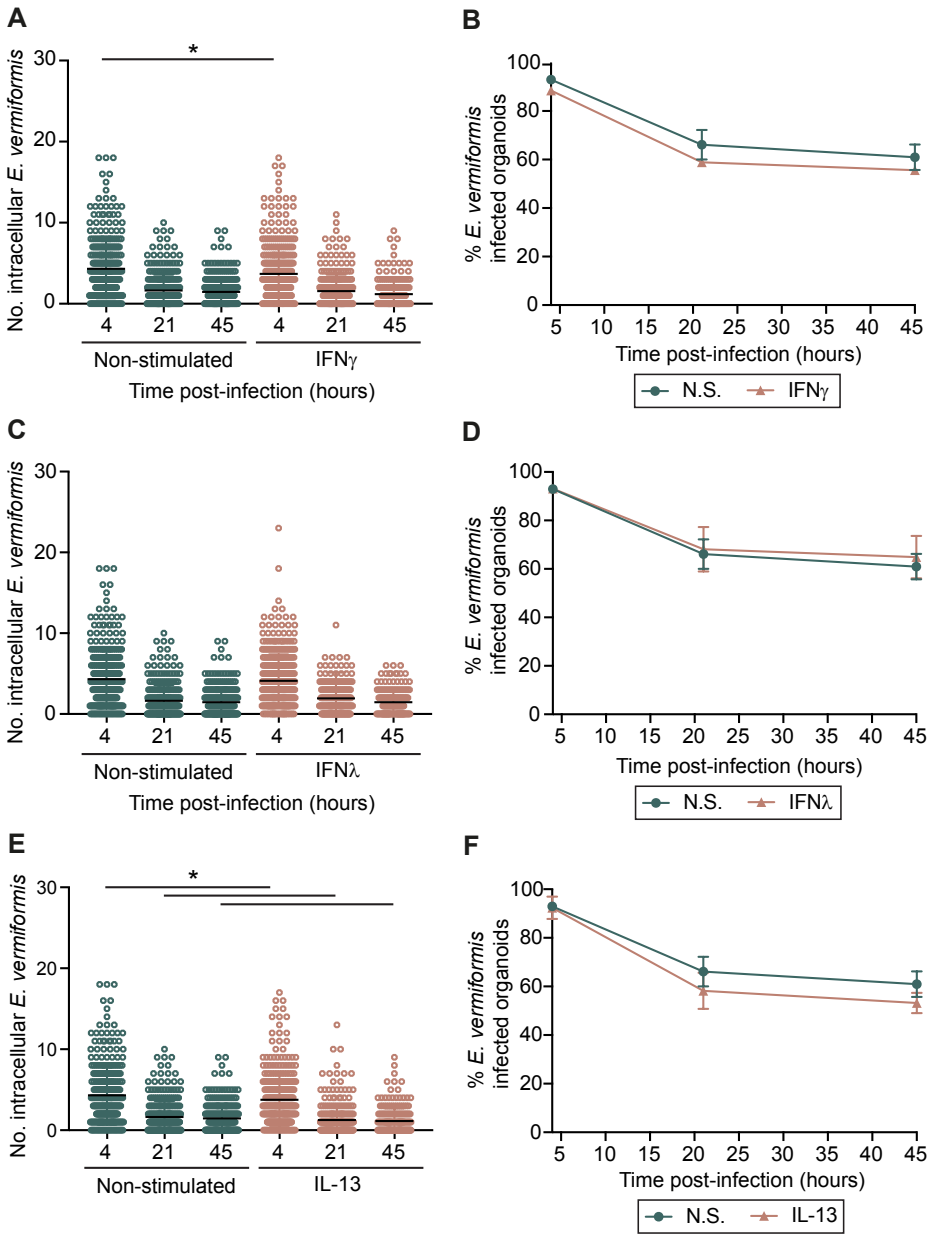

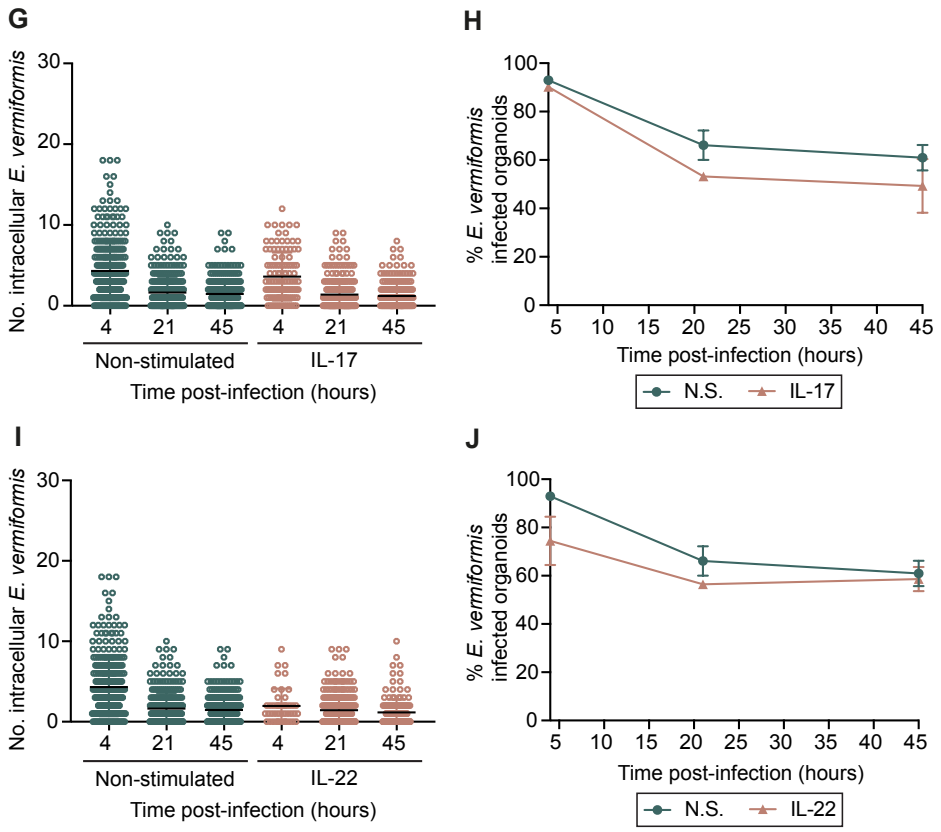

Fig. 5.7 IFN-γ, INFλ, IL-13, IL-17 and IL-22 treated small intestine organoids after *E. vermiformis* infection

Three- to four- day old small intestine organoids infected with *E. vermiformis* (orange) or non-infected controls (green) were treated with 2 ng/ml of IFN-γ (A, B), IFN-λ (C, D), IL-13 (E, F), IL-17 (G, H) or IL-22 (I, J). The number of intracellular *E. vermiformis* and their percentage were determined at 4, 21 and 45 hours post-infection. Data are representative of at least two independent experiments. Mean ($\pm$ SD) and non-parametric *t*-test with Welch's correction were plotted. Data are representative of at least two independent experiments. *P $<$ 0.05.

To further investigate the roles of IL-13 or IL-22 in the context of *in vitro E. vermiformis* infection, dose titrations were performed in order to evaluate if the effect seen was dose-dependent. Thus, *E. vermiformis*-infected organoids were stimulated with 0, 5, 10 or 20 ng/ml of mouse recombinant IL-13 or mouse recombinant IL-22. To determine the effects of the cytokine treatment, the number of intracellular parasites was determined (Figure 5.8).

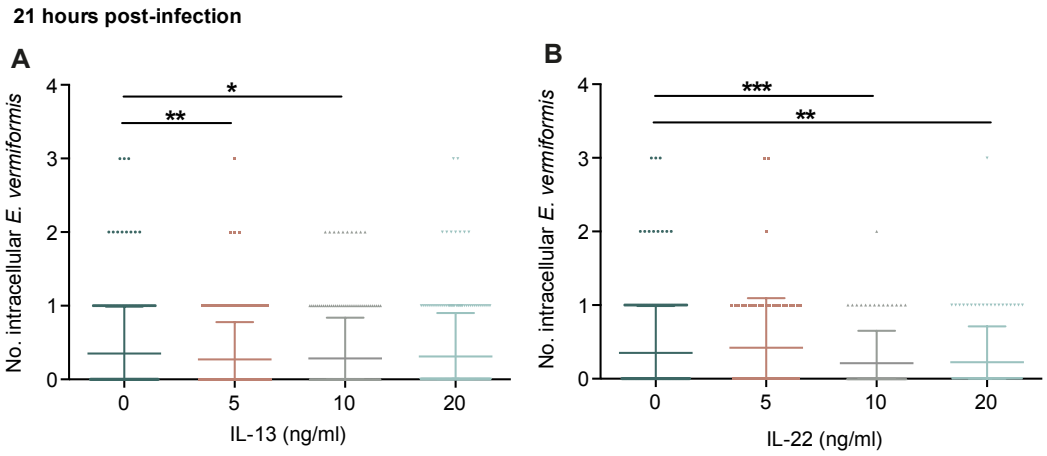

Fig. 5.8 Effect of dose titration of recombinant IL-13 or IL-22 on small intestine organoids after *E. vermiformis* infection

Three- to four-day old small intestine organoids were infected with *E. vermiformis* and treated with 0 ng/ml (green), 5 ng/ml (orange), 10 ng/ml (grey) or 20 ng/ml (blue) of mouse recombinant IL-13 (A) or IL-22 (B). The number of intracellular *E. vermiformis* was determined at 21 post-infection. Mean (± SD) and non-parametric *t*-test with Welch's correction were plotted. Data are representative of at least two independent experiments. *P < 0.05 **P < 0.01 ***P < 0.001.

The results showed that treatment with 5 or 10 ng/ml of mouse recombinant IL-13 led to a reduction of the number of intracellular parasites per organoid (Figure 5.8A). However, no significant differences were observed between the organoids treated with 5 or 10 ng/ml of mouse recombinant IL-13. A significant reduction of the number of intracellular *E. vermiformis* was also seen when infected organoids were treated with 10 or 20 ng/ml of mouse recombinant IL-22 (Figure 5.8B). IL-22 is known to promote intestinal epithelial proliferation [198]. By supplementing organoid medium with mouse recombinant IL-22 I induced an acceleration of the organoid growth. Consequently, when the data from 21 hours post-infection, a high number of organoids was burst in the IL-22-treated conditions (data not shown). Therefore, the reduction in the number of intracellular parasites could be an indirect effect of the alterations induced to the organoid by the IL-22 treatment.

Further investigation would be required to dissect the mechanisms involved in the potential protection against *E. vermiformis* conferred by both IL-13 or IL-22.

5.4 Screening of small intestine organoids cytokine production after *E. vermiformis* infection

The intestinal epithelium is exposed to numerous cytokines during inflammation. These cytokines are typically produced by the cells that are present in the local environment and by the intestinal epithelial cells themselves [199]. In order to further understand the interaction between the intestinal epithelium and pathogens, I investigated the ability of small intestine organoids to produce cytokines. For that, 3- to 4-day old organoids were infected with *E. vermiformis* and supernatant was collected at 4, 21, 45, 69 and 96 hours post-infection. Medium was renewed at 45 hours post-infection. For the quantification of cytokine production, I used the LEGENDplex mouse inflammatory panel. This assay provides higher detection sensitivity than traditional ELISA methods, and included the quantification of 13 cytokines, including: IL-1α, IL-1β, IL-6, IL-10, IL-12p70, IL-17A, IL-23, IL-27, CCL2(MCP-1), IFN-β, IFN-γ, TNF-α, and GM-CS.

Disappointingly, the data collected showed no production of any of the above-mentioned cytokines by the *E. vermiformis*-infected small intestine organoids, at any time point (data not shown). The assay protocol did not fail to work, as the standard curve was correctly acquired. This result does not necessarily mean that small intestine organoids are incapable of producing cytokines after infection. Given the ratio between the number of organoids and volume of medium per well, there is a possibility that the assay was not sensitive enough for the detection of protein production by small intestine organoids.

5.5 Discussion

In this chapter, I wanted to further investigate the interplay between the host intestinal epithelial cells and *E. vermiformis*. Therefore, because the importance of IFN-γ in the protection against *E. vermiformis* infection had been previously established, both *in vivo* and *in vitro* [147, 134], *E- vermiformis*-infected small intestine organoids were treated with mouse recombinant IFN-γ. The results of this showed that treatment with IFN-γ led to a significant increase in the number of intracellular parasites per organoid; however, the percentage of infected organoids remains unchanged (Figures 5.2, 5.7A and 5.7B). This was a surprising result, as previous reports consistently associated IFN-γ with a protective effect against *E. vermiformis* infection. Specifically, Rose and colleagues showed that *E. vermiformis* development in murine fibroblast-like (L929) cells was inhibited by treatment with recombinant IFN-γ. Interestingly, cell pretreatment was required for an effective impairment of *E. vermiformis* growth, and the length of its duration was directly related to the reduction in the number of parasites. Furthermore, they showed that if IFN-γ treatment was given 24 hours post-infection or later, it did not confer protection as it had no effect on the development of sporozoites [147]. In the *E. vermiformis*-infected small intestinal organoid model, IFN-γ treatment was administered after sporozoite invasion of epithelial cells. Moreover, by the time medium was administered the cells had been incubated with the sporozoites for 15 min, due to matrigel polymerisation. Therefore, I hypothesise that the increase in the the number of intracellular *E. vermiformis* could be the result of an indirect consequence, a negative effect induced by IFN-γ on the host epithelial cells. Furthermore, it was shown that IFN-γ has a detrimental effect over the IECs, which is strongly supported by the fact that non-infected IFN-γ-treated IECs showed an increase in the number of burst organoids over the first 45 hours post-treatment (Figure 5.6) that is accompanied by a decrease in the absolute number of organoids (Figure 5.4). IFN-γ is a pleiotropic cytokine with both pro- and anti-inflammatory roles in the context of intestinal inflammation [200]. Therefore,

an optimal balance of the levels of IFN-γ might be required to induce a protective response against *E. vermiformis*. Additionally, is has been shown that *in vivo* microbiota can induce the production of IFN-γ by immune cells at the intestinal barrier, consequently conferring on the host a higher protection to infection [201]. Therefore, in order to 'mimic' the *in vivo* conditions for *E. vermiformis*, pre-treatment of small intestine organoids with low doses of recombinant IFN-γ might be required.

Data also suggest that *E. vermiformis* infection has a detrimental effect on organoid viability, shown by the significant increase of burst organoids (Figure 5.6) and decrease of the absolute number of organoids in culture up to 45 hours post-infection (Figure 5.4), when compared with the non-infected controls. This could be a result of the sporozoite invasion process. Alternatively, *E. vermiformis* could be interfering with the availability of essential mechanisms for IEC proliferation. It has been shown that a variety of infectious organisms, including parasites like *Giardia intestinalis*, are able to induce the up-regulation host of arginases, consequently leading to a reduction of arginine, which in turn leads to a reduction in the proliferation of IECs [202]. Furthermore, there are multiple examples of IEC proliferation arrest by infectious pathogens, through various mechanisms, such as inhibition of host cell cytokinesis or induction of mitochondrial dysfunction [203, 204]. Further studies would be required to investigate how *E. vermiformis* induces the suppression of host proliferation mechanisms.

Treatment of *E. vermiformis*-infected organoids with mouse recombinant IL-13 led to a significant reduction of the number of intracellular parasites, suggesting an impairment of parasite growth. IL-13 is known to induce the production of mucin and the proliferation of goblet cells [205, 189]. On the other hand, it has been shown that the number of goblet cells decreases in association with the development of *E.vermiformis* [166]. Furthermore, it has been shown that *E. acervulina* and *E. tenella* infection is followed by decrease in the expression of IL-13 mRNA [206]. Specifically for *E. tenella*, it has been shown that IL-13

limits the egress of *E. tenella* sporozoites [207]. In contrast, *E. maxima* infection induces an increase in IL-13 mRNA expression [208]. This interplay between the IL-13 production and the proliferation of goblet cells could be the reason why IL-13-treated organoids show a lower number of intracellular *E. vermiformis*. Quantification of mucin production, or absolute numbers of goblet cells, might be required to provide answers on how IL-13 triggering of IECs confers protection against *E. vermiformis*.

IL-22 treatment of *E. vermiformis*-infected small intestinal organoids provided inconsistent results. Nevertheless, IL-22-treated organoids tended to show a lower number of intracellular *E. vermiformis*. IL-22 plays a crucial role in the maintenance of the integrity of the intestinal epithelial barrier. Additionally, IL-22 is known to facilitate the barrier defence mechanisms against pathogens, such as *T. gondii* [209]. To further investigate the effects of recombinant IL-22 on the *E. vermiformis*-infected organoids, a titration assay was performed. These results showed a significant decrease of intracellular *E. vermiformis* which correlated with the higher concentrations of recombinant IL-22. It is well established that IL-22 induces proliferation of IECs. A Ki67 proliferation analysis would be useful to further confirm my observations. Nonetheless, the data have shown that IL-22 activated small intestine organoids have an increased percentage of burst organoids, compared with the non-treated controls, which suggests that IL-22 leads to an accelerated proliferation of small intestinal organoids, ultimately leading to a reduction in the absolute number of organoids. Therefore, the observations on the reduction of the number of intracellular parasites could be a bias resulting from the reduction of the total number of organoids or an indirect effect resulting from the state of fitness of the small intestine organoids after treatment.

Finally, to grasp a better understanding on the epithelial cell response against *E. vermiformis*, I performed a screening analysis of the cytokine production by infected small intestine organoids. LEGENDplex data analysis of the medium of *E. vermiformis*-infected small intestine organoids did not detect the production of any of the target cytokines. This

result does not necessarily mean that IECs do not produce any of the target cytokines. The amount of cytokines produced could be below the detection level, given that I had seeded about 100 organoids per droplet of matrigel, which was supplemented with 500μl of organoid complete medium.

Altogether, these data suggest that IEC signalling can be triggered by cytokines. Further studies would be required to dissect the signalling mechanisms induced by IEC activation after infection. Specifically, detailed screening of gene expression and protein production by *E. vermiformis*-infected small intestine organoids would enable us to grasp a better understanding of IECs in the context of eimerian infections. Clearly, further technical work is required to define and design *in vitro* conditions in which to conduct these experiments.

Chapter 6

General Discussion

There is limited knowledge on how intestinal health is maintained. The intestinal epithelium represents a dynamic ecosystem in which mutualistic interactions between the host and external environment are cultivated. These interactions have a direct effect on immunophysiology and intestinal homeostasis. As means to perturbing this homeostasis and so revealing more about the fundamental mechanisms that maintain intestinal immunity at the epithelial barrier, in this project I investigated how the intestinal epithelium responds to *Eimeria spp.* infection, both *in vivo* and *in vitro*.

I first took an *in vivo* approach to the study of intestinal site-specific infection, namely the distal small intestine, by infecting animals with a mouse-specific intestinal parasite - *E. vermiformis*. In the context of mucosal inflammation, innate lymphoid cells (ILCs) have been reported to contribute to the maintenance of the integrity of the intestinal epithelium and defence against infection. Therefore, I focused on the ILC contribution to the protection against *E. vermiformis*. The deficiency of ILCs alone showed no increased susceptibility to *E. vermiformis* infection. Surprisingly, we observed that ILCs have a detrimental effect on the susceptibility to *E. vermiformis* infection in immunocompromised mice. Similar observations had been reported in which ILC2s were reported to have a role in inducing inflammation in the airway [175]. However, levels of ILC2s are very low in the intestine [78].

Therefore, in order to further understand the function of ILCs in the context of intestinal infection and inflammation, studies of the ILC cell subsets involved in the immune responses against *E. vermiformis* infection in a Rag2-sufficient or Rag2-deficient background would be fundamental. These studies could shed light on the protective immunological function of ILCs and the relevance of their function in parasitic diseases, thus contributing to the development of new targeting strategies for the defence against infections, when ILCs are shown to be associated with severe adverse events.

To study the interactions between intestinal epithelial cells (IECs) and pathogens, I successfully implemented an *in vitro* model of small intestine organoids that were infected with mouse *E. vermiformis* and *E. falciformis*, which infects distal small intestine and caecum/colon, respectively. Despite the differences in the intestinal site of infection, here I showed that by using a three-dimensional epithelium organoid model, which closely resembles their *in vivo* counterpart, both *Eimeria* species completed various rounds of asexual stages of development *in vitro*. However, given the complexity of this three-dimensional model, the development of reliable read-out techniques is required to gather accurate data on the spatial contribution of the various IECs.

Even though completion of the *E. falciformis* or *E. vermiformis* life cycles has not been achieved, the established small intestine organoid model is a promising tool for the study of the molecular and signalling mechanisms underlying the host-parasite or host intercellular interactions. Understanding of IEC function and translation of this understanding to humans, through the use of human biopsies to generate small intestine organoids, could contribute to the identification and exploration of new personalised therapeutic al targets.

References

[1] Lance W Peterson and David Artis. Intestinal epithelial cells: regulators of barrier function and immune homeostasis. *Nature reviews. Immunology*, 14(3):141, 2014.

[2] Hugo J Snippert, Laurens G Van Der Flier, Toshiro Sato, Johan H Van Es, Maaike Van Den Born, Carla Kroon-Veenboer, Nick Barker, Allon M Klein, Jacco Van Rheenen, Benjamin D Simons, et al. Intestinal crypt homeostasis results from neutral competition between symmetrically dividing lgr5 stem cells. *Cell*, 143(1):134–144, 2010.

[3] Laurens G van der Flier and Hans Clevers. Stem cells, self-renewal, and differentiation in the intestinal epithelium. *Annual review of physiology*, 71:241–260, 2009.

[4] Amanda M Marchiando, Le Shen, W Vallen Graham, Karen L Edelblum, Carrie A Duckworth, Yanfang Guan, Marshall H Montrose, Jerrold R Turner, and Alastair JM Watson. The epithelial barrier is maintained by in vivo tight junction expansion during pathologic intestinal epithelial shedding. *Gastroenterology*, 140(4):1208–1218, 2011.

[5] Malin EV Johansson, Mia Phillipson, Joel Petersson, Anna Velcich, Lena Holm, and Gunnar C Hansson. The inner of the two muc2 mucin-dependent mucus layers in colon is devoid of bacteria. *Proceedings of the national academy of sciences*, 105(39):15064–15069, 2008.

[6] Maria Van der Sluis, Barbara AE De Koning, Adrianus CJM De Bruijn, Anna Velcich, Jules PP Meijerink, Johannes B Van Goudoever, Hans A Büller, Jan Dekker, Isabelle Van Seuningen, Ingrid B Renes, et al. Muc2-deficient mice spontaneously develop colitis, indicating that muc2 is critical for colonic protection. *Gastroenterology*, 131(1):117–129, 2006.

[7] Anna Velcich, WanCai Yang, Joerg Heyer, Alessandra Fragale, Courtney Nicholas, Stephanie Viani, Raju Kucherlapati, Martin Lipkin, Kan Yang, and Leonard Augenlicht. Colorectal cancer in mice genetically deficient in the mucin muc2. *Science*, 295(5560):1726–1729, 2002.

[8] Joachim Mankertz and Jörg-Dieter Schulzke. Altered permeability in inflammatory bowel disease: pathophysiology and clinical implications. *Current opinion in gastroenterology*, 23(4):379–383, 2007.

[9] Jacques Amar, Chantal Chabo, Aurélie Waget, Pascale Klopp, Christelle Vachoux, Luis G Bermúdez-Humarán, Natalia Smirnova, Mathieu Bergé, Thierry Sulpice, Sampo Lahtinen, et al. Intestinal mucosal adherence and translocation of commensal

bacteria at the early onset of type 2 diabetes: molecular mechanisms and probiotic treatment. *EMBO molecular medicine*, 3(9):559–572, 2011.

[10] Jason M Brenchley, David A Price, Timothy W Schacker, Tedi E Asher, Guido Silvestri, Srinivas Rao, Zachary Kazzaz, Ethan Bornstein, Olivier Lambotte, Daniel Altmann, et al. Microbial translocation is a cause of systemic immune activation in chronic hiv infection. *Nature medicine*, 12(12):1365, 2006.

[11] Netanya G Sandler, Christopher Koh, Annelys Roque, Jason L Eccleston, Rebecca B Siegel, Mary Demino, David E Kleiner, Steven G Deeks, T Jake Liang, Theo Heller, et al. Host response to translocated microbial products predicts outcomes of patients with hbv or hcv infection. *Gastroenterology*, 141(4):1220–1230, 2011.

[12] Kerstin Berer, Marsilius Mues, Michail Koutrolos, Zakeya Al Rasbi, Marina Boziki, Caroline Johner, Hartmut Wekerle, and Gurumoorthy Krishnamoorthy. Commensal microbiota and myelin autoantigen cooperate to trigger autoimmune demyelination. *Nature*, 479(7374):538, 2011.

[13] Yun Kyung Lee, Juscilene S Menezes, Yoshinori Umesaki, and Sarkis K Mazmanian. Proinflammatory t-cell responses to gut microbiota promote experimental autoimmune encephalomyelitis. *Proceedings of the National Academy of Sciences*, 108(Supplement 1):4615–4622, 2011.

[14] Li Wen, Ruth E Ley, Pavel V Volchkov, Peter B Stranges, Lia Avanesyan, Austin C Stonebraker, Changyun Hu, F Susan Wong, Gregory L Szot, Jeffrey A Bluestone, et al. Innate immunity and intestinal microbiota in the development of type 1 diabetes. *Nature*, 455(7216):1109, 2008.

[15] Maria Rescigno. The intestinal epithelial barrier in the control of homeostasis and immunity. *Trends in immunology*, 32(6):256–264, 2011.

[16] Toshiro Sato, Robert G Vries, Hugo J Snippert, Marc Van De Wetering, Nick Barker, Daniel E Stange, Johan H Van Es, Arie Abo, Pekka Kujala, Peter J Peters, et al. Single lgr5 stem cells build crypt-villus structures *in vitro* without a mesenchymal niche. *Nature*, 459(7244):262, 2009.

[17] Ashok R Gunawardene, Bernard M Corfe, and Carolyn A Staton. Classification and functions of enteroendocrine cells of the lower gastrointestinal tract. *International journal of experimental pathology*, 92(4):219–231, 2011.

[18] Allison J Bancroft, Andrew NJ McKenzie, and Richard K Grencis. A critical role for il-13 in resistance to intestinal nematode infection. *The Journal of Immunology*, 160(7):3453–3461, 1998.

[19] Valerie Steenwinckel, Jamila Louahed, Muriel M Lemaire, Caroline Sommereyns, Guy Warnier, Andrew McKenzie, Frank Brombacher, Jacques Van Snick, and Jean-Christophe Renauld. Il-9 promotes il-13-dependent paneth cell hyperplasia and up-regulation of innate immunity mediators in intestinal mucosa. *The journal of immunology*, 182(8):4737–4743, 2009.

[20] Meera G Nair, Katherine J Guild, Yurong Du, Colby Zaph, George D Yancopoulos, David M Valenzuela, Andrew Murphy, Sean Stevens, Margaret Karow, and David Artis. Goblet cell-derived resistin-like molecule β augments cd4+ t cell production of ifn-γ and infection-induced intestinal inflammation. *The Journal of Immunology*, 181(7):4709–4715, 2008.

[21] DR Taupin, K Kinoshita, and DK Podolsky. Intestinal trefoil factor confers colonic epithelial resistance to apoptosis. *Proceedings of the National Academy of Sciences*, 97(2):799–804, 2000.

[22] Sohini Mukherjee, Hui Zheng, Mehabaw Derebe, Keith Callenberg, Carrie L Partch, Darcy Rollins, Daniel C Propheter, Josep Rizo, Michael Grabe, Qiu-Xing Jiang, et al. Antibacterial membrane attack by a pore-forming intestinal c-type lectin. *Nature*, 505(7481):103, 2014.

[23] Shipra Vaishnava, Miwako Yamamoto, Kari M Severson, Kelly A Ruhn, Xiaofei Yu, Omry Koren, Ruth Ley, Edward K Wakeland, and Lora V Hooper. The antibacterial lectin regiiiγ promotes the spatial segregation of microbiota and host in the intestine. *Science*, 334(6053):255–258, 2011.

[24] Ulf Meyer-Hoffert, Mathias W Hornef, Birgitta Henriques-Normark, Lars-Göran Axelsson, Tore Midtvedt, Katrin Pütsep, and Mats Andersson. Secreted enteric antimicrobial activity localises to the mucus surface layer. *Gut*, 57(6):764–771, 2008.

[25] Reinoud EA de Groot, Henner F Farin, Marie Macurkova, Johan H van Es, Hans C Clevers, and Hendrik C Korswagen. Retromer dependent recycling of the wnt secretion factor wls is dispensable for stem cell maintenance in the mammalian intestinal epithelium. *PloS one*, 8(10):e76971, 2013.

[26] Jim Geiser, Koen JT Venken, Robert C De Lisle, and Glen K Andrews. A mouse model of acrodermatitis enteropathica: loss of intestine zinc transporter zip4 (slc39a4) disrupts the stem cell niche and intestine integrity. *PLoS genetics*, 8(6):e1002766, 2012.

[27] Toshiro Sato, Johan H Van Es, Hugo J Snippert, Daniel E Stange, Robert G Vries, Maaike Van Den Born, Nick Barker, Noah F Shroyer, Marc Van De Wetering, and Hans Clevers. Paneth cells constitute the niche for lgr5 stem cells in intestinal crypts. *Nature*, 469(7330):415, 2011.

[28] Hans C Clevers and Charles L Bevins. Paneth cells: maestros of the small intestinal crypts. *Annual review of physiology*, 75:289–311, 2013.

[29] Timon E Adolph, Michal F Tomczak, Lukas Niederreiter, Hyun-Jeong Ko, Janne Böck, Eduardo Martinez-Naves, Jonathan N Glickman, Markus Tschurtschenthaler, John Hartwig, Shuhei Hosomi, et al. Paneth cells as a site of origin for intestinal inflammation. *Nature*, 503(7475):272, 2013.

[30] Ken Cadwell, John Liu, Sarah L Brown, Hiroyuki Miyoshi, Joy Loh, Jochen Lennerz, Chieko Kishi, Wumesh KC, Javier A Carrero, Steven Hunt, et al. A unique role for autophagy and atg16l1 in paneth cells in murine and human intestine. *Nature*, 456(7219):259, 2008.

[31] Arthur Kaser and Richard S Blumberg. Autophagy, microbial sensing, endoplasmic reticulum stress, and epithelial function in inflammatory bowel disease. *Gastroenterology*, 140(6):1738–1747, 2011.

[32] Bo Liu, Ajay S Gulati, Viviana Cantillana, Stanley C Henry, Elyse A Schmidt, Xiaoju Daniell, Emily Grossniklaus, Alexi A Schoenborn, R Balfour Sartor, and Gregory A Taylor. Irgm1-deficient mice exhibit paneth cell abnormalities and increased susceptibility to acute intestinal inflammation. *American Journal of Physiology-Gastrointestinal and Liver Physiology*, 305(8):G573–G584, 2013.

[33] Kelli L VanDussen, Ta-Chiang Liu, Dalin Li, Fadi Towfic, Nir Modiano, Rachel Winter, Talin Haritunians, Kent D Taylor, Deepti Dhall, Stephan R Targan, et al. Genetic variants synthesize to produce paneth cell phenotypes that define subtypes of crohn's disease. *Gastroenterology*, 146(1):200–209, 2014.

[34] Hazel Cheng and CP Leblond. Origin, differentiation and renewal of the four main epithelial cell types in the mouse small intestine i. columnar cell. *Developmental Dynamics*, 141(4):461–479, 1974.

[35] Nick Barker, Johan H Van Es, Jeroen Kuipers, Pekka Kujala, Maaike Van Den Born, Miranda Cozijnsen, Andrea Haegebarth, Jeroen Korving, Harry Begthel, Peter J Peters, et al. Identification of stem cells in small intestine and colon by marker gene lgr5. *Nature*, 449(7165):1003–1007, 2007.

[36] Robert K Montgomery, Diana L Carlone, Camilla A Richmond, Loredana Farilla, Mariette EG Kranendonk, Daniel E Henderson, Nana Yaa Baffour-Awuah, Dana M Ambruzs, Laura K Fogli, Selma Algra, et al. Mouse telomerase reverse transcriptase (mtert) expression marks slowly cycling intestinal stem cells. *Proceedings of the National Academy of Sciences*, 108(1):179–184, 2011.

[37] Anne E Powell, Yang Wang, Yina Li, Emily J Poulin, Anna L Means, Mary K Washington, James N Higginbotham, Alwin Juchheim, Nripesh Prasad, Shawn E Levy, et al. The pan-erbb negative regulator lrig1 is an intestinal stem cell marker that functions as a tumor suppressor. *Cell*, 149(1):146–158, 2012.

[38] Eugenio Sangiorgi and Mario R Capecchi. Bmi1 is expressed in vivo in intestinal stem cells. *Nature genetics*, 40(7):915–920, 2008.

[39] Norifumi Takeda, Rajan Jain, Matthew R LeBoeuf, Qiaohong Wang, Min Min Lu, and Jonathan A Epstein. Interconversion between intestinal stem cell populations in distinct niches. *Science*, 334(6061):1420–1424, 2011.

[40] Simon JA Buczacki, Heather Ireland Zecchini, Anna M Nicholson, Roslin Russell, Louis Vermeulen, Richard Kemp, and Douglas J Winton. Intestinal label-retaining cells are secretory precursors expressing lgr5. *Nature*, 495(7439):65, 2013.

[41] Carlos Lopez-Garcia, Allon M Klein, Benjamin D Simons, and Douglas J Winton. Intestinal stem cell replacement follows a pattern of neutral drift. *Science*, 330(6005):822–825, 2010.

[42] Toshiro Sato and Hans Clevers. Growing self-organizing mini-guts from a single intestinal stem cell: mechanism and applications. *Science*, 340(6137):1190–1194, 2013.

[43] Vladimir Korinek, Nick Barker, Petra Moerer, Elly van Donselaar, Gerwin Huls, Peter J Peters, and Hans Clevers. Depletion of epithelial stem-cell compartments in the small intestine of mice lacking tcf-4. *Nature genetics*, 19(4), 1998.

[44] Henner F Farin, Johan H Van Es, and Hans Clevers. Redundant sources of wnt regulate intestinal stem cells and promote formation of paneth cells. *Gastroenterology*, 143(6):1518–1529, 2012.

[45] Bryan T MacDonald and Xi He. Frizzled and lrp5/6 receptors for wnt/β-catenin signaling. *Cold Spring Harbor perspectives in biology*, 4(12):a007880, 2012.

[46] Johan H van Es, Marielle E van Gijn, Orbicia Riccio, Maaike van den Born, et al. Notch/gamma-secretase inhibition turns proliferative cells in intestinal crypts and adenomas into goblet cells. *Nature*, 435(7044):959, 2005.

[47] Luca Pellegrinet, Veronica Rodilla, Zhenyi Liu, Shuang Chen, Ute Koch, Lluis Espinosa, Klaus H Kaestner, Raphael Kopan, Julian Lewis, and Freddy Radtke. Dll1-and dll4-mediated notch signaling are required for homeostasis of intestinal stem cells. *Gastroenterology*, 140(4):1230–1240, 2011.

[48] Johan H Van Es, Toshiro Sato, Marc Van De Wetering, Anna Lyubimova, Annie Ng Yee Nee, Alex Gregorieff, Nobuo Sasaki, Laura Zeinstra, Maaike Van Den Born, Jeroen Korving, et al. Dll1+ secretory progenitor cells revert to stem cells upon crypt damage. *Nature cell biology*, 14(10):1099–1104, 2012.

[49] Atsushi Suzuki, Sayaka Sekiya, Eriko Gunshima, Setsuko Fujii, and Hideki Taniguchi. Egf signaling activates proliferation and blocks apoptosis of mouse and human intestinal stem/progenitor cells in long-term monolayer cell culture. *Laboratory investigation*, 90(10):1425, 2010.

[50] Anna-Pavlina G Haramis, Harry Begthel, Maaike van den Born, Johan van Es, Suzanne Jonkheer, G Johan A Offerhaus, and Hans Clevers. De novo crypt formation and juvenile polyposis on bmp inhibition in mouse intestine. *Science*, 303(5664):1684–1686, 2004.

[51] Kelsey N Retting, Buer Song, Byeong S Yoon, and Karen M Lyons. Bmp canonical smad signaling through smad1 and smad5 is required for endochondral bone formation. *Development*, 136(7):1093–1104, 2009.

[52] Tae-Hee Kim, Silvia Escudero, and Ramesh A Shivdasani. Intact function of lgr5 receptor-expressing intestinal stem cells in the absence of paneth cells. *Proceedings of the National Academy of Sciences*, 109(10):3932–3937, 2012.

[53] Aurélie Durand, Bridgitte Donahue, Grégory Peignon, Franck Letourneur, Nicolas Cagnard, Christian Slomianny, Christine Perret, Noah F Shroyer, and Béatrice Romagnolo. Functional intestinal stem cells after paneth cell ablation induced by the loss of transcription factor math1 (atoh1). *Proceedings of the National Academy of Sciences*, 109(23):8965–8970, 2012.

[54] Neil A Mabbott, David S Donaldson, Hiroshi Ohno, Ifor R Williams, and Arvind Mahajan. Microfold (m) cells: important immunosurveillance posts in the intestinal epithelium. *Mucosal immunology*, 6(4):666–677, 2013.

[55] Kazunori Masahata, Eiji Umemoto, Hisako Kayama, Manato Kotani, Shota Nakamura, Takashi Kurakawa, Junichi Kikuta, Kazuyoshi Gotoh, Daisuke Motooka, Shintaro Sato, et al. Generation of colonic iga-secreting cells in the caecal patch. *Nature communications*, 5:3704, 2014.

[56] Oliver Pabst, Heike Herbrand, Tim Worbs, Michaela Friedrichsen, Sheng Yan, Matthias W Hoffmann, Heiner Körner, Günter Bernhardt, Reinhard Pabst, and Reinhold Förster. Cryptopatches and isolated lymphoid follicles: dynamic lymphoid tissues dispensable for the generation of intraepithelial lymphocytes. *European journal of immunology*, 35(1):98–107, 2005.

[57] Allan M Mowat and William W Agace. Regional specialization within the intestinal immune system. *Nature reviews. Immunology*, 14(10):667, 2014.

[58] Craig L Maynard, Charles O Elson, Robin D Hatton, and Casey T Weaver. Reciprocal interactions of the intestinal microbiota and immune system. *Nature*, 489(7415):231–241, 2012.

[59] Karen L Edelblum, Le Shen, Christopher R Weber, Amanda M Marchiando, Bryan S Clay, Yingmin Wang, Immo Prinz, Bernard Malissen, Anne I Sperling, and Jerrold R Turner. Dynamic migration of $\gamma\delta$ intraepithelial lymphocytes requires occludin. *Proceedings of the National Academy of Sciences*, 109(18):7097–7102, 2012.

[60] Marc Bonneville, Charles A Janeway, Kouichi Ito, Wayne Haser, Isao Ishida, Nobuki Nakanishit, and Susumu Tonegawa. Intestinal intraepithelial lymphocytes are a distinct set of $\gamma\delta$ t cells. *Nature*, 336(6198):479–481, 1988.

[61] Thomas Goodman and Leo Lefrançois. Expression of the γ-δ t-cell receptor on intestinal cd8+ intraepithelial lymphocytes. *Nature*, 333(6176):855–858, 1988.

[62] Hilde Cheroutre. Starting at the beginning: new perspectives on the biology of mucosal t cells. *Annu. Rev. Immunol.*, 22:217–246, 2004.

[63] S Sugahara, T Shimizu, Y Yoshida, T Aiba, S Yamagiwa, H Asakura, and T Abo. Extrathymic derivation of gut lymphocytes in parabiotic mice. *Immunology*, 96(1):57, 1999.

[64] Susumu Suzuki, Satoshi Sugahara, Takao Shimizu, Takashi Tada, Masahiro Minagawa, Satoshi Maruyama, Hisami Watanabe, Hisashi Saito, Hiromichi Ishikawa, Katsuyoshi Hatakeyama, et al. Low level of mixing of partner cells seen in extrathymic t cells in the liver and intestine of parabiotic mice: its biological implication. *European journal of immunology*, 28(11):3719–3729, 1998.

[65] Thierry Chardes, Dominique Buzoni-Gatel, Anne Lepage, Francoise Bernard, and Daniel Bout. Toxoplasma gondii oral infection induces specific cytotoxic cd8 alpha/beta+ thy-1+ gut intraepithelial lymphocytes, lytic for parasite-infected enterocytes. *The Journal of Immunology*, 153(10):4596–4603, 1994.

[66] Stefan Müller, Myriam Bühler-Jungo, and Christoph Mueller. Intestinal intraepithelial lymphocytes exert potent protective cytotoxic activity during an acute virus infection. *The Journal of Immunology*, 164(4):1986–1994, 2000.

[67] PA Offit and KI Dudzik. Rotavirus-specific cytotoxic t lymphocytes appear at the intestinal mucosal surface after rotavirus infection. *Journal of virology*, 63(8):3507–3512, 1989.

[68] John Shires, Efstathios Theodoridis, and Adrian C Hayday. Biological insights into tcr$\gamma\delta$+ and tcr$\alpha\beta$+ intraepithelial lymphocytes provided by serial analysis of gene expression (sage). *Immunity*, 15(3):419–434, 2001.

[69] Delphine Guy-Grand, Michele Malassis-Seris, Chantal Briottet, and P Vassalli. Cytotoxic differentiation of mouse gut thymodependent and independent intraepithelial t lymphocytes is induced locally. correlation between functional assays, presence of perforin and granzyme transcripts, and cytoplasmic granules. *Journal of Experimental Medicine*, 173(6):1549–1552, 1991.

[70] Tuula Arstila, T Petteri Arstila, Sébastien Calbo, Françoise Selz, Michèle Malassis-Seris, Pierre Vassalli, Philippe Kourilsky, and Delphine Guy-Grand. Identical t cell clones are located within the mouse gut epithelium and lamina propria and circulate in the thoracic duct lymph. *Journal of Experimental Medicine*, 191(5):823–834, 2000.

[71] MJ Barnes, T Griseri, AMF Johnson, W Young, F Powrie, and A Izcue. Ctla-4 promotes foxp3 induction and regulatory t cell accumulation in the intestinal lamina propria. *Mucosal immunology*, 6(2):324, 2013.

[72] Christoph SN Klose and David Artis. Innate lymphoid cells as regulators of immunity, inflammation and tissue homeostasis. *Nature immunology*, 17(7):765–775, 2016.

[73] Hergen Spits, David Artis, Marco Colonna, Andreas Diefenbach, James P Di Santo, Gerard Eberl, Shigeo Koyasu, Richard M Locksley, Andrew NJ McKenzie, Reina E Mebius, et al. Innate lymphoid cells–a proposal for uniform nomenclature. *Nature reviews. Immunology*, 13(2):145, 2013.

[74] William E Carson, Judith G Giri, MatthewJ Lindemann, Michael L Linett, Minoo Ahdieh, Raymond Paxton, Dirk Anderson, June Eisenmann, Kenneth Grabstein, and Michael A Caligiuri. Interleukin (il) 15 is a novel cytokine that activates human natural killer cells via components of the il-2 receptor. *Journal of Experimental Medicine*, 180(4):1395–1403, 1994.

[75] Hergen Spits and James P Di Santo. The expanding family of innate lymphoid cells: regulators and effectors of immunity and tissue remodeling. *Nature immunology*, 12(1):21–27, 2011.

[76] Jochem H Bernink, Lisette Krabbendam, Kristine Germar, Esther de Jong, Konrad Gronke, Michael Kofoed-Nielsen, J Marius Munneke, Mette D Hazenberg, Julien Villaudy, Christianne J Buskens, et al. Interleukin-12 and-23 control plasticity of cd127+ group 1 and group 3 innate lymphoid cells in the intestinal lamina propria. *Immunity*, 43(1):146–160, 2015.

[77] Jochem H Bernink, Charlotte P Peters, Marius Munneke, Anje A Te Velde, Sybren L Meijer, Kees Weijer, Hulda S Hreggvidsdottir, Sigrid E Heinsbroek, Nicolas Legrand, Christianne J Buskens, et al. Human type 1 innate lymphoid cells accumulate in inflamed mucosal tissues. *Nature immunology*, 14(3):221–229, 2013.

[78] Jenny M Mjösberg, Sara Trifari, Natasha K Crellin, Charlotte P Peters, Cornelis M Van Drunen, Berber Piet, Wytske J Fokkens, Tom Cupedo, and Hergen Spits. Human il-25-and il-33-responsive type 2 innate lymphoid cells are defined by expression of crth2 and cd161. *Nature immunology*, 12(11):1055–1062, 2011.

[79] Alan Hanash, Jarrod Dudakov, Guoqiang Hua, Chen Liu, Lynette Fouser, Richard Kolesnick, Bruce Blazar, and Marcel van den Brink. Il-22 protects intestinal stem cells from immune-mediated tissue damage and regulates sensitivity to graft vs. host disease (126.31), 2012.

[80] Elke Scandella, Beatrice Bolinger, Evelyn Lattmann, Simone Miller, Stéphanie Favre, Dan R Littman, Daniela Finke, Sanjiv A Luther, Tobias Junt, and Burkhard Ludewig. Restoration of lymphoid organ integrity through the interaction of lymphoid tissue–inducer cells with stroma of the t cell zone. *Nature immunology*, 9(6):667–675, 2008.

[81] Gregory F Sonnenberg, Laurel A Monticelli, Theresa Alenghat, Thomas C Fung, Natalie A Hutnick, Jun Kunisawa, Naoko Shibata, Stephanie Grunberg, Rohini Sinha, Adam M Zahm, et al. Innate lymphoid cells promote anatomical containment of lymphoid-resident commensal bacteria. *Science*, 336(6086):1321–1325, 2012.

[82] Emelyne Lecuyer, Sabine Rakotobe, Helene Lengline-Garnier, Corinne Lebreton, Marion Picard, Catherine Juste, Remi Fritzen, Gerard Eberl, Kathy D McCoy, Andrew J Macpherson, et al. Segmented filamentous bacterium uses secondary and tertiary lymphoid tissues to induce gut iga and specific t helper 17 cell responses. *Immunity*, 40(4):608–620, 2014.

[83] Christoph SN Klose, Elina A Kiss, Vera Schwierzeck, Karolina Ebert, Thomas Hoyler, Yannick d'Hargues, Nathalie Goppert, Andrew L Croxford, Ari Waisman, Yakup Tanriver, et al. At-bet gradient controls the fate and function of ccr6^{-} ror γ t^{+} innate lymphoid cells. *Nature*, 494(7436):261, 2013.

[84] Christoph SN Klose, Melanie Flach, Luisa Möhle, Leif Rogell, Thomas Hoyler, Karolina Ebert, Carola Fabiunke, Dietmar Pfeifer, Veronika Sexl, Diogo Fonseca-Pereira, et al. Differentiation of type 1 ilcs from a common progenitor to all helper-like innate lymphoid cell lineages. *Cell*, 157(2):340–356, 2014.

[85] Ana Reynders, Nadia Yessaad, Thien-Phong Vu Manh, Marc Dalod, Aurore Fenis, Camille Aubry, Georgios Nikitas, Bertrand Escalière, Jean Christophe Renauld, Olivier Dussurget, et al. Identity, regulation and *in vivo* function of gut nkp46+ rorγt+ and nkp46+ rorγt- lymphoid cells. *The EMBO journal*, 30(14):2934–2947, 2011.

[86] Alessandra Geremia, Carolina V Arancibia-Cárcamo, Myles PP Fleming, Nigel Rust, Baljit Singh, Neil J Mortensen, Simon PL Travis, and Fiona Powrie. Il-23–responsive innate lymphoid cells are increased in inflammatory bowel disease. *Journal of Experimental Medicine*, pages jem–20101712, 2011.

[87] Wolfgang Hueber, Bruce E Sands, Steve Lewitzky, Marc Vandemeulebroecke, Walter Reinisch, Peter DR Higgins, Jan Wehkamp, Brian G Feagan, Michael D Yao, Marek Karczewski, et al. Secukinumab, a human anti-il-17a monoclonal antibody, for moderate to severe crohn9s disease: unexpected results of a randomised, double-blind placebo-controlled trial. *Gut*, 61(12):1693–1700, 2012.

[88] Jacob S Lee, Cristina M Tato, Barbara Joyce-Shaikh, Muhammet F Gulen, Corinne Cayatte, Yi Chen, Wendy M Blumenschein, Michael Judo, Gulesi Ayanoglu, Terrill K McClanahan, et al. Interleukin-23-independent il-17 production regulates intestinal epithelial permeability. *Immunity*, 43(4):727–738, 2015.

[89] Per Brandtzaeg, Inger Nina Farstad, Finn-Eirik Johansen, H Craig Morton, Inger Natvig Norderhaug, and Takeshi Yamanaka. The b-cell system of human mucosae and exocrine glands. *Immunological reviews*, 171(1):45–87, 1999.

[90] Per Brandtzaeg and Finn-Eirik Johansen. Mucosal b cells: phenotypic characteristics, transcriptional regulation, and homing properties. *Immunological reviews*, 206(1):32–63, 2005.

[91] Per Brandtzaeg and KÅRE TOLO. Mucosal penetrability enhanced by serum-derived antibodies. *Nature*, 266(5599):262–263, 1977.

[92] Ruth J Napier, Erin J Adams, Marielle C Gold, and David M Lewinsohn. The role of mucosal associated invariant t cells in antimicrobial immunity. *Frontiers in immunology*, 6, 2015.

[93] Lars Kjer-Nielsen, Onisha Patel, Alexandra J Corbett, Jerome Le Nours, Bronwyn Meehan, Ligong Liu, Mugdha Bhati, Zhenjun Chen, Lyudmila Kostenko, Rangsima Reantragoon, et al. Mr1 presents microbial vitamin b metabolites to mait cells. *Nature*, 491(7426):717, 2012.

[94] Lionel Le Bourhis, Lucia Guerri, Mathilde Dusseaux, Emmanuel Martin, Claire Soudais, and Olivier Lantz. Mucosal-associated invariant t cells: unconventional development and function. *Trends in immunology*, 32(5):212–218, 2011.

[95] Onisha Patel, Lars Kjer-Nielsen, Jerome Le Nours, Sidonia BG Eckle, Richard Birkinshaw, Travis Beddoe, Alexandra J Corbett, Ligong Liu, John J Miles, Bronwyn Meehan, et al. Recognition of vitamin b metabolites by mucosal-associated invariant t cells. *Nature communications*, 4:2142, 2013.

[96] Gerhard Wingender and Mitchell Kronenberg. Invariant natural killer t cells in the response to bacteria: the advent of specific antigens. *Future microbiology*, 1(3):325–340, 2006.

[97] Victor Arrunategui-Correa and Hyun Sil Kim. The role of cd1d in the immune response against listeria infection. *Cellular immunology*, 227(2):109–120, 2004.

[98] Masashi Emoto, Izumi Yoshizawa, Yoshiko Emoto, Mamiko Miamoto, Robert Hurwitz, and Stefan HE Kaufmann. Rapid development of a gamma interferon-secreting glycolipid/cd1d-specific vα14+ nk1. 1- t-cell subset after bacterial infection. *Infection and immunity*, 74(10):5903–5913, 2006.

[99] Thomas Ranson, Søren Bregenholt, Agnes Lehuen, Olivier Gaillot, Maria C Leite-de Moraes, André Herbelin, Patrick Berche, and James P Di Santo. Invariant vα14+ nkt cells participate in the early response to enteric listeria monocytogenes infection. *The Journal of Immunology*, 175(2):1137–1144, 2005.

[100] Kendra S Carmon, Qiushi Lin, Xing Gong, Anthony Thomas, and Qingyun Liu. Lgr5 interacts and cointernalizes with wnt receptors to modulate wnt/β-catenin signaling. *Molecular and cellular biology*, 32(11):2054–2064, 2012.

[101] Wim de Lau, Nick Barker, Teck Y Low, Bon-Kyoung Koo, Vivian SW Li, Hans Teunissen, Pekka Kujala, Andrea Haegebarth, Peter J Peters, Marc van de Wetering, et al. Lgr5 homologues associate with wnt receptors and mediate r-spondin signalling. *Nature*, 476(7360):293, 2011.

[102] Johan H van Es, Philippe Jay, Alex Gregorieff, Marielle E van Gijn, Suzanne Jonkheer, Pantelis Hatzis, Andrea Thiele, Maaike van den Born, Harry Begthel, Thomas Brabletz, et al. Wnt signalling induces maturation of paneth cells in intestinal crypts. *Nature cell biology*, 7(4):381, 2005.

[103] Vivian WY Wong, Daniel E Stange, Mahalia E Page, Simon Buczacki, Agnieszka Wabik, Satoshi Itami, Marc Van De Wetering, Richard Poulsom, Nicholas A Wright, Matthew WB Trotter, et al. Lrig1 controls intestinal stem cell homeostasis by negative regulation of erbb signalling. *Nature cell biology*, 14(4):401, 2012.

[104] Shiro Yui, Tetsuya Nakamura, Toshiro Sato, Yasuhiro Nemoto, Tomohiro Mizutani, Xiu Zheng, Shizuko Ichinose, Takashi Nagaishi, Ryuichi Okamoto, Kiichiro Tsuchiya, et al. Functional engraftment of colon epithelium expanded in vitro from a single adult lgr5+ stem cell. *Nature medicine*, 18(4):618–623, 2012.

[105] Rami A Dalloul and Hyun S Lillehoj. Poultry coccidiosis: recent advancements in control measures and vaccine development. *Expert review of vaccines*, 5(1):143–163, 2006.

[106] RB Williams. A compartmentalised model for the estimation of the cost of coccidiosis to the world's chicken production industry. *International journal for parasitology*, 29(8):1209–1229, 1999.

[107] Dawn M Walker, Steve Oghumu, Gaurav Gupta, Bradford S McGwire, Mark E Drew, and Abhay R Satoskar. Mechanisms of cellular invasion by intracellular parasites. *Cellular and molecular life sciences*, 71(7):1245–1263, 2014.

[108] Michael D Ruff. Important parasites in poultry production systems. *Veterinary parasitology*, 84(3-4):337–347, 1999.

[109] Sabina I Belli, Nicholas C Smith, and David JP Ferguson. The coccidian oocyst: a tough nut to crack! *Trends in parasitology*, 22(9):416–423, 2006.

[110] Jörg Stange, Matthew R Hepworth, Sebastian Rausch, Lara Zajic, Anja A Kühl, Catherine Uyttenhove, Jean-Christophe Renauld, Susanne Hartmann, and Richard Lucius. Il-22 mediates host defense against an intestinal intracellular parasite in the absence of ifn-γ at the cost of th17-driven immunopathology. *The Journal of Immunology*, 188(5):2410–2418, 2012.

[111] Stefanie Wiedmer, Joerg Stange, Thomas Kurth, Wilfrid Bleiss, Rolf Entzeroth, and Michael Kurth. New insights into the excystation process and oocyst morphology of rodent eimeria species. *Protist*, 162(4):668–678, 2011.

[112] Vern B Carruthers and LD Sibley. Sequential protein secretion from three distinct organelles of toxoplasma gondii accompanies invasion of human fibroblasts. *European journal of cell biology*, 73(2):114–123, 1997.

[113] Donatella Giovannini, Stephan Späth, Céline Lacroix, Audrey Perazzi, Daniel Bargieri, Vanessa Lagal, Camille Lebugle, Audrey Combe, Sabine Thiberge, Patricia Baldacci, et al. Independent roles of apical membrane antigen 1 and rhoptry neck proteins during host cell invasion by apicomplexa. *Cell host & microbe*, 10(6):591–602, 2011.

[114] Jessica S Tyler, Moritz Treeck, and John C Boothroyd. Focus on the ringleader: the role of ama1 in apicomplexan invasion and replication. *Trends in parasitology*, 27(9):410–420, 2011.

[115] Klaus Lingelbach and Keith A Joiner. The parasitophorous vacuole membrane surrounding plasmodium and toxoplasma: an unusual compartment in infected cells. *Journal of cell science*, 111(11):1467–1475, 1998.

[116] Bang Shen and L David Sibley. The moving junction, a key portal to host cell invasion by apicomplexan parasites. *Current opinion in microbiology*, 15(4):449–455, 2012.

[117] Karine Frénal, Valérie Polonais, Jean-Baptiste Marq, Rolf Stratmann, Julien Limenitakis, and Dominique Soldati-Favre. Functional dissection of the apicomplexan glideosome molecular architecture. *Cell host & microbe*, 8(4):343–357, 2010.

[118] Vern B Carruthers and Fiona M Tomley. Microneme proteins in apicomplexans. In *Molecular Mechanisms of Parasite Invasion*, pages 33–45. Springer, 2008.

[119] Kalpana Lal, Elizabeth Bromley, Richard Oakes, Judith Helena Prieto, Sanya J Sanderson, Dominic Kurian, Lawrence Hunt, John R Yates, Jonathan M Wastling, Robert E Sinden, et al. Proteomic comparison of four *Eimeria tenella* life-cycle stages: Unsporulated oocyst, sporulated oocyst, sporozoite and second-generation merozoite. *Proteomics*, 9(19):4566–4576, 2009.

[120] Hong Y Han, Jiao J Lin, Qi P Zhao, Hui Dong, Lian L Jiang, Mei Q Xu, Shun H Zhu, and Bing Huang. Identification of differentially expressed genes in early stages of eimeria tenella by suppression subtractive hybridization and cdna microarray. *Journal of Parasitology*, 96(1):95–102, 2010.

[121] Sarah Tammy Nicole Keeton and Christine B Navarre. Coccidiosis in large and small ruminants. *Veterinary Clinics of North America: Food Animal Practice*, 2017.

[122] GM Mesfin, JE Bellamy, and PH Stockdale. The pathological changes caused by *Eimeria falciformis* var pragensis in mice. *Canadian Journal of Comparative Medicine*, 42(4):496, 1978.

[123] BYRON L BLAGBURN and KENNETH S TODD. Pathological changes and immunity associated with experimental eimeria vermiformis infections in mus musculus. *Journal of Eukaryotic Microbiology*, 31(4):556–561, 1984.

[124] Kyoko Inagaki-Ohara, Fitriya Nurannisa Dewi, Hajime Hisaeda, Adrian L Smith, Fumiko Jimi, Maki Miyahira, Ayman Samir Farid Abdel-Aleem, Yoichiro Horii, and Yukifumi Nawa. Intestinal intraepithelial lymphocytes sustain the epithelial barrier function against *Eimeria vermiformis* infection. *Infection and immunity*, 74(9):5292–5301, 2006.

[125] NC Smith, KS Ovington, P Deplazes, and J Eckert. Cytokine and immunoglobulin subclass responses of rats to infection with eimeria nieschulzi. *Parasitology*, 111(1):51–57, 1995.

[126] ME Rose, D Wakelin, and P Hesketh. Interferon-gamma-mediated effects upon immunity to coccidial infections in the mouse. *Parasite immunology*, 13(1):63–74, 1991.

[127] Scott J Roberts, Adrian L Smith, A Brian West, Li Wen, R Craig Findly, Michael J Owen, and Adrian C Hayday. T-cell alpha beta+ and gamma delta+ deficient mice display abnormal but distinct phenotypes toward a natural, widespread infection of the intestinal epithelium. *Proceedings of the National Academy of Sciences*, 93(21):11774–11779, 1996.

[128] JOHN V ERNST, BILL CHOBOTAR, and DATUS M HAMMOND. The oocysts of eimeria vermiformis sp. n. and e. papillata sp. n.(protozoa: Eimeriidae) from the mouse mus musclus. *Journal of Eukaryotic Microbiology*, 18(2):221–223, 1971.

[129] Kenneth S Todd and Donald L Lepp. The life cycle of *Eimeria vermiformis* ernst, chobotar and hammond, 1971 in the mouse *Mus musculus*. *Journal of Eukaryotic Microbiology*, 18(2):332–337, 1971.

[130] Jr KS Todd, Donald L Lepp, and Charles V Trayser. Development of the asexual cycle of eimeria vermiformis ernst, chobotar, and hammond, 1971, from the mouse, mus musculus, in dexamethasone-treated rats, rattus norvegicus. *The Journal of parasitology*, 57(5):1137–1138, 1971.

[131] Kenneth S Todd Jr and Donald L Lepp. Completion of the life cycle of eimeria vermiformis ernst, chobotar, and hammond, 1971, from the mouse, mus musculus, in dexamethasone-treated rats, rattus norvegicus. *The Journal of parasitology*, 58(2):400, 1972.

[132] M Elaine Rose, Dawn G Owen, and Patricia Hesketh. Susceptibility to coccidiosis: effect of strain of mouse on reproduction of eimeria vermiformis. *Parasitology*, 88(1):45–54, 1984.

[133] ME Rose, P Hesketh, and D Wakelin. Immune control of murine coccidiosis: $Cd4^+$ and $cd8^+$ t lymphocytes contribute differentially in resistance to primary and secondary infections. *Parasitology-Cambridge*, 105:349–349, 1992.

[134] M ELAINE Rose, D Wakelin, and P Hesketh. Gamma interferon controls *Eimeria vermiformis* primary infection in balb/c mice. *Infection and immunity*, 57(5):1599–1603, 1989.

[135] AL Smith and AC Hayday. Genetic analysis of the essential components of the immunoprotective response to infection with *Eimeria vermiformis*. *International journal for parasitology*, 28(7):1061–1069, 1998.

[136] M Elaine Rose, Patricia Hesketh, Lisa Rothwell, and Robert A Gramzinski. T-cell receptor $\gamma\delta$ lymphocytes and *Eimeria vermiformis* infection. *Infection and immunity*, 64(11):4854–4858, 1996.

[137] AL Smith and AC Hayday. An $\alpha\beta$ t-cell-independent immunoprotective response towards gut coccidia is supported by $\gamma\delta$ cells. *Immunology*, 101(3):325–332, 2000.

[138] R Craig Findly, Scott J Roberts, and Adrian C Hayday. Dynamic response of murine gut intraepithelial t cells after infection by the coccidian parasite eimeria. *European journal of immunology*, 23(10):2557–2564, 1993.

[139] Adrian L Smith and Adrian C Hayday. Genetic dissection of primary and secondary responses to a widespread natural pathogen of the gut, *Eimeria vermiformis*. *Infection and immunity*, 68(11):6273–6280, 2000.

[140] RG Strout, CA Ouellette, and DP Gangi. Eimeria tenella: Temperature and asexual development in cell culture. *Experimental parasitology*, 25:324–328, 1969.

[141] RG Strout, CA Ouellette, and DP Gangi. Effect of inoculum size on development of eimeria tenella in cell cultures. *The Journal of parasitology*, pages 406–411, 1969.

[142] DAVID J Doran et al. Eimeria tenella: from sporozoites to oocysts in cell culture. *Proceedings of the Helminthological Society of Washington*, 37:84–92, 1970.

[143] David J Doran. Increasing the yield of *Eimeria tenella* oocysts in cell culture. *The Journal of parasitology*, pages 891–900, 1971.

[144] TY Shi, XY Liu, LL Hao, JD Li, Abdel Nabi Gh, MH Abdille, and X Suo. Transfected *Eimeria tenella* could complete its endogenous development *in vitro*. *Journal of Parasitology*, 94(4):978–980, 2008.

[145] Gary L Kelley and Nabil N Youssef. Development in cell cultures of eimeria vermiformis ernst, chobotar and hammond, 1971. *Zeitschrift für Parasitenkunde*, 53(1):23–29, 1977.

[146] JH Adams and GR Bushell. The effect of protease inhibitors on *Eimeria vermiformis* invasion of cultured cells. *International journal for parasitology*, 18(5):683–685, 1988.

[147] M ELAINE Rose, AL Smith, and D Wakelin. Gamma interferon-mediated inhibition of *Eimeria vermiformis* growth in cultured fibroblasts and epithelial cells. *Infection and immunity*, 59(2):580–586, 1991.

[148] C Hermosilla, B Barbisch, A Heise, S Kowalik, and H Zahner. Development of *Eimeria bovis in vitro*: suitability of several bovine, human and porcine endothelial cell lines, bovine fetal gastrointestinal, madin-darby bovine kidney (mdbk) and african green monkey kidney (vero) cells. *Parasitology research*, 88(4):301–307, 2002.

[149] Carlos Hermosilla, Ivonne Stamm, Christian Menge, and Anja Taubert. Suitable *in vitro* culture of *Eimeria bovis* meront ii stages in bovine colonic epithelial cells and parasite-induced upregulation of cxcl10 and gm-csf gene transcription. *Parasitology research*, 114(8):3125–3136, 2015.

[150] Jan Hillern Behrendt, Carlos Hermosilla, Martin Hardt, Klaus Failing, Horst Zahner, and Anja Taubert. Pmn-mediated immune reactions against *Eimeria bovis*. *Veterinary parasitology*, 151(2):97–109, 2008.

[151] Jan H Behrendt, Anja Taubert, Horst Zahner, and Carlos Hermosilla. Studies on synchronous egress of coccidian parasites (*Neospora caninum, Toxoplasma gondii, Eimeria bovis*) from bovine endothelial host cells mediated by calcium ionophore a23187. *Veterinary research communications*, 32(4):325–332, 2008.

[152] Bin Yang, Jennifer B Treweek, Rajan P Kulkarni, Benjamin E Deverman, Chun-Kan Chen, Eric Lubeck, Sheel Shah, Long Cai, and Viviana Gradinaru. Single-cell phenotyping within transparent intact tissue through whole-body clearing. *Cell*, 158(4):945–958, 2014.

[153] Yoichi Shinkai, Kong-Peng Lam, Eugene M Oltz, Valerie Stewart, Monica Mendelsohn, Jean Charron, Milton Datta, Faith Young, Alan M Stall, Frederick W Alt, et al. Rag-2-deficient mice lack mature lymphocytes owing to inability to initiate v (d) j rearrangement. *Cell*, 68(5):855–867, 1992.

[154] Peter Mombaerts, Alan R Clarke, Michael A Rudnicki, John Iacomini, Shigeyoshi Itohara, Juan J Lafaille, Lili Wang, Yoshiaki Ichikawa, Rudolf Jaenisch, Martin L Hooper, et al. Mutations in t-cell antigen receptor genes α and β block thymocyte development at different stages. *Nature*, 360(6401):225–231, 1992.

[155] Shigeyoshi Itohara, Peter Mombaerts, Juan Lafaille, John Iacomini, Andrew Nelson, Alan R Clarke, Martin L Hooper, Andrew Farr, and Susumu Tonegawa. T cell receptor δ gene mutant mice: independent generation of $\alpha\beta$ t cells and programmed rearrangements of $\gamma\delta$ tcr genes. *Cell*, 72(3):337–348, 1993.

[156] James P DiSanto, Werner Müller, Delphine Guy-Grand, Alain Fischer, and Klaus Rajewsky. Lymphoid development in mice with a targeted deletion of the interleukin 2 receptor gamma chain. *Proceedings of the National Academy of Sciences*, 92(2):377–381, 1995.

[157] James P Lodolce, David L Boone, Sophia Chai, Rachel E Swain, Themistocles Dassopoulos, Shanthi Trettin, and Averil Ma. Il-15 receptor maintains lymphoid homeostasis by supporting lymphocyte homing and proliferation. *Immunity*, 9(5):669–676, 1998.

[158] Jacques J Peschon, Philip J Morrissey, Kenneth H Grabstein, Fred J Ramsdell, Eugene Maraskovsky, Brian C Gliniak, Linda S Park, Steven F Ziegler, Dooglas E Williams, Carol B Ware, et al. Early lymphocyte expansion is severely impaired in interleukin 7 receptor-deficient mice. *Journal of Experimental Medicine*, 180(5):1955–1960, 1994.

[159] Michael Kurth and Rolf Entzeroth. Improved excystation protocol for eimeria nieschulzi (apikomplexa, coccidia). *Parasitology research*, 102(4):819–822, 2008.

[160] Patricia Aparicio-Domingo, Monica Romera-Hernandez, Julien J Karrich, Ferry Cornelissen, Natalie Papazian, Dicky J Lindenbergh-Kortleve, James A Butler, Louis Boon, Mark C Coles, Janneke N Samsom, et al. Type 3 innate lymphoid cells maintain intestinal epithelial stem cells after tissue damage. *Journal of Experimental Medicine*, pages jem–20150318, 2015.

[161] M Elaine Rose, P Hesketh, and D Wakelin. Cytotoxic effects of natural killer cells have no significant role in controlling infection with the intracellular protozoon *Eimeria vermiformis*. *Infection and immunity*, 63(9):3711–3714, 1995.

[162] AL Smith, ME Rose, and D Wakelin. The role of natural killer cells in resistance to coccidiosis: investigations in a murine model. *Clinical & Experimental Immunology*, 97(2):273–279, 1994.

[163] WT Johnston, MW Shirley, AL Smith, and MB Gravenor. Modelling host cell availability and the crowding effect in eimeria infections. *International journal for parasitology*, 31(10):1070–1081, 2001.

[164] Kazushige Maki, Shinji Sunaga, Yoshinori Komagata, Yuzo Kodaira, Ayako Mabuchi, Hajime Karasuyama, Kozo Yokomuro, Jun-Ichi Miyazaki, and Koichi Ikuta. Interleukin 7 receptor-deficient mice lack gammadelta t cells. *Proceedings of the National Academy of Sciences*, 93(14):7172–7177, 1996.

[165] Cedric Vonarbourg and Andreas Diefenbach. Multifaceted roles of interleukin-7 signaling for the development and function of innate lymphoid cells. In *Seminars in immunology*, volume 24, pages 165–174. Elsevier, 2012.

[166] Bui Khanh Linh, Toshiharu Hayashi, and Yoichiro Horii. *Eimeria vermiformis* infection reduces goblet cells by multiplication in the crypt cells of the small intestine of c57bl/6 mice. *Parasitology research*, 104(4):789–794, 2009.

[167] Marco L Schito, John R Barta, and Bill Chobotar. Comparison of four murine eimeria species in immunocompetent and immunodeficient mice. *The Journal of parasitology*, pages 255–262, 1996.

[168] Ulrike Fiebiger, Stefan Bereswill, and Markus M Heimesaat. Dissecting the interplay between intestinal microbiota and host immunity in health and disease: lessons learned from germfree and gnotobiotic animal models. *European Journal of Microbiology and Immunology*, 6(4):253–271, 2016.

[169] Randi Lundberg, Martin I Bahl, Tine R Licht, Martin F Toft, and Axel K Hansen. Microbiota composition of simultaneously colonized mice housed under either a gnotobiotic isolator or individually ventilated cage regime. *Scientific Reports*, 7, 2017.

[170] Yasmine Belkaid and Timothy W Hand. Role of the microbiota in immunity and inflammation. *Cell*, 157(1):121–141, 2014.

[171] Elke Gülden, Nalini K Vudattu, Songyan Deng, Paula Preston-Hurlburt, Mark Mamula, James C Reed, Sindhu Mohandas, Betsy C Herold, Richard Torres, Silvio M Vieira, et al. Microbiota control immune regulation in humanized mice. *JCI insight*, 2(21), 2017.

[172] Christa Thoene-Reineke, André Fischer, Christian Friese, Dana Briesemeister, Ulf B Göbel, Thomas Kammertoens, Stefan Bereswill, and Markus M Heimesaat. Composition of intestinal microbiota in immune-deficient mice kept in three different housing conditions. *PLoS One*, 9(11):e113406, 2014.

[173] Kerim Hoorweg, Charlotte P Peters, Ferry Cornelissen, Patricia Aparicio-Domingo, Natalie Papazian, Geert Kazemier, Jenny M Mjösberg, Hergen Spits, and Tom Cupedo. Functional differences between human nkp44- and nkp44+ rorc+ innate lymphoid cells. *Frontiers in immunology*, 3, 2012.

[174] Jian Li, Andria L Doty, Atif Iqbal, and Sarah C Glover. The differential frequency of lineage- crth2- cd45+ nkp44- cd117- cd127+ ilc subset in the inflamed terminal ileum of patients with crohn's disease. *Cellular immunology*, 304:63–68, 2016.

[175] Hideaki Morita, Ken Arae, Hirotoshi Unno, Kousuke Miyauchi, Sumika Toyama, Aya Nambu, Keisuke Oboki, Tatsukuni Ohno, Kenichiro Motomura, Akira Matsuda, et al. An interleukin-33-mast cell-interleukin-2 axis suppresses papain-induced allergic inflammation by promoting regulatory t cell numbers. *Immunity*, 43(1):175–186, 2015.

[176] Manuela Schmid, Maik J Lehmann, Richard Lucius, and Nishith Gupta. Apicomplexan parasite, *Eimeria falciformis*, co-opts host tryptophan catabolism for life cycle progression in mouse. *Journal of Biological Chemistry*, 287(24):20197–20207, 2012.

[177] Joachim Müller and Andrew Hemphill. *In vitro* culture systems for the study of apicomplexan parasites in farm animals. *International journal for parasitology*, 43(2):115–124, 2013.

[178] John H Adams and Kenneth S Todd. Transmission electron microscopy of intracellular sporozoites of *Eimeria vermiformis* (apicomplexa, eucoccidiida) in the mouse. *Journal of Eukaryotic Microbiology*, 30(1):114–118, 1983.

[179] GM Mesfin and James EC Bellamy. The life cycle of eimeria falciformis var. pragensis (sporozoa: Coccidia) in the mouse, *Mus musculus*. *The Journal of parasitology*, pages 696–705, 1978.

[180] WH Clair and JW Osborne. Crypt fission and crypt number in the small and large bowel of postnatal rats. *Cell Proliferation*, 18(3):255–262, 1985.

[181] Chris S Hughes, Lynne M Postovit, and Gilles A Lajoie. Matrigel: a complex protein mixture required for optimal growth of cell culture. *Proteomics*, 10(9):1886–1890, 2010.

[182] Michelle Kelleher and FionaM Tomley. Transient expression of β-galactosidase in differentiating sporozoites of *Eimeria tenella*. *Molecular and biochemical parasitology*, 97(1):21–31, 1998.

[183] M Elaine Rose and BJ Millard. *Eimeria vermiformis*: host strains and the developmental cycle. *Experimental parasitology*, 60(3):285–293, 1985.

[184] Penny H Hamid, Joerg Hirzmann, Katharina Kerner, Gerald Gimpl, Guenter Lochnit, Carlos R Hermosilla, and Anja Taubert. *Eimeria bovi*s infection modulates endothelial host cell cholesterol metabolism for successful replication. *Veterinary research*, 46(1):100, 2015.

[185] Porfirio Nava, Stefan Koch, Mike G Laukoetter, Winston Y Lee, Keli Kolegraff, Christopher T Capaldo, Neal Beeman, Caroline Addis, Kirsten Gerner-Smidt, Irmgard Neumaier, et al. Interferon-γ regulates intestinal epithelial homeostasis through converging β-catenin signaling pathways. *Immunity*, 32(3):392–402, 2010.

[186] Megan T Baldridge, Sanghyun Lee, Judy J Brown, Nicole McAllister, Kelly Urbanek, Terence S Dermody, Timothy J Nice, and Herbert W Virgin. Expression of ifnlr1 on intestinal epithelial cells is critical to the antiviral effects of interferon lambda against norovirus and reovirus. *Journal of virology*, 91(7):e02079–16, 2017.

[187] Johanna Pott, Tanel Mahlakõiv, Markus Mordstein, Claudia U Duerr, Thomas Michiels, Silvia Stockinger, Peter Staeheli, and Mathias W Hornef. Ifn-λ determines the intestinal epithelial antiviral host defense. *Proceedings of the National Academy of Sciences*, 108(19):7944–7949, 2011.

[188] Pedro P Hernández, Tanel Mahlakõiv, Ines Yang, Vera Schwierzeck, Nam Nguyen, Fabian Guendel, Konrad Gronke, Bernhard Ryffel, Christoph Hölscher, Laure Dumoutier, et al. Interferon-[lambda] and interleukin 22 act synergistically for the induction of interferon-stimulated genes and control of rotavirus infection. *Nature immunology*, 16(7):698–707, 2015.

[189] S Kanoh, T Tanabe, and BK Rubin. Il-13-induced muc5ac production and goblet cell differentiation is steroid resistant in human airway cells. *Clinical & Experimental Allergy*, 41(12):1747–1756, 2011.

[190] Rei Kawashima, Yuki I Kawamura, Rie Kato, Noriko Mizutani, Noriko Toyama-Sorimachi, and Taeko Dohi. Il-13 receptor $\alpha 2$ promotes epithelial cell regeneration from radiation–induced small intestinal injury in mice. *Gastroenterology*, 131(1):130–141, 2006.

[191] Emilio Del Cacho, Margarita Gallego, Hyun Soon Lillehoj, Joaquín Quílez, Erik P Lillehoj, Ana Ramo, and Caridad Sánchez-Acedo. Il-17a regulates *Eimeria tenella* schizont maturation and migration in avian coccidiosis. *Veterinary research*, 45(1):25, 2014.

[192] Lei Zhang, Renqiang Liu, Meng Song, Yanxin Hu, Baoliang Pan, Jianping Cai, and Ming Wang. *Eimeria tenella*: interleukin 17 contributes to host immunopathology in the gut during experimental infection. *Experimental parasitology*, 133(2):121–130, 2013.

[193] Stefanie Eyerich, Kilian Eyerich, Andrea Cavani, and Carsten Schmidt-Weber. Il-17 and il-22: siblings, not twins. *Trends in immunology*, 31(9):354–361, 2010.

[194] Spencer C Liang, Xiang-Yang Tan, Deborah P Luxenberg, Riyez Karim, Kyriaki Dunussi-Joannopoulos, Mary Collins, and Lynette A Fouser. Interleukin (il)-22 and il-17 are coexpressed by th17 cells and cooperatively enhance expression of antimicrobial peptides. *Journal of Experimental Medicine*, 203(10):2271–2279, 2006.

[195] Sabine Middendorp, Kerstin Schneeberger, Caroline L Wiegerinck, Michal Mokry, Ronald DL Akkerman, Simone Wijngaarden, Hans Clevers, and Edward ES Nieuwenhuis. Adult stem cells in the small intestine are intrinsically programmed with their location-specific function. *Stem Cells*, 32(5):1083–1091, 2014.

[196] Elmer R Pfefferkorn, Matthew Eckel, and Scott Rebhun. Interferon-γ suppresses the growth of toxoplasma gondii in human fibroblasts through starvation for tryptophan. *Molecular and biochemical parasitology*, 20(3):215–224, 1986.

[197] Xiangshu Wen, Tomoya Kudo, Laura Payne, Xisheng Wang, Laurel Rodgers, and Yasuhiro Suzuki. Predominant interferon-γ-mediated expression of cxcl9, cxcl10, and ccl5 proteins in the brain during chronic infection with toxoplasma gondii in balb/c mice resistant to development of toxoplasmic encephalitis. *Journal of Interferon & Cytokine Research*, 30(9):653–660, 2010.

[198] Caroline A Lindemans, Marco Calafiore, Anna M Mertelsmann, Margaret H O'connor, Jarrod A Dudakov, Robert R Jenq, Enrico Velardi, Lauren F Young, Odette M Smith, Gillian Lawrence, et al. Interleukin-22 promotes intestinal stem cell-mediated epithelial regeneration. *Nature*, 528(7583):560, 2015.

[199] Markus F Neurath. Cytokines in inflammatory bowel disease. *Nature reviews. Immunology*, 14(5):329, 2014.

[200] Christoph Thelemann, Remzi Onur Eren, Manuel Coutaz, Jennifer Brasseit, Hanifa Bouzourene, Muriel Rosa, Anais Duval, Christine Lavanchy, Vanessa Mack, Christoph Mueller, et al. Interferon-γ induces expression of mhc class ii on intestinal epithelial cells and protects mice from colitis. *PLoS One*, 9(1):e86844, 2014.

[201] Sophie Thiemann, Nathiana Smit, Urmi Roy, Till Robin Lesker, Eric JC Gálvez, Julia Helmecke, Marijana Basic, Andre Bleich, Andrew L Goodman, Ulrich Kalinke, et al. Enhancement of ifnγ production by distinct commensals ameliorates salmonella-induced disease. *Cell Host & Microbe*, 21(6):682–694, 2017.

[202] Britta Stadelmann, María C Merino, Lo Persson, and Staffan G Svärd. Arginine consumption by the intestinal parasite giardia intestinalis reduces proliferation of intestinal epithelial cells. *PloS one*, 7(9):e45325, 2012.

[203] Caixia Ma, Mark E Wickham, Julian A Guttman, Wanyin Deng, John Walker, Karen L Madsen, Kevan Jacobson, Wayne A Vogl, B Brett Finlay, and Bruce A Vallance. Citrobacter rodentium infection causes both mitochondrial dysfunction and intestinal epithelial barrier disruption in vivo: role of mitochondrial associated protein (map). *Cellular microbiology*, 8(10):1669–1686, 2006.

[204] António JM Santos, Charlotte H Durkin, Sophie Helaine, Emmanuel Boucrot, and David W Holden. Clustered intracellular salmonella enterica serovar typhimurium blocks host cell cytokinesis. *Infection and immunity*, 84(7):2149–2158, 2016.

[205] Hazel C Atherton, Gareth Jones, and Henry Danahay. Il-13-induced changes in the goblet cell density of human bronchial epithelial cell cultures: Map kinase and phosphatidylinositol 3-kinase regulation. *American Journal of Physiology-Lung Cellular and Molecular Physiology*, 285(3):L730–L739, 2003.

[206] Yeong Ho Hong, Hyun S Lillehoj, Sung Hyen Lee, Rami A Dalloul, and Erik P Lillehoj. Analysis of chicken cytokine and chemokine gene expression following eimeria acervulina and eimeria tenella infections. *Veterinary immunology and immunopathology*, 114(3):209–223, 2006.

[207] Xiaojuan Dong, Ghada H Abdelnabi, Sung H Lee, Guangxing Li, Hong Jin, Hyun S Lillehoj, and Xun Suo. Enhanced egress of intracellular eimeria tenella sporozoites by splenic lymphocytes from coccidian-infected chickens. *Infection and immunity*, 79(8):3465–3470, 2011.

[208] Yeong Ho Hong, Hyun S Lillehoj, Erik P Lillehoj, and Sung Hyen Lee. Changes in immune-related gene expression and intestinal lymphocyte subpopulations following eimeria maxima infection of chickens. *Veterinary immunology and immunopathology*, 114(3):259–272, 2006.

[209] Melba Muñoz, Celine Eidenschenk, Naruhisa Ota, Kit Wong, Uwe Lohmann, Anja A Kühl, Xiaoting Wang, Paolo Manzanillo, Yun Li, Sascha Rutz, et al. Interleukin-22 induces interleukin-18 expression from epithelial cells during intestinal infection. *Immunity*, 42(2):321–331, 2015.

Appendix A

Supplementary Data

A.1 Chapter 4: supplementary data

Table A.1 Phenotypic characterization of small intestine organoids: 20% matrigel

Days post-passage	Cysts	1 to 2 buds	2 to 3 buds	6+ buds
1	42%	54%	3%	1%
2	17%	62%	12%	9%
3	8%	48%	27/%	17%
4	4%	26%	25%	45%
5	0%	12%	15%	73%

Table A.2 Phenotypic characterization of small intestine organoids: 50% matrigel

Days post-passage	Cysts	1 to 2 buds	2 to 3 buds	6+ buds
1	54%	46%	0%	0%
2	26%	42%	25%	7%
3	18%	38%	27%	17%
4	2%	23%	19%	56%
5	2%	17%	11%	70%

Table A.3 Phenotypic characterization of small intestine organoids: 70% matrigel

Days post-passage	Cysts	1 to 2 buds	2 to 3 buds	6+ buds
1	57%	42%	1%	0%
2	45%	43%	10%	2%
3	17%	55%	23%	5%
4	8%	41%	28%	23%
5	3%	19%	21%	57%

Table A.4 Phenotypic characterization of small intestine organoids: 90% matrigel

Days post-passage	Cysts	1 to 2 buds	2 to 3 buds	6+ buds
1	59%	39%	2%	0%
2	34%	46%	13%	8%
3	17%	55%	23%	5%
4	4%	26%	31%	39%
5	1%	24%	11%	64%

Table A.5 Phenotypic characterization of small intestine organoids: 10% R-spondin 1 supernatant

Days post-passage	Cysts	1 to 2 buds	2 to 3 buds	6+ buds
1	90%	39.3%	0.7%	0%
2	18%	61.3%	12.7%	8%
3	8%	54%	19.3%	18.7%
4	4.7%	40%	19.3%	36%
5	1.3%	15.3%	20.7%	62.7%

Table A.6 Phenotypic characterization of small intestine organoids: 20% R-spondin 1 supernatant

Days post-passage	Cysts	1 to 2 buds	2 to 3 buds	6+ buds
1	55.3%	44%	0.7%	0%
2	30%	49.3%	17.3%	3.3%
3	11.3%	52.7%	22%	14%
4	6%	25.3%	26%	42%
5	4%	17.3%	16%	62%